UNIVERSIDADE ESTADUAL PAULISTA - UNESP
CÂMPUS DE JABOTICABAL

# CARBON DIOXIDE DYNAMICS THROUGH ORBITAL AND TERRESTRIAL MEASUREMENTS ON AMAZONIAN CROP AND FOREST LANDS

**Fernando Saragosa Rossi**
Computer science

**2023**

**UNIVERSIDADE ESTADUAL PAULISTA - UNESP**
**CÂMPUS DE JABOTICABAL**

# CARBON DIOXIDE DYNAMICS THROUGH ORBITAL AND TERRESTRIAL MEASUREMENTS ON AMAZONIAN CROP AND FOREST LANDS

**Fernando Saragosa Rossi**

**Advisor: Prof. Dr. Newton La Scala Júnior**

**Co-Advisor: Prof. Dr. Carlos Antonio da Silva Junior**

The thesis presented to the College of Agricultural and Veterinarian Sciences – UNESP, Jaboticabal Campus, as partial fulfillment of the Doctor degree in Agronomy (Soil Science).

**2023**

R831c

Rossi, Fernando Saragosa
Carbon dioxide dynamics through orbital and terrestrial measurements on Amazonian crop and forest lands / Fernando Saragosa Rossi. -- Jaboticabal, 2023
134 f. : il., tabs., mapas

Tese (doutorado) - Universidade Estadual Paulista (Unesp), Faculdade de Ciências Agrárias e Veterinárias, Jaboticabal
Orientador: Newton La Scala Junior
Coorientador: Carlos Antonio da Silva Junior

1. Agricultura. 2. Gases de efeito estufa. 3. Dióxido de carbono. 4. Uso da terra e cobertura da terra. I. Título.

Sistema de geração automática de fichas catalográficas da Unesp. Biblioteca da Faculdade de Ciências Agrárias e Veterinárias, Jaboticabal. Dados fornecidos pelo autor(a).

Essa ficha não pode ser modificada.

**unesp**

**UNIVERSIDADE ESTADUAL PAULISTA**

**Câmpus de Jaboticabal**

unesp Jaboticabal

**CERTIFICADO DE APROVAÇÃO**

TÍTULO DA TESE: CARBON DIOXIDE DYNAMICS TROUGH ORBITAL AND TERRESTRIAL MEASUREMENTS ON AMAZONIAN CROP FOREST LANDS

**AUTOR: FERNANDO SARAGOSA ROSSI**

**ORIENTADOR: NEWTON LA SCALA JUNIOR**

**COORIENTADOR: CARLOS ANTONIO DA SILVA JUNIOR**

Aprovado como parte das exigências para obtenção do Título de Doutor em Agronomia (Ciência do Solo), pela Comissão Examinadora:

Prof. Dr. NEWTON LA SCALA JUNIOR (Participaçao Virtual)
Departamento de Engenharia e Ciencias Exatas DECEx / FCAV UNESP Jaboticabal

Prof. Dr. PAULO EDUARDO TEODORO (Participaçao Virtual)
Departamento de Agronomia / Universidade Federal de Mato Grosso do Sul - gov.br

Documento assinado digitalmente
PAULO EDUARDO TEODORO
Data: 30/01/2023 16:30:50-0300
Verifique em https://verificador.iti.br

Prof. Dr. ALAN RODRIGO PANOSSO (Participaçao Virtual)
Departamento de Engenharia e Ciencias Exatas DECEx / FCAV UNESP Jaboticabal

Prof. Dr. JOSÉ FRANCISCO DE OLIVEIRA JUNIOR (Participaçao Virtual)
Departamento de Meteorologia / Universidade Federal de Alagoas UFAL - Maceió/AL gov.br

Documento assinado digitalment
Jose Francisco de Oliveira Junior
Data: 04/05/2023 14:50:26-0300
CPF: 894.868.804-49

Prof. Dr. GLAUCO DE SOUZA ROLIM (Participaçao Virtual)
Departamento de Engenharia e Ciencias Exatas DECEx / FCAV UNESP Jaboticabal

Jaboticabal, 30 de janeiro de 2023

## AUTHOR'S CURRICULUM DATA

**FERNANDO SARAGOSA ROSSI** – Son of Osvaldo Saragosa Rossi and Ana Aparecida Bandini Rossi, he was born in Ivaté - PR, on March 11, 1986. He attended minor elementary school at the Escola Estadual Ouro Verde and the middle school at the Colégio Ágora, in that same school he finished high school in 2003. From 2005 to 2006, he attended the technician/professional course in Technician in Informatics. Escola Tecnica de Viçosa, ETEV, Brazil and also took a technical/professional course in Technician in Electrotechnics. Charles Babbage Teaching Institution, UNIORKA, Brazil. In 2007, he joined the Computer Science course at Universidade Paulista, UNIP, Brazil with the course completion work entitled "Prototype in Interactivity Software for Digital TV" under the guidance of professor Mário Henrique Souza Pardo. He worked from 2011 to 2015 at the company Odebrecht Energia e Infraestrutura. In 2018, he started the Master's degree in Mestrado em Biodiversidade e Agroecossistemas Amazônicos, at the Universidade do Estado de Mato Grosso, UNEMAT, Campus of Alta Floresta - MT. On February 12, 2017, he submitted to the Master's defense, approved as a Master in Biodiversidade e Agroecossistemas Amazônicos. In March 2020, he started his Ph.D. course in Agronomy (Soil Science) also from FCAV-UNESP. In January 2023, he submitted the doctoral thesis to an examination panel, and received his Ph.D. degree in Agronomy (Soil Science) at UNESP/FCAV.

“You can look at a mistake as bullshit to be forgotten or as a result that points you in a new direction.”

Steve Jobs

## I DEDICATE

To my father **Osvaldo Saragosa Rossi** and my mother **Ana Aparecida Bandini Rossi** for their unconditional support in all the difficult moments of my life. This work is dedicated to them. Eternal gratitude.

## ACKNOWLEDGMENTS


Firstly, to my parents, Ana and Osvaldo, for always believing in me, for still supporting me, for their love, understanding, trust and especially for the teachings they gave me for life, you are the most influential teachers I have in my life. My sister Fernanda too, for her love and friendship.

I thank my companion Auana Vicente Tiago for all her patience and dedication to me.

To my advisor and friend, Dr. Newton La Scala Júnior, for their patience, guidance, trust, support, friendship. Thank you very much for contributing to my professional, personal and intellectual development. I will be eternally grateful to you for my training as a scientist.

To my co-advisor, Dr. Carlos Antonio da Silva Junior, for having received me so fraternally in his life, in the laboratory at UNEMAT -SINOP / Alta Floresta and always ready to clarify all my doubts, his contribution was indispensable. Mainly for his friendship besides being a teacher. Thank you very much.

Special thanks to a friend who welcomed me with open arms from the beginning of my doctoral journey, Gustavo André de Araújo Santos.

To the members who participated in my qualification exam: Dr. Glauco De Souza Rolim and Dr. Alan Rodrigo Panosso.

To the examination panel members of the thesis defense: Dr. Glauco De Souza Rolim, Dr. Alan Rodrigo Panosso, Dr Paulo Eduardo Teodoro and Dr José Francisco de Oliveira Júnior.

To my colleagues at the GAAF (UNEMAT-SINOP).

To the professors of the Departament of Engineering and Mathematical Sciences, thanks for the pleasant coexistence during my journey.

Thanks also at Universidade Estadual Paulista, Câmpus de Jaboticabal and Programa de pós-graduação em Agronomia (Ciência do Solo) for the opportunity to be able to study his doctorate in one of the best programs in the country.

This study was financed in part by the Coordenação de Aperfeiçoamento de Pessoal de Nível Superior - Brasil (CAPES) - Finance Code 001.

The databases SCOPUS, ScienceDirect, WEB OF SCIENCE, SCIELO, and the Periódico Capes facilitated the search for my literature review and understanding of my results.

And to all who contributed directly and indirectly to the conduct of my study.

## SUMMARY

## DINÂMICA DO DIÓXIDO DE CARBONO ATRAVÉS DE MEDIÇÕES ORBITAIS E TERRESTRES EM TERRAS DE CULTIVO E FLORESTAS AMAZÔNICAS

**ABSTRACT -** A emissão de dióxido de carbono ($CO_2$) do solo é reconhecida como o segundo maior fluxo de carbono (C) entre os ecossistemas terrestres e a atmosfera. Nas áreas agrícolas, é um processo resultante da interação de diferentes fatores, tais como clima, condições do solo e investimento tecnológico. Assim, estudos capazes de caracterizar a dinâmica do $CO_2$ são importantes na busca da compreensão das relações entre os atributos do solo em diferentes sistemas de produção. O trabalho foi realizado em quatro capítulos, desenvolvidos no estado de Mato Grosso e Mato Grosso do Sul. No capítulo 1, foram apresentadas as considerações gerais do estudo. No capítulo 2, avaliamos a variabilidade temporal da emissão de $CO_2$ do solo e sua relação com variáveis relacionadas como fluxo de $CO_2$ ($CO_2$Flux) derivado de processos fotossintéticos, Índice de Vegetação Melhorada (EVI), Produtividade Primária Bruta (GPP), Índice de Área Foliar (LAI), Temperatura do Solo (Ts) e Umidade do Solo (Us), no ano safra 2020/2021 na Fazenda Aurora, que está localizada no município de Cláudia no Estado do Mato Grosso com os diferentes usos e ocupação do solo: soja de baixo potencial de rendimento (SB); floresta nativa (FN); soja de alto potencial de rendimento (SA); bom pasto (PB) e pasto degradado (PD). Influência significativa ($p < 0,01$) foi encontrada neste capítulo para todas as variáveis analisadas e entre os diferentes usos do solo e cobertura da terra. Os valores $FCO_2$ para SA e SB com os valores mais baixos e para FN com os valores mais altos sendo o oposto para $CO_2$Flux. No capítulo 3, foi avaliada a relação entre o fluxo de dióxido de carbono no solo e os índices multiespectrais da vegetação em um sistema de monocultura de espécies de eucalipto, no campo experimental da Universidade Federal de Mato Grosso do Sul, Campus de Chapadão do Sul onde a área é composta por cinco espécies de eucalipto: *E. camaldulensis, E. uroplylla, E. saligna, E. grandis e E. urograndis* e *Corymbria citriodora*. No capítulo 3, a umidade do solo apresenta uma correlação negativa entre $FCO_2$ e significativa ($p < 0,05$), provou ser um dos fatores importantes no controle da respiração do solo. Os índices de vegetação NDRE (Normalized Difference Red-Edge Index), NDVI (Normalized Difference Vegetation Index), SAVI (Soil-Adjusted Vegetation Index) e MSAVI (Modified Soil-Adjusted Vegetation Index) mostraram maior correlação negativa com FCO2, e uma influência significativa de $p < 0,001$ para as espécies E. camaldulensis, E. saligna e E. uroplylla. No capítulo 4, a detecção remota foi usada para avaliar a dinâmica espaço-temporal do $CO_2$ de 2015 a 2018 no estado de Mato Grosso, que é a principal fronteira agrícola do Brasil. Os resultados do capítulo 4 mostraram que a variabilidade temporal do fluxo de $CO_2$ está positivamente correlacionada com a precipitação, enquanto que o $X_{CO2}$ está negativamente correlacionado com a precipitação. Portanto, não somente o $X_{CO2}$, mas também o fluxo de $CO_2$ estão diretamente relacionados ao uso da terra e à mudança de cobertura do solo (LULCC) em sistemas complexos que são afetados por variáveis e processos climáticos, como a fotossíntese e a respiração do solo.

**Keywords:** Fluxo de $CO_2$, Uso da terra e cobertura da terra, Agricultura, Gases de efeito estufa

# CARBON DIOXIDE DYNAMICS THROUGH ORBITAL AND TERRESTRIAL MEASUREMENTS ON AMAZONIAN CROP AND FOREST LANDS

**ABSTRACT -** The soil carbon dioxide ($CO_2$) emission, is recognized as the second largest carbon (C) flux between terrestrial ecosystems and the atmosphere. In agricultural areas it is a process resulting from the interaction of different factors, such as climate, soil conditions and technological investment. Thus, studies capable of characterizing the dynamics of $CO_2$ are important in the search for understanding the relationships between soil attributes in different production systems. The work was conducted in four chapters, developed in the state of Mato Grosso and Mato Grosso do Sul. In chapter 1, the general considerations of the study were presented. In chapter 2, we evaluated the temporal variability of $CO_2$ emission from soil and its relation with related variables as $CO_2$ flux ($CO_2$Flux) derived from photosynthetic processes, Enhanced vegetation index (EVI), Gross Primary Productivity (GPP), Leaf Area Index (LAI), Soil Temperature (Ts) and Soil Moisture (Ms), in the crop year 2020/2021 in Aurora Farm, which is located in the municipality of Cláudia in the State of Mato Grosso with the different land uses and occupation: low yield potential soybean (SB); native forest (FN); high yield potential soybean (SA); good pasture (PB) and degraded pasture (PD). Significant influence ($p < 0.01$) was found in this chapter for all variables analyzed and between the different land uses and land cover. The $FCO_2$ values for SA and SB with the lowest values and for FN with the highest values being the opposite for $CO_2$Flux. In chapter 3, were evaluated the relation between the flux of carbon dioxide from soil and multispectral indices of vegetation in a monoculture system of eucalypt species, in the experimental field of the Federal University of Mato Grosso do Sul, Campus de Chapadão do Sul where the area is composed of five species of eucalyptus: *E*. *camaldulensis*, *E*. *uroplylla*, *E*. *saligna*, *E*. *grandis* and *E*. *urograndis* and *Corymbria citriodora*. In chapter 3 soil moisture has a negative correlation between $FCO_2$ and significant ($p < 0.05$), proved to be one of the important factors in controlling soil respiration. The vegetation indices NDRE (Normalized Difference Red-Edge Index), NDVI (Normalized Difference Vegetation Index), SAVI (Soil-Adjusted Vegetation Index) and MSAVI (Modified Soil Adjusted Vegetation Index) showed higher negative correlation with $FCO_2$, and a significant influence of $p < 0.001$ for *E*. *camaldulensis*, *E*. *saligna* and *E*. *uroplylla* species. In chapter 4, remote sensing was used to evaluate the spatio-temporal dynamics of $CO_2$ from 2015 to 2018 in the state of Mato Grosso, which is the main agricultural frontier in Brazil. The results of chapter 4 showed that the temporal variability of $CO_2$ flux is positively correlated with precipitation, while $X_{CO2}$ is negatively correlated with precipitation. Therefore, not only $X_{CO2}$, but also $CO_2$flux are directly related to land use and land cover change (LULCC) in complex systems that are affected by climatic variables and processes, such as photosynthesis and soil respiration.

**Keywords:** $CO_2$ flux, Land use and land cover, Agriculture, Greenhouse Gas

# LIST OF ABBREVIATIONS AND ACRONYMS

**Al -** Aluminum

**ANOVA -** Analysis of Variance

**APAR -** Absorbed Photosynthetically Active Radiation

**ARVI2 -** Atmospherically Resistant Vegetation Index 2

**ATSAVI -** Ajusted Transformed Soil-Ajusted VI

**BWDRVI -** Blue-Wide Dynamic Range Vegetation Index

**CCCI -** Canopy Chlorophyll Content Index

**CHIRPS -** Climate Hazards Group Infrared Precipitation with Station

**CIgreen -** Chlorophyll Index Green

**CIrededge -** Chlorophyll Index RedEdge

**CVI -** Chlorophyll Vegetation Index

**DFOV -** Diagonal Field of View

**DVI -** Difference Vegetation Index

**ESA -** European Space Agency

**EVEI2 -** Enhanced Vegetation Index 2

**EVI -** Enhanced vegetation index

**EVI -** Improved Vegetation Index

**fAPAR -** Fraction of photosynthetically active radiation absorbed by vegetation

**$FCO_2$ -** Soil $CO_2$ emission

**FN -** Native Forest

**GCP -** Ground Control Points

**GDVI -** Difference NIR/Green Difference Vegetation Index

**GEMI -** Global Environment Monitoring Index

**GHG -** Greenhouse Gas

**GNDVI -** Green Normalized Difference Vegetation Index

**GPP -** Gross Primary Productivity

**GRNDVI -** Green-Red NDVI

**GRVI -** Green-Red Vegetation Index)

**GSAVI -** Green Soil Adjusted Vegetation Index

**GTVI -** Green Triangle Vegetation Index

**HFOV -** Horizontal Field of View

**HV -** Healthy Vegetation

**IBGE -** Brazilian Institute of Geography and Statistics

**INMET -** National Institute of Meteorology

**IPCC -** Intergovernmental Panel on Climate Change

**IPVI -** Infrared Percentage Vegetation Index

**LAI -** Leaf Area Index

**LAPIG -** Image Processing and Geoprocessing Laboratory

**LogR -** Log Ratio

**LSMM -** Linear Spectral Mixture Model

**LULC -** Land Use and Land Cover

**MODIS -** Moderate Resolution Imaging Spectroradiometer

**MSAVI -** Modified Soil Adjusted Vegetation Index

**MSRNir_Red -** Modified Simple Ratio NIR/RED

**NASA/POWER -** National Aeronautics and Space Administration / Prediction of Worldwide Energy Resources

**NDFI -** Normalized Difference Fraction Index

**NDRE -** Normalized Difference Red-Edge Index

**NDVI -** Normalized difference vegetation index

**NGRDI -** Normalized Green-Red Difference Index

**NIR -** Near-infrared

**NOAA -** National Oceanic and Atmospheric Administration

**NormR1 -** Normalized G

**NormR2 -** Normalized NIR

**NormR3 -** Normalized R

**OCO-2 -** Orbiting Carbon Observatory-2

**PAR -** Photosynthetically Active Radiation

**PB -** Productive Pasture

**PCA -** Principal Component Analysis

**PD -** Degraded Pasture

**PDF -** Probability Density Function

**PRI -** Photosynthetic Vegetation Index

**PVC -** Polyvinyl Chloride

**RGR** - Red Green Ratio Index

**RI -** Redness Index

**RTK -** Real Time Kinematic

**SA -** High-Yield Potential Soybean

**SAVI -** Soil Adjusted Vegetation Index

**SB -** Low-Yield Potential Soybean

**SM -** Soil moisture

**SMAP -** Soil Moisture Active Passive

**SMT -** State of Mato Grosso

**SPI -** Standardized Precipitation Index

**sPRI -** Scaled Value Of PRI

**ST -** Soil temperature

**TDR -** Time Domain Reflectometry

**TES -** Tropospheric Emission Spectrometer

**VFOV -** Vertical Field of View

**VIs -** Vegetation Indices

**$VPD_{scalar}$ -** Water Vapor Pressure Deficit

**WDRVI -** Wide Dynamic Range Vegetation Index

**ε -** Light-Use Efficiency

# LIST OF FIGURES

**Page**

**CHAPTER 2 – IMPLICATIONS OF $CO_2$ EMISSIONS ON THE MAIN LAND AND FOREST USES IN THE BRAZILIAN AMAZON[1]**



[1] This chapter corresponds to the scientific article submitted to the Environmental Research, Volume 220, 01 March 2023, 8.431 Impact Factor.

**CHAPTER 3 – RELATION BETWEEN SOIL RESPIRATION AND MULTIPLE VARIABLES ON EUCALYPTUS SPECIES CROP IN SOUTHWESTERN BRAZILIAN CERRADO**



**CHAPTER 4 – CARBON DIOXIDE SPATIAL VARIABILITY AND DYNAMICS FOR CONTRASTING LAND USES IN CENTRAL BRAZIL AGRICULTURAL FRONTIER FROM REMOTE SENSING DATA[2]**



[2] This chapter corresponds to the scientific article published in the Journal of South American Earth Sciences https://doi.org/10.1016/j.jsames.2022.103809.

# LIST OF TABLES

**Page**



[3] This chapter corresponds to the scientific article submitted to the Environmental Research, Volume 220, 01 March 2023, 8.431 Impact Factor.

# CHAPTER 1 – GENERAL CONSIDERATIONS

## 1 INTRODUCTION

The conversion of land use and land cover is currently one of the main impacts to the environment, and as consequence of the loss of local biodiversity and carbon emissions. This data survey is essential to report on the fulfillment of the goals signed with the civil society and international organizations, besides being important in the elaboration of strategies for the improvement of public policies. While the preservation and conservation of vegetation is necessary for $CO_2$ recycling, there is a need for large-scale food production, relative to the world population increase.

The expansion and modernization of agriculture implies on socio-environmental impacts such as the different areas occupied by soybean cultivation and thus, forest areas were replaced by agriculture, promoting intensification of the forest fragmentation process (ITAQUI, 2002; SILVA; LIMA, 2018b). However, the factors favorable to soybean farming and the support of the Federal Government were fundamental for its rapid expansion in the country (BATISTA FARIAS, 2018; SOARES; SPOLADOR; OTHERS, 2016).

The soil is an important carbon pool, and its quantity variation has direct interference in $CO_2$ concentrations, and can signal low or high concentrations of this important greenhouse gas (GHG) in the system. Therefore, soil $CO_2$ emission rates ($FCO_2$) is directly related to loss or gain of soil organic carbon, arising from the complex dynamics among soil attributes and the climatic conditions (LAL; NEGASSA; LORENZ, 2015; SILVA-OLAYA et al., 2013b) related to emissions variations, due to its great variability in time and space (DE BORTOLI TEIXEIRA et al., 2011; EPRON et al., 2006).

For better estimates of soil respiration, it is first necessary to describe its temporal variability and the relation among soil respiration and environmental variables, such as soil temperature and soil moisture (SILVA et al., 2019; XAVIER et al., 2020), both with orbital and in situ sensors. In this context, several studies seek the comprehension of agricultural practices and their respective productivities effects on increasing atmospheric concentrations of GHGs, particularly $CO_2$ (LA SCALA; BOLONHEZI; PEREIRA, 2006; MOITINHO et al., 2015; SILVA et al., 2019).

Thus, few works have sought to compare environmental variables assessed via remote sensing techniques against those obtained in situ with the flux chamber, and especially to compare $CO_2$ emission data in areas of different levels of soybean crop productivity. Understanding the spatial variability of $CO_2$ emission at different levels of data acquisition in agricultural areas becomes important for the conduction of a controlled and sustainable management of the culture for the preservation of carbon in the soil, thus contributing to the reduction of the greenhouse effect and the agility in measurement with orbital data.

Sensors onboard land monitoring satellites obtain data that assist in understanding the global distribution of vegetation types, agricultural crops, as well as their biophysical and structural properties in spatial-temporal variations (DIDAN et al., 2015). Vegetation indices allow monitoring seasonal, interannual and long-term variations in vegetation structure, phenological and biophysical parameters (HUETE et al., 2002), as well as changes in climatic variables.

The hypothesis of this study is that changes in land use affects either the soil $CO_2$ emission ($FCO_2$) or the $CO_2$ flux model ($CO_2$Flux) and those could be related to vegetative aspects like Enhanced Vegetation Index (EVI) and Leaf Area Index (LAI), resulting from modifications of the land use and land cover (LULC) system and environmental factors, which exhibit spatial and temporal variability.

Thus, the objective of the study is to evaluate the spatial and temporal characteristics of $FCO_2$ and $CO_2$Flux as function of climate and multispectral vegetation indexes in contrasting land uses in crop and forest lands of the state of Mato Grosso and Mato Grosso do Sul, Brazil.

## 1.3 LITERATURE REVIEW

### 1.3.1 Greenhouse Gases (GHGs)

In recent decades, climate change results from increasing concentrations of the carbon dioxide ($CO_2$), methane ($CH_4$), nitrous oxide ($N_2O$) and the Chlorofluorocarbons (CFC's) among others in the atmosphere (IPCC, 2020). The rates of $CO_2$, $CH_4$ and $N_2O$ concentrations in 2019 reached levels of 409.9 (±0.4) parts per million (ppm), 1866.3 (±3.3) parts per billion (ppb) and 332.1 (±0.4) ppb respectively with an increase from 1750 to 2019 of 131, 6 ± 2.9 ppm (47.3%), 1137 ± 10 ppb (156%) and 62 ± 6 ppb (23.0%) and an effective radiative forcing (ERF) of halogenated components in 2019 was 0.4 W $m^{-2}$, an increase of 3.5 % since 2011 (BYERS et al., 2022). The increase of these gases concentration in the atmosphere has been significant (IPCC; OTHERS, 2013; ZHENG et al., 2019), where Earth's global temperature has increased by 0.5 to 1 °C in the last 100 years (CHEN; XIN, 2017; MIKHAYLOV et al., 2020).

Anthropic actions such as fossil fuel burning, agriculture and land use change are the main sources of GHGs with 66%, 20% and 14% respectively of $CO_2$ emissions to the atmosphere (BRUHWILER et al., 2021; SHUKLA et al., 2019). In Brazil, the fires from deforestation account for 180 to 200 Mt C year$^{-1}$ (megatons of carbon per year) being higher than the burning of fossil fuel in the country of 70 to 90 Mt C year$^{-1}$ , making Brazil the 5$^{th}$ largest emitter of the world (SANQUETTA et al., 2022; SANTILLI et al., 2005). The contributions of total $CO_2$ emissions in Brazil by agriculture is represented by 20 to 25% for global warming (HOUGHTON et al., 2001).

Soil tillage by plowing and harrowing leads to a decrease in organic material and an increase in the oxidation of organic carbon into $CO_2$ by breaking up soil aggregates. The dynamics of N in the soil is intrinsically related to the emission of $N_2O$, which is influenced by the presence of nitrogen-fixing plants and additions of mineral nitrogen fertilizer. The degradation process by agriculture soil management causes the microbiota under anaerobic conditions to oxidize $CO_2$ to $CH_4$ (GUENET et al., 2021; TIWARI; SINGH; SINGH, 2020).

Terrestrial ecosystems composed of vegetation and soil are currently considered important carbon sinks, particularly soils. There are several ways in which proper management of the earth's biosphere, particularly soils, can significantly reduce the increase in GHGs.

### 1.3.2 Carbon in soil

Soil is an important carbon reservoir, in the first 100 cm depth, globally between 1,300 - 2,000 Pg (petagram) of carbon are stored, corresponding to twice the concentration of atmospheric carbon (LAL, 2003; MAYER et al., 2019). Changes in land use and land cover can have significant impacts on the concentration of carbon dioxide (ROSSI et al., 2022) and other GHGs in the atmosphere (SCHUMAN; JANZEN; HERRICK, 2002; SCHWANDNER et al., 2017).

Recently, research has pointed out that soil management is a decisive factor in the soil organic carbon sequestration, such as the no-till farming system, which allows crop rotation, straw maintenance on the soil surface with the use of cover crops and sowing without soil disturbance, providing a significant increase in soil C stock (TONELLO; AZEREDO, 2021).

Tropical soils store 506 Pg of carbon (MARÍN-SPIOTTA; SHARMA, 2013) of which 66 Pg of carbon are in soils of the Amazon (BATJES, 1999), and 47 Pg of carbon in the Brazilian legal Amazon (BATJES, 1999). Considering the first 30 cm of depth, the soils of the Brazilian territory, store around 36,4 Pg of carbon (BERNOUX et al., 2002). However, assessing changes in soil C stocks still has its barriers, due to the difficulties in detecting small modifications (OLIVEIRA, 2018).

Soil carbon is present in living organic matter, which accounts for less than 4 percent of total soil organic carbon, and in dead organic matter, which returns most of the total soil organic carbon (about 98 percent) (REGO et al., 2013; SIQUEIRA et al., 2021).

The soil organic C stock is determined by the annual balance of the addition of photosynthesized C and the loss of organic C due to its oxidation to $CO_2$ by heterotrophic microorganisms. Decomposition processes and transformation rates are strongly influenced by climate, type and quality of organic matter, chemical and physicochemical associations of organic matter with soil mineral components, and the location of organic matter in the soil (ALMEIDA; SANCHES, 2014; MÜTZENBERG, 2020).

The three main processes responsible for carbon sequestration in soils are humification, aggregation and sedimentation. At the same time, the processes responsible for carbon losses in the soil are erosion, decomposition, volatilization and leaching (LAL, 1997; RUFINO et al., 2022). The physical protection of soil organic matter by the mineral fraction of the soil during the process of aggregate formation has been a fundamental process for the increase of soil C stocks (DE M. SÁ et al., 2001).

The conversion of a natural ecosystem into agriculture and/or pasture may have an important influence on the fate of the C stored in the soil (FERNANDES; FERNANDES, 2008; NEILL et al., 1997; RODRIGUES, 2021). In soils under natural vegetation, the preservation of organic matter tends to be maximum, because soil disturbance is minimal, and the contribution of carbon in forests is higher than in cultivated areas. In cultivated areas, the levels of organic matter, as a rule, decrease, since the organic fractions are more exposed to attack by microorganisms, due to greater soil disturbance and de-structuring (CHRISTENSEN, 2020).

However, several factors such as soil and climatic conditions can lead to an increase or decrease in soil C contents. Thus, studies in broad scenarios are essential, in order to help reduce the variability of results and promote the homogeneity of information (CIDIN, 2016).

### 1.3.3 Land use and land cover change

Forest ecosystems, collaborate through their functions in reducing climate change, mainly by absorbing a significant part of carbon dioxide emissions and storing large amounts of carbon in biomass and soils (COLLALTI et al., 2019; LE QUÉRÉ et al., 2018), in addition to the importance for watershed protection, soil, climate regulation and biodiversity conservation (BONAN, 2008; ROY; RAVAN, 1996).

Forests store up to about 45% of terrestrial carbon (YAO et al., 2018). Approximately 2.4 ± 0.4 Pg of Carbon per year is absorbed by the global forest ecosystem, reaching the equivalent of 60% of the cumulative carbon emissions from global fossil consumption (FU et al., 2015). The Amazon presents itself as one of the great potentialities to capture carbon, since it is estimated as the largest tropical forest in the world, and responsible for sequestering 14% of the planet's carbon (BRIENEN et al., 2015).

During the development process, trees absorb $CO_2$ and release $O_2$ in photosynthesis, on the contrary, in respiration, they release carbon dioxide, in reduced amounts in relation to that absorbed (BARBOSA, 2015; PIRES, 2019). Thus, one can consider the practices for climate change mitigation, reforestation, restoration of degraded forests and forest protection (BERENGUER et al., 2014; HOUGHTON; UNRUH; LEFEBVRE, 1993; ZHANG; XU, 2003).

Forestry and agribusiness have driven the production of soybean and eucalyptus monocultures in Brazil (SANTOS, 2019). The increase in soybean and eucalyptus planting is as a result of the demand for the spread of this activity largely influenced by the Brazilian state (LAMEIRA et al., 2017).

The expansion of soybean cultivation in Brazil in the last two decades has reached large proportions, bringing important changes to the model of territorial occupation and the development of the national economy. Soybean expansion differs from other crops in relation to its impact on land use change, especially in the Amazon and Cerrado biomes (VALE; CARVALHO; ABDALA, 2021). Second largest world soybean producer and largest exporter since 2003, Brazil has increased its production following the global trend of growth in demand and supply of soybeans (LIMA, 2006).

Soybean (*Glycine max* (L.) Merr.) is one of the commodities that presents the greatest prominence in the national and international market, being one of the most consumed and produced grains in the world (FAOSTAT, [s.d.]). In Brazil it has a significant socioeconomic importance, thus becoming one of the main vehicles of development and the main product of agriculture in the country (HIRAKURI; LAZZAROTTO, 2014).

In addition to soybeans, Brazil also stands out as one of the largest producers of eucalyptus (*Eucalyptus* spp.), with high levels of productivity due to favorable soil conditions, climate, and land availability (ABREU; FEIO, 2021; IBÁ, 2020). The increase in forest plantations in Brazilian territory reaches approximately 8.7 million hectares, with eucalyptus plantations predominantly occupying 7.47 million hectares, corresponding to 33% of the total area of eucalyptus plantations in the world (ALMEIDA; VIEIRA, 2022; MAPBIOMAS, 2021; ZHANG; WANG, 2021). Strengthening the production of paper, pulp, furniture and biofuels (LIMA et al., 2020).

However, one of the main concerns about GHG's has been the conversion of natural vegetation for agriculture and cattle ranching (MCTI, 2014; SILVA; LIMA, 2018a; SILVA et al., 2018), which result in significant amounts of $CO_2$ emissions to the atmosphere, either by burning the aerial biomass or subsequent loss in soil carbon stocks (IPCC, 2014). This influence still seems to be indirect, since it is being established over degraded pasture areas from failed cattle ranching projects, in most cases.

Carbon loss is faster in the conversion from native vegetation to an agricultural system located in the tropics, due to the combination of high humidity and temperature throughout the season (SCHOLES; VAN BREEMEN, 1997). The main losses of soil organic matter are stimulated by soil disturbance, greater variations in soil temperature and moisture, breakdown of aggregates, and the decrease in soil cover. The reduction of the most active fraction of soil organic matter affects several functions in the soil, being composed of humic substances of low molecular weight, as well as plant and animal residues and their primary decomposition products.

#### 1.3.4 Remote Sensing

Remote sensing is a technique that is becoming prominent in agricultural activities, in plant evaluations through biophysical parameters, and in several other fields of science through ground, airborne or orbital sensors that act actively or passively, recording the interaction of electromagnetic energy with the environment (DA SILVA JUNIOR et al., 2018; XU et al., 2020). The phenomena of absorption, reflection and transmission relies on the interaction of electromagnetic energy with the targets of interest (LIU, 2015). The ability of an object to absorb, reflect, and transmit electromagnetic radiation is referred to as absorptance, reflectance, and transmittance, respectively (XUE; SU, 2017). Transmission is done through the components that make up the leaf, when the radiation is reflected by the leaves (TSAI et al., 2019). Among the three phenomena, the energy reflected by objects is the most used in studies by most researchers using orbital and sub-orbital sensors (DENG et al., 2019).

In photosynthesis, plants have higher absorbance in the wavelength corresponding to the blue and red bands and higher reflectance in the near infrared range (NIR) (GITELSON et al., 2021). Much of this absorbed radiation and made by the pigments of chlorophylls "a" (430 - 660 nm) and "b" (450 - 650 nm) existing in chloroplasts, with high absorption in the blue and red bands (GITELSON et al., 2006). One of the major factors of the low absorption and reflectance of incident energy is the pigmentation contained in the leaves. With the loss of chlorophyll from a plant indicates that it is in the senescence stage, thus having a reflectance in the red range (MERZLYAK et al., 1999; MURAOKA et al., 2010).

In remote sensing, the vegetation is a complex target, since it presents leaf manifestations non-uniformity of structure inter and intra vegetation in the same plant, besides the soil spectral interference. The variability of the red and near infrared energy reflected by the vegetation that reaches the sensor will vary with solar irradiance, atmospheric conditions, substrate type, canopy structure and composition. The radiance is received by the optical components and then converted into electrical signals, then transformed into a digital numerical value associated with the pixels of the satellite images at the time of imaging.

By using satellite images, we can perform analysis by means of vegetation indices (IR) to highlight the spectral behavior of biomass in relation to the soil and other targets of the earth's surface, in order to assess natural resources and monitor vegetation cover. Commonly, vegetations indices rely on the arithmetic operations combination by using two or more spectral bands, in order to provide stable information about the surface compared to reflectance measurements (DA SILVA et al., 2017). Studies use this combination of spectral bands to analyze biomass and carbon stock over coffee plantation areas by using the Normalized Difference Vegetation Index (NDVI), the Photosynthetic Vegetation Index (PRI) and the $CO_2$flux model, which is based on the NDVI and PRI by means of Landsat images (COLTRI et al., 2009).

The discrimination between deficient and adequate boron levels in *Eucalyptus* spp. juveniles can be based on the wavelengths of the MSI/Sentinel-2 sensor system with the data from this sensor support the method of discrimination of adequate B nutrition in areas with planting of the species (DAMASCENO et al., 2023). In other studies used structural equation modeling (SEM) and factor analysis on corn varieties allowed to identify which agronomic variables and which NDVI, NDRE and SAVI indices are most associated with crop grain yield (SANTANA et al., 2022).

Nowadays, there are several vegetation indices developed for different applications and research assessment abroad the science. This proves that the use of remote sensing techniques is capable of supplying research on spatial and temporal scales of vegetation, both locally and globally.

# CHAPTER 2 – VARIATIONS OF CO2 EMISSIONS ON DIFFERENT VEGETATIONS COVERS IN THE BRAZILIAN AMAZON[4]

**ABSTRACT:** Soil carbon dioxide ($CO_2$) emission in agricultural areas is a process resulting from the interaction of several factors, such as climate, soil and management conditions. Agricultural practices directly affect the carbon dynamics between soil and atmosphere. Here, we evaluated the temporal variability (2020/2021 crop season) of soil $CO_2$ emission and its relationship with related variables as $CO_2$ flux model, Enhanced vegetation index (EVI), Gross Primary Productivity (GPP), Leaf Area Index (LAI) from orbital data and soil temperature, soil moisture and soil $CO_2$ emission in situ collection, over native forest, productive pasture, degraded pasture, high-yield potential soybean and low-yield potential soybean areas. Significant influence ($p < 0.01$) was observed for all variables and between the different land uses and land occupation. September and October presented lower soil $CO_2$ emission, recording low means of soil moisture and soil temperature, and no differences were observed among treatments. On the other hand, there was a significant effect of $CO_2$ flux model in the areas of productive pasture, high-yield potential soybean and low-yield potential soybean. The months with the highest $CO_2$ flux model values, regardless the land use and land cover, were October and November, the beginning of the rainy season. There were positive correlations between soil $CO_2$ emission and GPP (0.208), LAI (0.354), EVI (0.363) and soil moisture (0.280), and negative correlations between soil $CO_2$ emission and soil temperature (-0.240) and $CO_2$ flux model (-0.314). The land uses and land covers showed negative correlations between these variables, except for the $CO_2$ flux model variable. Soil $CO_2$ emission values were lower for high-yield potential soybean (averages from 0.834 to 6.835 μmol $m^{-2}$ $s^{-1}$) and low-yield potential soybean (from 0.943 to 5.686 μmol $m^{-2}$ $s^{-1}$) and higher for native forest (from 2.279 to 8.131 μmol $m^{-2}$ $s^{-1}$), whereas for $CO_2$ flux model the opposite behavior was observed.

**Keywords:** Land use and land cover; Sustainability; climate change; greenhouse gases

[4] This chapter corresponds to the scientific article submitted to the Environmental Research, Volume 220, 01 March 2023, 8.431 Impact Factor.

## 2.1 INTRODUCTION

Climate change is one of the main challenges for society and is probably the most widespread threat to humanity due to the earth's growing population and the resulting increased concentration of carbon dioxide ($CO_2$) released into the atmosphere (NASROLLAHI et al., 2020; RIBEIRO; RYBSKI; KROPP, 2019). As the world's population increases, the need for large-scale food production arises, agricultural expansion and increased food production have been among the major impacts of humanity on the environment that include climate change, greenhouse gas (GHG) emissions (AWUCHI et al., 2020; REHMAN et al., 2021a, 2021b, 2022). Land use and land cover change for commodity production is one of Brazil's main sources of GHGs, making the country responsible for 2.8% of global emissions (DE AREA LEÃO PEREIRA et al., 2020).

Soybean (*Glycine max* (L.) Merr.) is one of the most important commodities in the national and international market, being one of the most consumed and produced grains in the world (FAOSTAT, [s.d.]). In Brazil it has an expressive socioeconomic importance, thus becoming one of the main vehicles of development and the main agricultural product of the country (HIRAKURI; LAZZAROTTO, 2014). However, one of the main concerns about GHG's has been the conversion of natural vegetation for agriculture and cattle ranching (MCTI, 2014; SILVA; LIMA, 2018a; SILVA et al., 2018), that result in significant amounts of $CO_2$ emissions to the atmosphere, either by burning the above-ground biomass or subsequent loss in soil carbon stocks (IPCC, 2014).

Soil $CO_2$ emission in agricultural areas has proven to be a complex phenomenon, as it has great spatial and temporal variability due to its relationship with various soil properties (LA SCALA; BOLONHEZI; PEREIRA, 2006; SILVA et al., 2019, 2020). For better estimates of soil respiration, it is first necessary to describe its temporal variability and the relationships with environmental variables that can be continuously monitored, such as temperature and humidity (SILVA et al., 2019; XAVIER et al., 2020), both with orbital sensors and *in loco*, which makes it possible to monitor other related parameters.

In this context, several studies have elucidated the effects of agricultural practices and their respective productivity on the increasing atmospheric concentrations of GHGs, particularly $CO_2$ (LA SCALA; BOLONHEZI; PEREIRA, 2006;

MOITINHO et al., 2015; SILVA et al., 2019). In the soil, $CO_2$ is produced through biochemical reactions directly related to the biological activity of microorganisms and root respiration, which are mainly influenced by soil temperature and humidity (BOND-LAMBERTY; THOMSON, 2010; OERTEL et al., 2016; PRIES et al., 2017).

According to Intergovernmental Panel on Climate Change (2014), Inadequate agricultural land management practices are responsible for approximately a quarter of global GHG emissions, including deforestation, agricultural methane emissions, and nitrous oxide emissions in fertilized soils. In this context, soil carbon accumulation in agricultural systems is a promising strategy to mitigate the atmospheric increment of $CO_2$ (DOSSOU-YOVO et al., 2016), thus reducing the greenhouse gas balance and the carbon footprint associated with agricultural production, as examples in meat and sugarcane production respectively (DE FIGUEIREDO et al., 2017).

Nevertheless, environmental variables that tangent to this prospect demand comparison, where *in loco* data obtained with the soil respiration chamber can be related to carbon sequestration efficiency estimates related to vegetation in agricultural areas. Understanding the spatial and temporal variability of $CO_2$ at different levels of data acquisition in farming lands becomes important for conducting controlled and sustainable crop management for soil carbon preservation, thus contributing to the mitigation of the extended greenhouse effect.

For the generation of objective information in near-real-time, remote sensing is a tool that provides and contributes to the distinction and characterization of forests, agriculture, climate, among others (ALMEIDA et al., 2019; LIU et al., 2020b). On-board sensors from ground monitoring satellites obtain data that assist in understanding the global distribution of vegetation types, agricultural crops, as well as their biophysical and structural properties in spatio-temporal variations (DIDAN, 2015). For example, one of the products generated by Moderate-Resolution Imaging Spectroradiometer (MODIS) sensor are the vegetation indices (VIs), which perform spectral transformations of two or more bands and enable the visualization of vegetation properties and temporal inter-comparisons of terrestrial photosynthetic activity and canopy structural variations, enabling for example the monitoring of areas with soybean (DA SILVA et al., 2017). The VIs allow monitoring of seasonal, inter-annual and long-term variations in vegetation structure, phenological and biophysical parameters (HUETE et al., 2002), besides changes in climatic variables, such as precipitation (GOUVEIA et al., 2008). Furthermore, it is also possible to acquire and estimate other variables through spectral bands, such as Gross Primary Productivity (GPP) (ROSSI; SANTOS, 2020) and carbon dioxide flux ($CO_2$Flux) through photosynthesis and respiration (DELLA-SILVA et al., 2022; ROSSI et al., 2022; SILVA JUNIOR et al., 2019).

In view of the biogeochemical carbon cycle and its great relation to climate, the observation of soil $CO_2$ emission, moisture and soil temperature dynamics, as well as the relation of variables obtained by means of remote orbital sensing techniques related to the emission and/or absorption of atmospheric carbon in the biotic carbon pool are potentially associated to the type of land use and occupation.

Thus, our objective was to verify the relation of soil carbon emission with remotely sensed variables of $CO_2$ flux model ($CO_2$Flux), GPP, vegetation indices and leaf area index, as well as in situ metrics of soil moisture and temperature, conditioned to different land uses and land covers of an agricultural are in northern Mato Grosso.

## 2.2 MATERIAL AND METHODS

### 2.2.1 Studied area

The study was carried out in the 2020/2021 crop season at Aurora Farm, located in the municipality of Cláudia, Midwest region of Brazil (Figure 1) southern Amazon ecoregion, with a total area of 3.843,561 km² (IBGE, 2021) According to Köppen's classification, the region's climate is type Aw (tropical climate, with dry winter) (ALVARES et al., 2013), with a rainy period from October to April and a dry period from May to September. Annual rainfall is approximately 1970 mm, and average monthly temperatures range between 24 and 27 °C (SOUZA et al., 2013a). The soil of the area was classified as yellow latosol, according to the Brazilian Soil Classification System (SIBCS) (EMBRAPA_SOLOS, 2020; EMBRAPA, 2018).

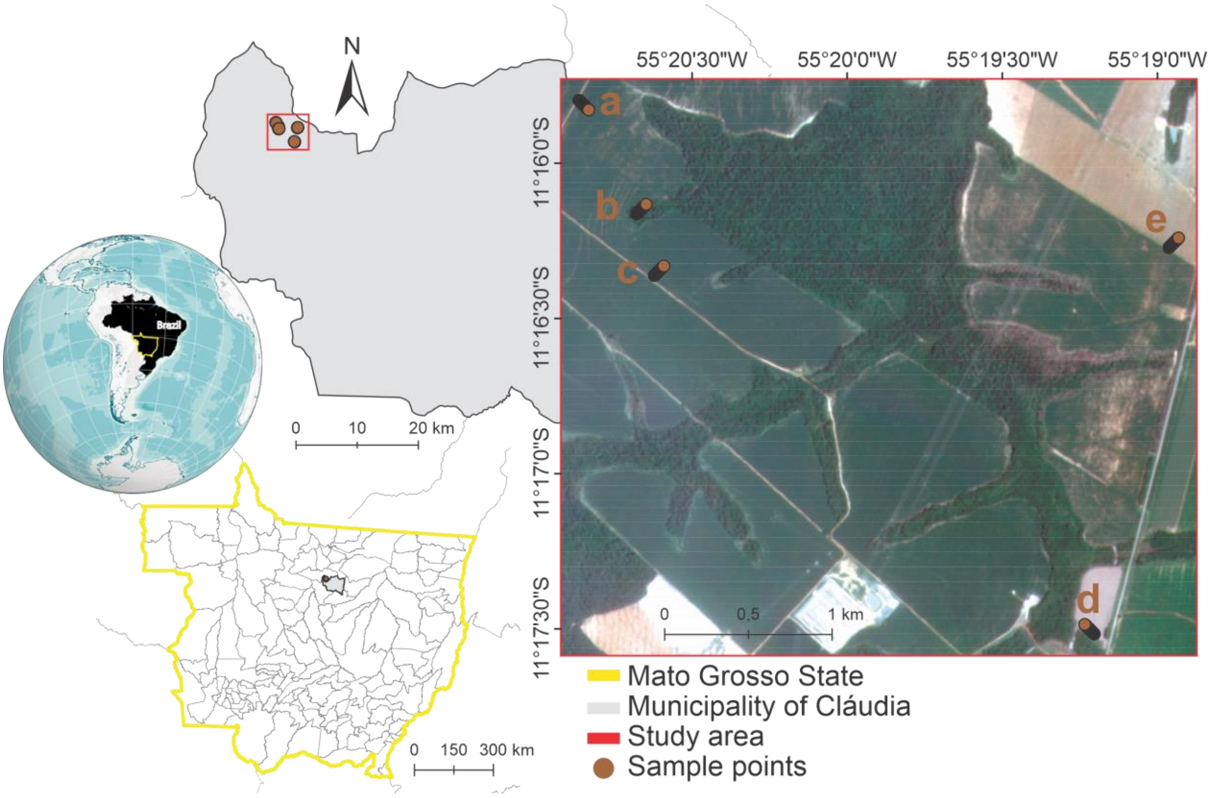


**Figure 1.** Study area located in the State of Mato Grosso with the different land uses and occupation in the Amazon ecoregion: a) low-yield potential soybean (SB); b) native forest (FN); c) high-yield potential soybean (SA); d) productive pasture (PB) and e) degraded pasture (PD) in the municipality of Cláudia.

Five areas with distinct uses were chosen according to availability and ease of access. The native forest is in an initial regeneration stage due to environmental intervention, such as clear-cutting, agricultural cultivation, or fire/burning that has occurred in the last 10 years. The pasture areas are in the process of changing to rice in the first crop grown on the site, and the later to soybean and corn crops. Previously, there was pasture in the area, and farming on the site began in 2015.

### 2.2.2 Vegetation Indices

Vegetation indices (VIs) have been developed to highlight the combinations of surface reflectance at two or more wavelengths designed to highlight a particular property of vegetation in order to exclude soil and other terrestrial targets. The numerical values of these indices can vary between -1 and 1, in which vegetation is commonly indicated by positive values, as there is greater reflectance in the near-infrared wavelength than in the red (HUETE et al., 2002; SOLANO et al., 2010). Some targets, such as water and snow, exhibit higher reflectance at the red (600 – 750 nm) wavelength region, as compared with the near-infrared (750 – 1100 nm) region. With the emergence of the Moderate-Resolution Imaging Spectroradiometer (MODIS) sensor, Huete et al. (1997) proposed an Enhanced Vegetation Index (EVI) (Equation 1) that minimizes the effects of soil and atmosphere by considering the blue spectral band.

$$EVI = g\frac{\rho_{NIR} - \rho_{RED}}{\rho_{NIR} + (c_1 \cdot \rho_{RED}) - (c_2 \cdot \rho_{BLUE}) + L} \quad (1)$$

where $\rho_{NIR}$, $\rho_{RED}$, and $\rho_{BLUE}$ are the reflectances in the near-infrared, red, and blue spectral ranges, respectively; *g* is the gain factor (2.5); $c_1$ and $c_2$ are the correction coefficients for red (6) and blue (7.5) atmospheric effects, respectively; and *L* is the correction factor for soil interference (1). The coefficients adopted in the EVI equation according to Huete et al. (1994, 1997).

The Soil Adjusted Vegetation Index (SAVI) (Equation 2), takes into account the effects of exposed soil in the analyzed images (that is, when the surface is not completely covered by vegetation) to adjust Normalized Difference Vegetation Index (NDVI).

$$SAVI = \frac{(1 + L_s)(\rho_{NIR} - \rho_{RED})}{(L_s + \rho_{NIR} + \rho_{RED})} \quad (2)$$

where *Ls* is a constant called the adjustment factor of SAVI and can assume values of 0.25–1 depending on the soil cover. According to Huete (1988), a value for Ls of 0.25 is indicated for dense vegetation, of 0.5 for intermediate density, and of 1 for low density vegetation. When Ls is equal to 0, the assigned SAVI value is equal to the NDVI. Huete (1988) suggested an optimal value of Ls = 0.5 to account for first-order soil background variations.

Leaf Area Index (LAI) (Equation 3) is a biophysical index defined by the ratio between the leaf area of a vegetation per unit area used by this vegetation, being an indicator of the biomass of each image pixel, as computed by the following empirical equation (ALLEN et al., 2002). Surface Energy Balance Algorithm for Land (SEBAL) was designed to calculate the components that make up the energy balance locally and regionally, from limited surface data, by using empirical relationships and physical parametrization (BASTIAANSSEN et al., 1998a, 1998b; MARTINS; GALVANI, 2020).

$$LAI = \frac{\ln\left(\frac{0.69 - SAVI}{0.59}\right)}{0.91} \quad (3)$$

The constants used in equation 3 are assigned according to (ALLEN et al., 2002).

### 2.2.3 Planet© Images

Planet© is a California-based company that has manufactured and launched several nano-satellites such as "Doves" or PlanetScope that constitute the largest constellation of orbital imaging satellites on the earth. PlanetScope can image any part of the earth and provides data in four spectral bands between 454 and 860 nm with a 3-meter spatial resolution. Atmospheric corrections of the PlanetScope images were carried out at the stage of preliminary processing and correction factors for each spectral band are present in the metadata of each scene.

Planet platform (https://www.planet.com/products/platform) is a fully automated cloud-based platform for downloading, processing, and managing images online. The images acquired by the platform were needed to run the $CO_2$Flux, EVI, and LAI models, where NDVI is based on red and NIR, and PRI is based on blue and green bands.

### 2.2.4 Gross primary production (GPP)

The MOD and MYD17A2H products related to gross primary production is a cumulative composite of GPP (kg C $m^{-2}$ $d^{-8}$) values based on the concept of the solar radiation-use efficiency by vegetation (ε). By this logic, primary production is linearly related to absorbed photosynthetically active radiation (APAR) (RUNNING et al., 1999; RUNNING; ZHAO, 2019). APAR can be calculated as the product of the incident photosynthetically active radiation (PAR) in the visible spectral range 0.4 μm - 0.7 μm, assumed as 45% of the total incident solar radiation, and the fraction of photosynthetically active radiation absorbed by the vegetation cover (FPAR) (HEINSCH, 2003).

One of the major challenges in using such models is to obtain the light-use efficiency $\varepsilon$ over a large area, due to its dependence on environmental factors and the vegetation itself. One solution is to relate $\varepsilon$ according to its maximum value ($\varepsilon_{max}$) plus the environmental contributions synthesized by the minimum air temperature ($T_{minscalar}$) and the water status of the vegetation ($VPD_{scalar}$ - water vapor pressure deficit) (FIELD; RANDERSON; MALMSTRÖM, 1995).

In this study, MODIS GPP (Gross Primary Productivity), version 6 was used with the 8-day average. Pixel values referring to digital numbers from MODIS images were converted into biophysical values from kg (kilogram) to g (gram) by multiplying 0.0001 and transformed to daily by dividing by 8 (8-day), at the end we have the transformed GPP measurement unit from kg C $m^{-2}$ $d^{-8}$ to g C $m^{-2}$ $day^{-1}$ (Equation 4).

$$GPP = \frac{GPP \cdot 0.0001}{8} \tag{4}$$

**2.2.5 $CO_2$ Model Data**

The $CO_2$Flux model was used (RAHMAN et al., 2001) to estimate the efficiency of the vegetation-related carbon sequestration process, which is the photosynthesis rate derived from photosynthetic processes. For this, the photochemical reflectance index (PRI) (Equation 5) was calculated (GAMON; SERRANO; SURFUS, 1997) using the green and blue spectral bands. The PRI is related to the amount of carotenoid pigments in leaves, which indicates the $CO_2$ storage rate (BARNES et al., 2017; DELLA-SILVA et al., 2022; RAHMAN et al., 2001).

$$PRI = \frac{\rho_{BLUE} - \rho_{GREEN}}{\rho_{BLUE} + \rho_{GREEN}} \tag{5}$$

where $\rho_{BLUE}$ is the blue spectral band reflectance and $\rho_{GREEN}$ is the green spectral band reflectance.

Since our goal was to use PRI as an efficiency factor, we derived a scaled value of PRI (sPRI) to represent an adjusted range of 0 to 1. Therefore, it is necessary to generate the sPRI (Equation 6) (MARTINS; BAPTISTA, 2013).

$$sPRI = \frac{PRI + 1}{2} \tag{6}$$

Hence, the $CO_2$Flux (µmol m$^{-2}$ s$^{-1}$) is the multiplied result of the NDVI and sPRI. There is a relationship where it may be possible to capture the carbon sequestration absorptions using the PRI index, which indicates the efficient use of light during photosynthesis, and the NDVI, which demonstrates the vigor of the photosynthetically active vegetation (RAHMAN et al., 2001). For more coherent estimates of $CO_2$Flux in Brazil, the fitting of flux data associated with the $CO_2$Flux model with direct measurement of $CO_2$ fluxes by Turbulent Vortex Covariance (Eddy Covariance) (GOULDEN et al., 1996) was applied. Santos, (2017) determined a coefficient of $R^2$ = 0, 8185 and the regression model y = -66.207x + 13.63 between the direct measurement of $CO_2$ fluxes and the $CO_2$Flux model, the best correlation is given in Equation (7).

$$CO_2Flux = 13.63 - \left(66.207 \cdot (NDVI \cdot sPRI)\right) \tag{7}$$

In this model, the linear and angular coefficients are presented as NDVI and PRI vegetation models and should be fitted according to environmental characteristics. The $CO_2$Flux model expressed in Equation (7) was fitted to Amazonian standards, where negative values (-) indicate net absorption of carbon (photosynthesis) by the surface and positive values (+) indicate loss of carbon to the atmosphere (respiration).

### 2.2.6 Assessing soil $CO_2$ emission, temperature, and moisture

For the assessments of soil $CO_2$ emission ($FCO_2$), we used the LI-COR portable system, model LI-8100 (LI-COR Bioscience, Nebraska, USA) (Figure 2a), which monitors the $CO_2$ concentration variations inside the soil respiration chamber (Figure 2b) by means of optical absorption spectroscopy in the infrared spectral region. The soil respiration chamber is a closed system with an internal volume of 854.2 cm$^3$ and a circular contact area of 83.7 $cm^2$ and is coupled over PVC collars that were previously inserted into the soil 24 hours before collection.


**Figure 2.** LI-COR model LI-8100 portable system (a) connected to the soil chamber (b), soil moisture sensor (c) and soil temperature sensor (d).

The *on-site* measurements were performed in a 100-meter transect with 20 sample points for each land use and land cover (LULC) (Figure 3), with seven collections comprising before sowing, during the phenological stage, and after soybean harvest (Table 1), carried out in the morning from 8 am to 10 am in each LULC. The spatial distribution of the *in situ* collection points were distributed every five meters, so that each point could be represented in a different pixel.


**Figure 3.** Locations of the land uses and land cover of the experiment. a) native forest; b) productive pasture; c) degraded pasture; d) high-yield potential soybean; e) low-yield potential soybean.

**Table 1.** Collection dates for each land use and land cover and soybean soil preparation, sowing, and harvesting periods.

| Collection date | Julian Day | Period |
|---|---|---|
| 09/26/2020 | 270 | Before soybean sowing |
| 10/08/2020 | 282 | During the soybean phenological stage |
| 11/05/2020 | 310 | During the soybean phenological stage |
| 11/26/2020 | 331 | During the soybean phenological stage |
| 01/21/2021 | 21 | During the soybean phenological stage |
| 03/06/2021 | 65 | During the soybean phenological stage |
| 03/24/2021 | 83 | After soybean harvesting |

The $FCO_2$ was evaluated at each point by a fit of the $CO_2$ air concentration inside the chamber as a function of a polynomial regression over time after its closure. The measurement mode for determining the soil $CO_2$ emission took 90 seconds at each sampling point, and the $CO_2$ concentration inside the chamber was determined every 2.5 seconds, approximately (SÁ et al., 2019).

The Soil temperature (Ts) was monitored using a Digital Spit-Type Thermometer (DELLT DT-625) (Figure 2d). It consists of a 20 cm rod inserted into the soil at 5 cm from where the PVC collars were previously installed for the evaluation of soil $CO_2$ emission. Similarly, the Soil Moisture (Ms) was recorded using a TDR – Time Domain Reflectometry (Hydrosense TM, Campbell Scientific, Australia) (Figure 2c), consisting of a probe with two 12-cm rods inserted inside the soil, perpendicular to the surface at 5 cm from the PVC collars. The soil moisture value is derived from the time it takes for an electric current to travel the distance of 32 mm from one rod to the other. The soil temperature and moisture evaluations were performed concurrently with the soil $CO_2$ emission evaluations.

### 2.2.7 Statistical analysis

Data were submitted to analysis of variance (ANOVA) for comparison of land use and land cover (LULC) at each evaluation date. Means were grouped by the Scott-Knott test at 5% probability. Subsequently, to verify the interrelationship between the variables and LULC of each experiment, data were analyzed by principal component analysis (PCA), and a biplot was generated with the first two components due to the straightforward interpretation of these results. In this biplot, confidence ellipses were constructed for each LULC evaluated. Additionally, Pearson's correlation was applied to verify the relationship between the studied variables, and then a plot was generated to analyze the results. All analyses were performed on the R 3.6.3 (R CORE TEAM, 2022) software using the packages "FactoMineR" (LÊ; JOSSE; HUSSON, 2008), "factoextra" (KASSAMBARA; MUNDT, 2020), "ExpDes.pt" (FERREIRA; CAVALCANTI; NOGUEIRA, 2021) and "GGally" (SCHLOERKE et al., 2021).

## 2.3 RESULTS

Analysis of variance (ANOVA) was the statistical test used to determine the difference between the means of land use and land cover and observed days. The analysis of variance revealed significance level ($p < 0.01$) for the variables atmospheric ($FCO_2$ and $CO_2$Flux), vegetative (LAI, EVI and GPP), and physical (Ms) variables. The physical variable Ts differed from the others by presenting significance at 5% probability level ($p < 0.05$). On the other hand, all variables analyzed showed the same significance level ($p < 0.01$) among the different LULC (FN, PB, PD, SA and SB) and for the evaluations from sowing to soybean harvesting, besides a significant interaction between these effects (LULC and Date) for the variables analyzed (Table 2). Factor analysis was used to describe the variability among the independent and possibly correlated variables. The analysis showed that land use and land cover (LULC) and time series dates showed a maximum significant value for all variables atmospheric, vegetative, and physical as described in the Table 2. Therefore, the pattern of temporal variation of the variables differs depending on the soil cover on the days evaluated according to the significant F-test, rejecting the hypothesis of H0, and applying the test for comparison of means.

**Table 2.** Analysis of variance for the seven variables among the five land uses and land cover (LULC) for the dates.

| Source of variation† | DF | Mean Square | | | | | | |
|---|---|---|---|---|---|---|---|---|
| | | Ms | Ts | $FCO_2$ | $CO_2$Flux | LAI | EVI | GPP |
| Date | 6 | 1396.358** | 529.818* | 132.437** | 645.805** | 60.200** | 1.584** | 0.040686** |
| LULC | 4 | 59.345** | 514.757** | 44.044** | 961.383** | 71.224** | 1.254** | 0.005449** |
| LULC x Date | 24 | 50.474** | 185.559** | 25.581** | 142.735** | 12.318** | 0.386** | 0.002095** |
| Residual | 665 | 8.905 | 0.671 | 8.309 | 0.426 | 0.024 | 0.001 | 0.000002 |
| Mean | | 8.519 | 27.443 | 3.884 | 1.623 | 2.267 | 0.380 | 0.035 |

† Statistical significances of $p \leq 0.05$ and $p < 0.01$ are represented by * and **, respectively.

The mean soil moisture (Ms), regardless of the LULC and Julian days evaluated, was 8.52% (Table 2). The Ms presented significant differences throughout the days studied especially after November 5th, and the highest difference between the LULC is noted for March 6th. This differentiation was not observed for Julian days 270 (September 26th), 282 (October 08th) and 83 (March 24th) (Figure 4a). For the different LULC among the Julian days (lowercase letters) with SA (high-yield potential soybean), the highest Ms values was observed in January and March (Julian days 21 and 83) (Figure 4a), unlike SB (low-yield potential soybean) and PD (degraded pasture), which maintained higher Ms between November, January and March (Julian days 310, 21, 65, and 83). The highest Ms for FN (native forest) was recorded in March (Julian days 65 and 83), as well as for PB (productive pasture).

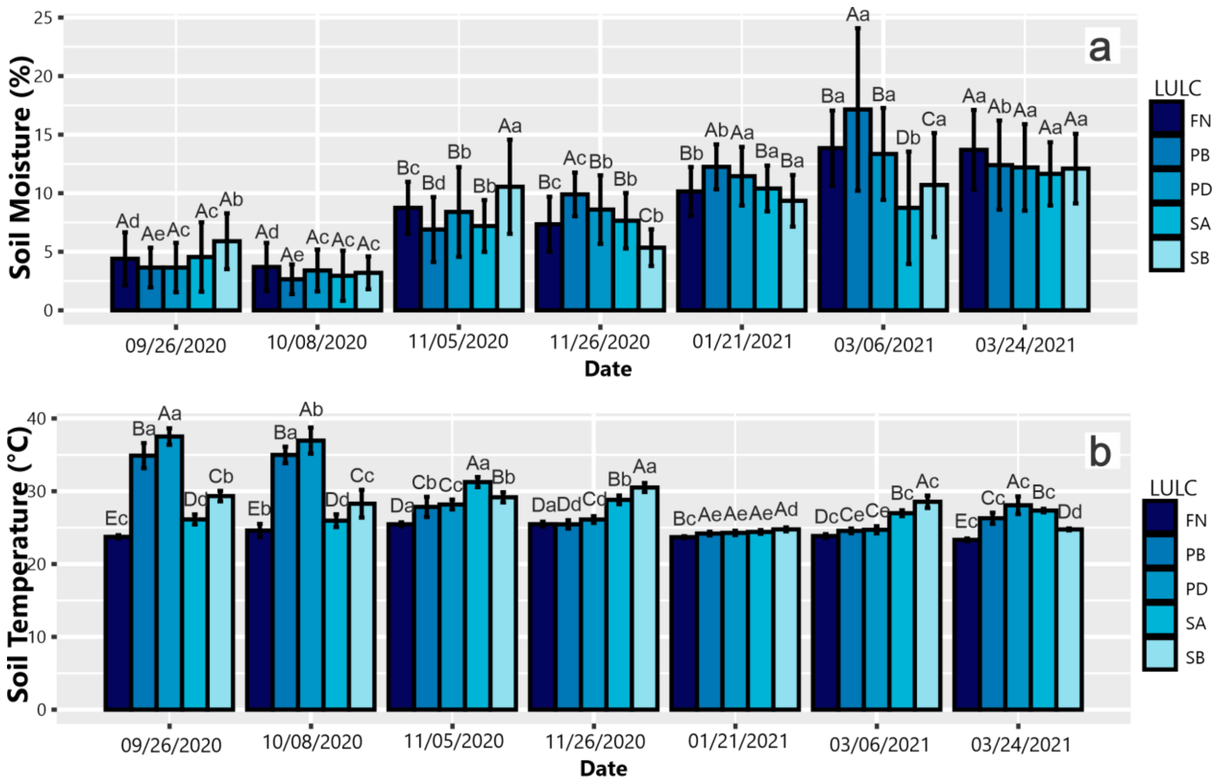


**Figure 4.** Grouping of means and the standard deviation of the variables a) Soil Moisture (Ms) and b) Soil Temperature (Ts) evaluated on different dates in the land uses and land cover (LULC) of native forest (FN), productive pasture (PB), degraded pasture (PD), high-yield soybean (SA) and low-yield soybean (SB). Means followed by uppercase letters do not differ in land use and land cover within each day and lowercase letters do not differ for the dates by Scott-Knott test at 5% probability.

For the periods evaluated (near sowing, during profiling, and post-harvest), the mean Soil Temperature (Ts) obtained in the LULC was 27.44 °C. In Ts there were differences between the days observed for all types of LULC (Figure 4b). In September, October and March (Julian day 270, 282 and 83), the Ts were higher for the PD soil and lower for FN. SA obtained the highest records on Julian day 310 (05/November) relative to FN, PB, PD and SB, and SB on 331 and 65 (26/November and 06/March) relative to FN, PB, PD and SA. For Julian day 21 (21/January), the lowest Ts record was observed for FN, while there was no difference among the other LULC. This means that Ts were high for the other environments.

When evaluating the Ts of each LULC within the observed days, FN recorded higher Ts on Julian days 310 and 331 (November 05$^{th}$ and November 26$^{th}$), unlike PB, which was on Julian days 270 and 282 (September 26$^{th}$ and October 08$^{th}$). The PD, SA, and SB recorded only a single day of high Ts (Julian days 270, 310, and 331, respectively).

Figure 5 shows the grouping of Ms and Ts for the different days and LULC studied. The mean soil moisture was significantly higher for Julian days 65 and 83 (Figure 5), with no difference between the LULC regardless of the days observed, but in the overall mean, the highest moisture was obtained for PB (Figure 5).

The lowest mean Ts were recorded from Julian day 21 onwards, corresponding with the highest mean humidity recorded. On the other hand, the highest mean Ts (30.3 °C and 30.2 °C) were on Julian days 270 and 282, which is probably related to the end of the dry season and beginning of the rainy season, as well as the lowest mean Ms.

The highest Ts was for PD (29.4 °C), followed by PB and SB (28.3 °C and 27.9 °C, respectively). The FN soil had the lowest temperature (24.3 °C), allowing it to maintain good Ms.

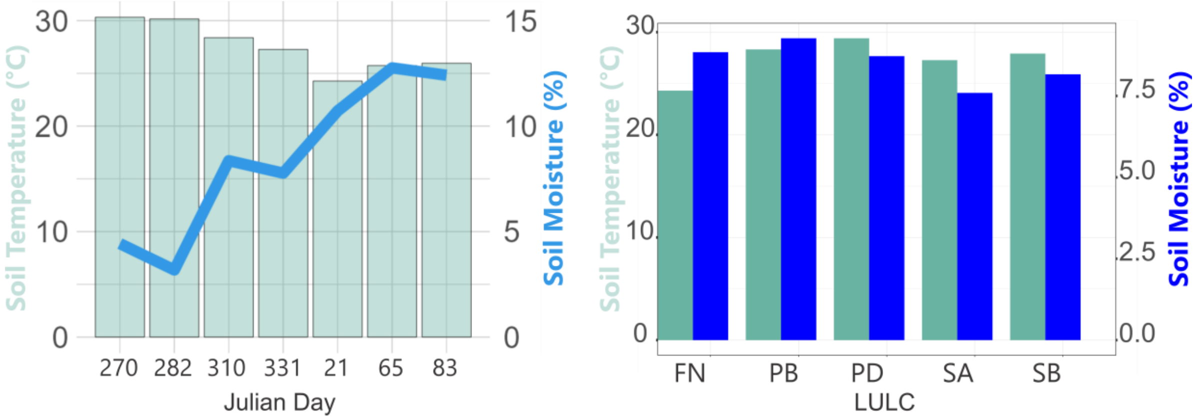


**Figure 5.** Grouping of means and the standard deviation of the variable Soil Temperature (Ts) and Soil Moisture (Ms) evaluated on different dates in the land uses and land cover (LULC) of native forest (FN), productive pasture (PB), degraded pasture (PD), high-yield soybean (SA) and low-yield soybean (SB). Means followed by uppercase letters do not differ in land use and land cover within each day and lowercase letters do not differ for the dates by Scott-Knott test at 5% probability.

Regarding the variable $FCO_2$, the mean value recorded during the time series considering all treatments was 3.88 µmol $m^{-2}$ $s^{-1}$ (Table 2). On Julian days 270 (September $26^{th}$) and 310 (November $05^{th}$), $FCO_2$ was highest for FN, on Julian days 282 (October $08^{th}$) and 331 (November $26^{th}$) for FN, PB and PD had the highest values of $FCO_2$ and lowest for SA and SB. PD, SA and SB treatments recorded the highest $FCO_2$ on Julian day 21 (January $21^{st}$) and the lowest for FN and PB. As for Julian days 65 (March $06^{th}$) and 83 (March $24^{th}$), FN and SA and PB and SA, respectively, corroborated for higher $FCO_2$ emissions (Figure 4a).

When we analyze the LULC, the FN had the highest emissions recorded on Julian days 310 and 65, while for PB the highest emission days were recorded on four Julian days 310, 331, 65, and 83. In PD and SB, the highest emission was observed on Julian day 21, different from what was observed for SA, with the highest emissions on Julian days 21, 65 and 83 (Figure 4a).

In general, total soil $CO_2$ emission ($FCO_2$) over time was higher in the FN area and in the SA and SB land uses, a lower amount than the other environments when compared to the overall means. However, when compared statistically, there is no significant difference among LULC for $FCO_2$ emission under the conditions established in this study.

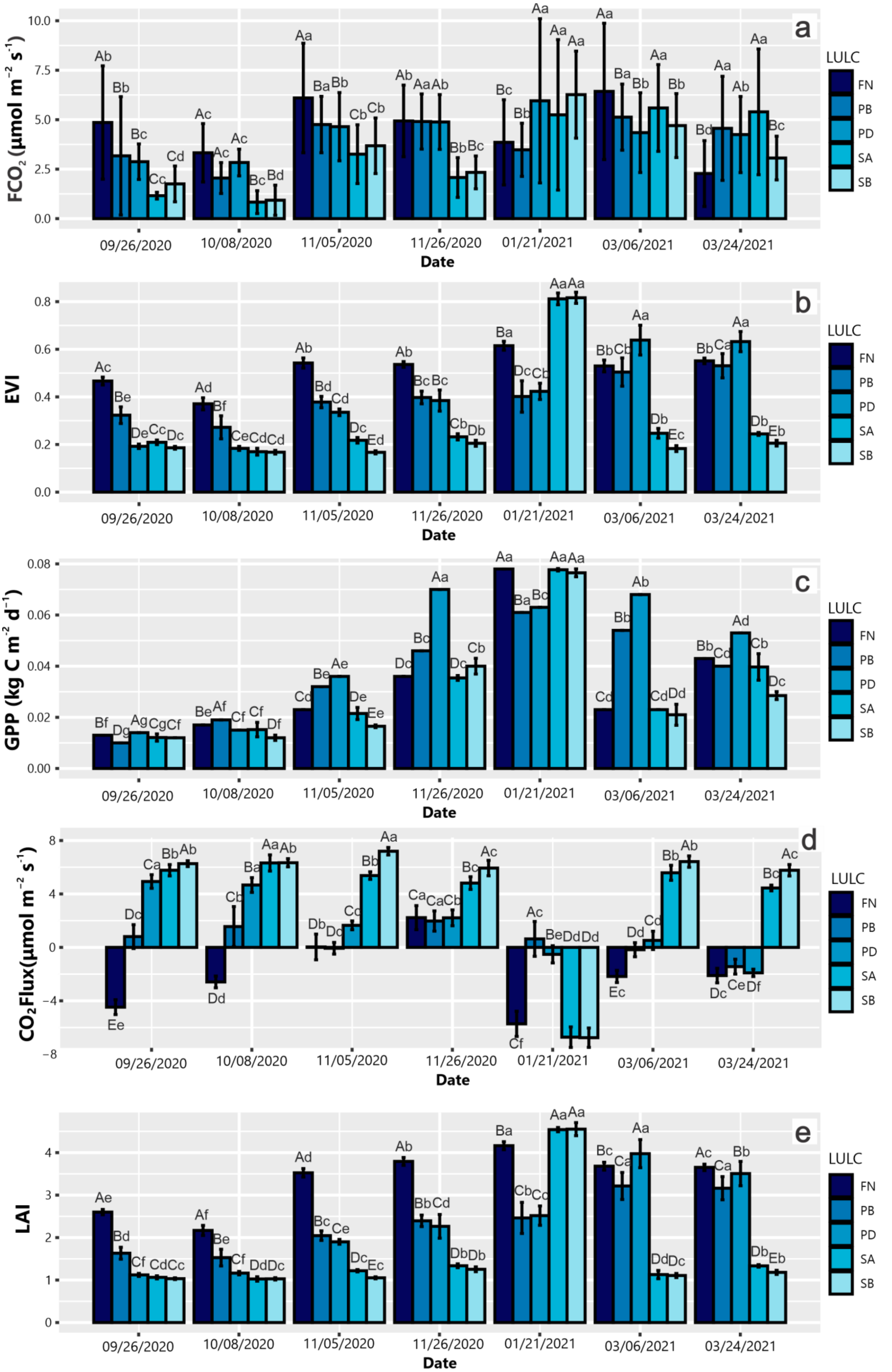
a
FCO2 (μmol m-2 s-1)
Date
09/26/2020
10/08/2020
11/05/2020
11/26/2020
01/21/2021
03/06/2021
03/24/2021
LULC
FN
PB
PD
SA
SB
b
EVI
c
GPP (kg C m-2 d-1)
d
CO2Flux(μmol m-2 s-1)
e
LAI

**Figure 6.** Grouping of means and the standard deviation of the variables a) $FCO_2$, b) EVI, c) GPP, d) $CO_2$Flux and e) LAI evaluated on different dates in the land uses and land cover (LULC) of native forest (FN), productive pasture (PB), degraded pasture (PD), high-yield soybean (SA) and low-yield soybean (SB). Means followed by uppercase letters do not differ in land use and land cover within each day and lowercase letters do not differ for the dates by Scott-Knott test at 5% probability.

The EVI data show a mean of 0.38, with the highest EVI recorded for FN (0.52). Subsequently, PB, PD, SA and SB showed an EVI of 0.40, 0.40, 0.31 and 0.28, respectively.

Analyzing the LULCs for the time series, the EVI index for FN was higher from Julian days 270 to 331 compared to the other LULCs (Figure 6b). There was variation among the LULCs from Julian day 21, in which SA and SB obtained higher EVI in this period, while for PD, the EVI was higher on Julian days 65 and 83. When observed the days within the LULCs, FN, SA and SB had highest EVI on Julian day 21, contrary to PD (Julian days 65 and 83) and PB (Julian day 83).

The mean GPP was 0.036, with the LULC averaging from 0.029 to 0.046 (SB and PD). In FN, PB and SB, the GPP was 0.033, 0.037 and 0.032, respectively. GPP values were higher for PD on five Julian days of the seven evaluated compared to FN, PB, SA and SB (Figure 6c). The other LULCs had higher averages on Julian day 282 (PB) and 21 (FN, SA and SB). When relating each LULC to the observed days, it can be seen that Julian day 21 had the highest mean GPP for FN, PB, SA, and SB, while PD had the highest mean GPP on Julian day 331.

The variability of $CO_2$Flux for each LULC is presented in Figure 6d. The mean $CO_2$Flux for all LULCs in the time series was 1.62 μmol $m^{-2}$ $s^{-1}$. SB had the highest $CO_2$Flux storage on six of the seven Julian days, with the highest mean recorded on Julian day 310, corresponding to November. However, on Julian day 282, the SB did not differ from the SA, i.e., both showed equal means for $CO_2$Flux. The PB has the highest $CO_2$Flux storage only on Julian day 21.

Observing the different LULC for the seven days, the FN and PB recorded $CO_2$Flux in larger amounts on Julian day 331, different from PD, which showed higher means on Julian days 270 and 282. For SA and SB, the highest values were on Julian days 282 and 310, respectively. Overall, FN and PB were the LULCs with the lowest $CO_2$Flux values, with the lowest concentration occurring in January.

The results found through the LAI in the different LULCs show a variation from 0.90 to 4.70, with an mean of 2.27. The FN stands out with the highest mean in the different days observed (3.37) (Figure 6e). Only on Julian days 21 and 65, the means were higher for SA, SB and PD. When we analyze the LAI for each LULC, there is a significant difference between the days observed, with the highest values verified on days 21 (FN, SA and SB), 65 (PB and PD) and 83 (PB).

Through PCA, we observed that the ordering of variables in each principal component (PC) of the axes was influenced by the degree of vegetation cover and moisture of land uses and land cover (Figure 7). Thus, PC1 contributed more to the variability of variables related to photosynthesis and LULC. Therefore, in PC2, the climatic factors affecting LULC influenced the variables humidity and temperature.

The first two PCs accumulated at least 67.3% of the total data variance across all dates (Figure 7). The first principal component (PC1) accounted for at least 50.4% of the total variance, while the second principal component (PC2) accounted for at least 16.1% of the total variance across collection days.

For Julian day 270 (September 26$^{th}$), FN and PB were associated with the variables $FCO_2$, LAI and EVI. The other LULC were close to the variables GPP, $CO_2$Flux, Ms and ST with emphasis on soybean with high productive potential, which showed great variability among the points collected. The variable $CO_2$Flux had the highest positive contribution, and the variables EVI and LAI had the highest negative contribution for PC1. On Julian day 282 (October 8th), FN and PB were associated with the variables EVI, GPP, $FCO_2$ and Ms. The other LULC were close to the variables ST and $CO_2$Flux with emphasis on native forest (FN) and high yield potential soybean (SA), which showed great variability among the points collected. $CO_2$Flux had the highest positive contribution, and the EVI had the highest negative contribution for PC1.

For Julian day 310 (November 5th), the FN, PB and PD were associated with the variables $FCO_2$, LAI, EVI and GPP. The other LULC were close to the variables $CO_2$Flux, Ms and ST with emphasis on the low-yield potential soybean (SB), which showed great variability between the points collected. The $CO_2$Flux had the highest positive contribution, and the variables EVI and LAI the highest negative contribution for PC1. On Julian day 331 (November 26th), FN, PB and PD were associated with the variables $FCO_2$, GPP, Ms, EVI and LAI. The other LULC were close to the variables $CO_2$Flux and Ts with emphasis on SA, which showed high variability among the points collected. The EVI and LAI had the highest positive contribution, and the $CO_2$Flux and Ts variables had the highest negative contribution for PC1.

For Julian day 21 (January 21st), the PB and PD were associated with the variables $CO_2$Flux and Ms. The other LULC were close to the variables GPP, LAI, EVI, $FCO_2$ and Ts with emphasis on the degraded pasture (PD), which showed high variability among the points collected. The $CO_2$Flux had the highest positive contribution and the variables GPP, EVI and LAI the highest negative contribution for PC1. On Julian day 65 (March 6th), SA and SB were associated with the variables $CO_2$Flux and Ts. The other LULC were close to the variables $FCO_2$, GPP, Ms, EVI and LAI with emphasis on the native forest, which showed great variability among the points collected. The $CO_2$Flux and Ts had the highest positive contribution and the variables EVI and LAI the highest negative contribution for PC1. On Julian day 83 (March 24th), FN, PB and PD were associated with the variables LAI, EVI, GPP, Ts, and Ms. The other LULC were close to the variables $CO_2$Flux and $FCO_2$ with emphasis on SA, which showed high variability among the points collected. The variable EVI and LAI had the highest positive contribution and the $CO_2$Flux the highest negative contribution for PC1.

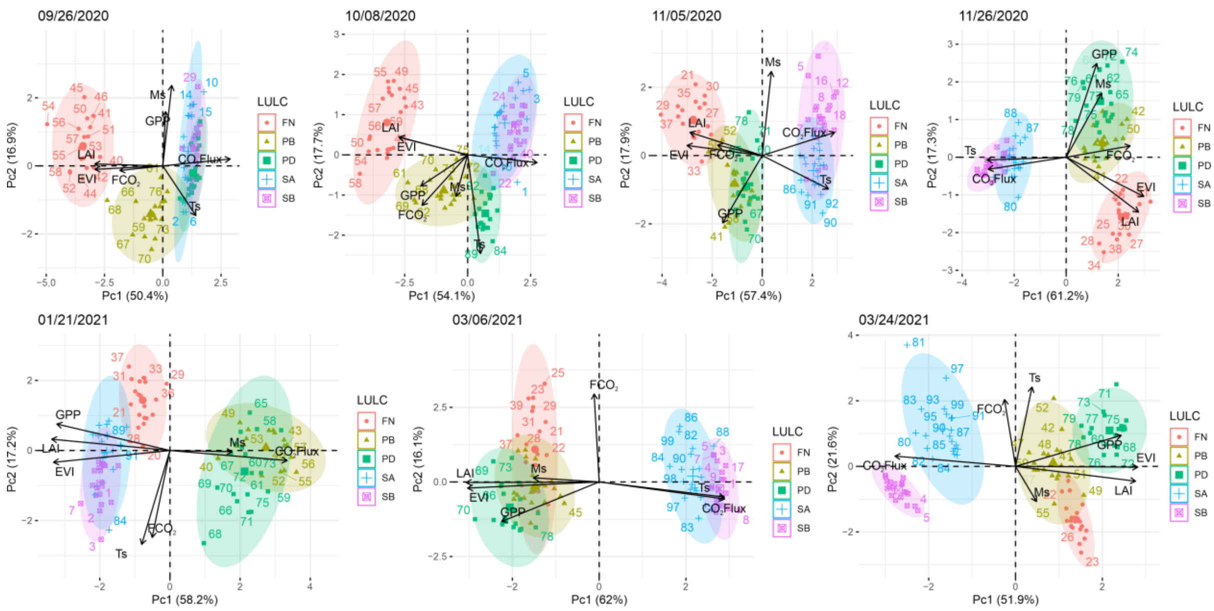


**Figure 7.** Principal component analysis for the variables $FCO_2$, Ms, Ts, $CO_2$Flux, EVI, LAI and GPP evaluated at different dates in the land uses and land cover (LULC) of native forest (FN), productive pasture (PB), degraded pasture (PD), high-yield soybean (SA) and low-yield soybean (SB).

For Ms, there was low-magnitude correlations between the variables GPP (0.477), LAI (0.414), EVI (0.381), $FCO_2$ (0.280), Ts (-0.444), and $CO_2$Flux (-0.243) (Figure 8). The LULCs showed positive correlations between these variables, except for Ts and $CO_2$Flux variables. The boxplot shows that Ms values are clustered in the first and the second quartiles for all LULC, as shown in the histogram and density plot of the continuous variables. The correlation between Ts and GPP (-0.491), LAI (-0.561), EVI (-0.533), Ms (-0.444) and $FCO_2$ (-0.240) were negative, while for $CO_2$Flux (0.459) were positive, but of low magnitude. LULC showed negative correlations between these variables, except for moisture and $CO_2$Flux variables. The boxplot shows low Ts values for FN, while PD and PB have the highest values, which clustered in the third quartile, as shown in the histogram and density plot of the continuous variables.

There were low magnitude correlations between $FCO_2$ and GPP (0.208), LAI (0.354), EVI (0.363) Ms (0.280), Ts (-0.240), and $CO_2$Flux (-0.314). The LULC showed negative correlations between these variables, except for the CO2Flux variable. From the boxplot, it can be seen that the $FCO_2$ values were lowest for SA and SB and highest for FN. There were low magnitude correlations between $CO_2$Flux and GPP (-0.582), LAI (-0.857), EVI (-0.890), $FCO_2$ (-0.314), Ms (-0.243), and Ts (0.459). From the boxplot, it can be seen that the $CO_2$Flux values were lowest for FN and highest for SA and SB.

There were positive correlations between EVI and GPP (0.715), LAI (0.979), $FCO_2$ (0.363) and Ms (0.381) and negative correlations between EVI and $CO_2$Flux (-0.890) and Ts (-0.533), with high magnitude for GPP, LAI and $CO_2$Flux. LULC showed positive correlations between these variables, except for Ts and $CO_2$Flux. From the boxplot, it can be seen that EVI values were lower for SA and SB and higher for FN, as shown in the histogram and density plot of the continuous variables.

The overall correlation between LAI and GPP was positive and significant (0.70). All LULC showed positive correlations between these variables. The boxplot shows that the LAI values were lower for SA and SB and higher for FN, as evidenced in the histogram and density plot of the continuous variables.

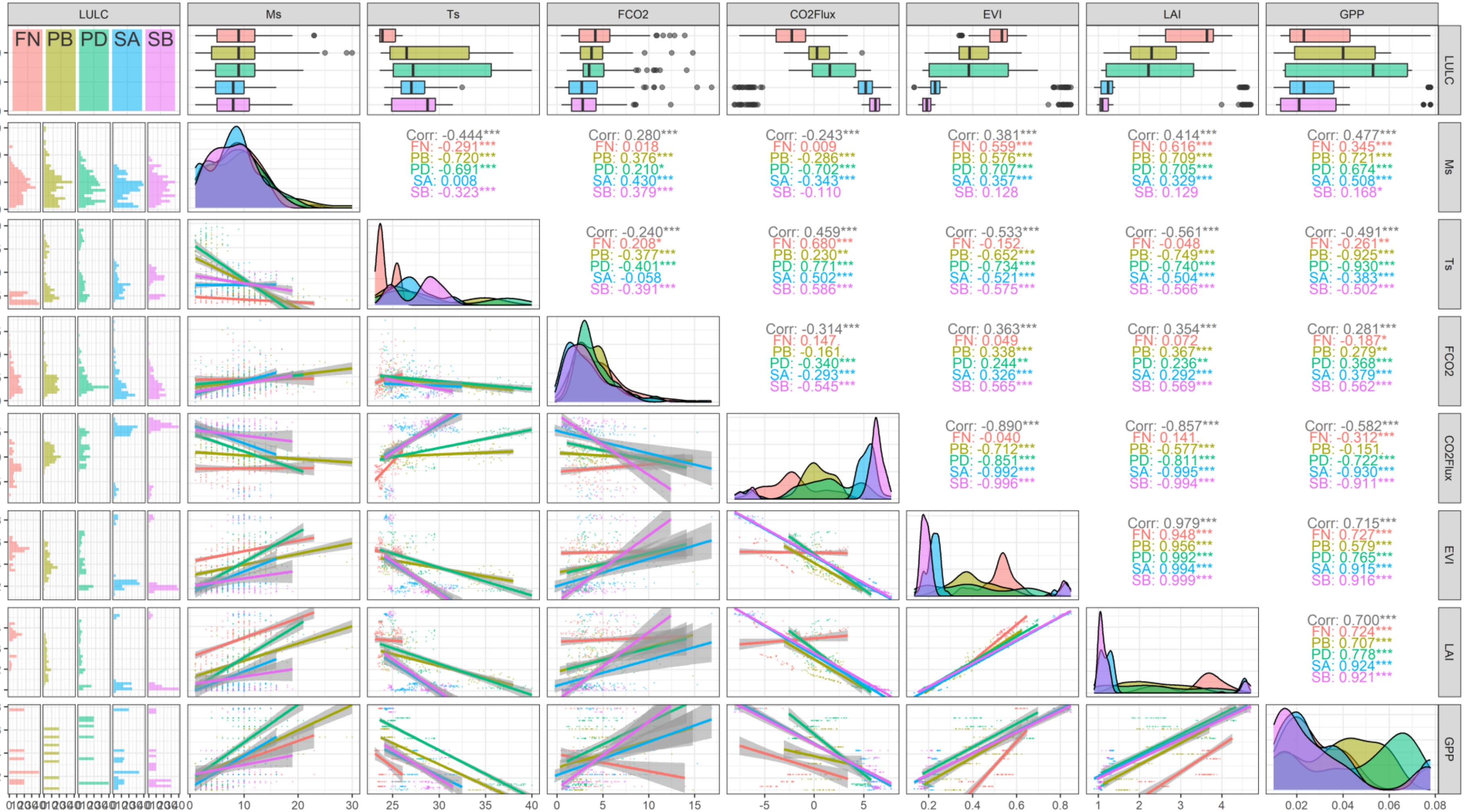


**Figure 8.** Pearson correlations for the variables $FCO_2$, Ms, Ts, $CO_2$Flux, EVI, LAI and GPP evaluated at different dates in the land uses and land cover (LULC) of native forest (FN), productive pasture (PB), degraded pasture (PD), high-yield soybean (SA) and low-yield soybean (SB).

## 2.4 DISCUSSION

Climate change worldwide is caused by anthropogenic actions such as land occupation (HE; ZHANG, 2022; HOUGHTON et al., 2012), ecosystem degradation (TCHOBSALA et al., 2021), urbanization and exploitation of natural resources (DANISH; ULUCAK; KHAN, 2020), which are enhanced by the growing world population (FRONTISTIS, 2021). This entire scenario goes through the carbon cycle dynamics, where solutions for reducing the concentrations of this element in the atmosphere are required.

The mean values of Soil Moisture (Ms) and Soil Temperature (Ts) were higher and lower, respectively, in the native forest than in the other land use and land cover (Figure 8). This fact was already expected since the native forest provides a higher volume of vegetation cover. No difference was found for the Ms variable between the first Julian days 270 and 282 (September and October), as well as the last Julian day 83 (March), which may be related to the previous dry period and the end of the rainy period. However, it can be seen a greater influence of the dry-rainy transition period on the degraded pasture area since the mean temperatures were higher than the other environments (Figure 8).

In our study, September and October (Julian days 270 and 282) had the lowest $FCO_2$ emission, recording low average humidity and high soil temperatures. Therefore, we found that the variable soil $CO_2$ emission ($FCO_2$) showed no difference for the LULCs, but did show a difference between the days observed. Throughout the days, there was a tendency to increase the $FCO_2$. This can be explained after the rainfall events during the observed days, increasing the $FCO_2$ flux. Soil temperature and soil moisture are influencing factors in the $CO_2$ (carbon dioxide) emission variability in soils and can be altered after a rainfall (PANOSSO et al., 2007). This occurs because the water drains into the soil and causes the $FCO_2$ found in the pores to escape, making a barrier that prevents the $FCO_2$ emission (ZANCHI et al., 2003).

Taking into account that the higher the values obtained for the Leaf Area Index (LAI), the better the ability of the vegetation to develop by absorbing sunlight and, therefore, the higher the $CO_2$ storage capacity, we highlight that the native forest (FN) was the environment with the highest LAI and, in a general way, the environment with the highest $CO_2$ concentration, regardless of the days observed. Castro Pereira et al. (2020) found that areas with high LAI values are sites where much of the vegetation is developing, absorbing a higher flux of energy radiation and a higher amount of carbon in the biomass.

Thus, the $CO_2$flux index ($CO_2$ flux) allows the estimation of carbon absorbed by the vegetation (DELLA-SILVA et al., 2022). Vegetated areas have high $CO_2$flux because the plants retain more carbon dioxide (TEOBALDO; BAPTISTA, 2016), allowing better development conditions for the vegetation. Thus, we verified in this study a difference in the $CO_2$ flux values between PB (productive pasture), SA (high-yield potential soybean) and SB (low-yield potential soybean). The months with the highest $CO_2$flux values, regardless the LULC, were recorded in October and November (Julian days 282 and 310), a transition period from dry to rainy season.

The interaction between land cover and atmosphere is weighted by the type of land cover, that is, its litter stock and organic matter. Principal component analysis allowed relating all LULCs and variables simultaneously (Figure 7). Overall, all LULCs during the time series were allocated to different quadrants, except native forest, which remained almost always in the same quadrant due to its high correlation with LAI and EVI. Similar results were reported by Jardim et al. (2022), who observed similarity in the occurrence of increased vegetative vigor in the forest canopy. According to these authors, such findings can be explained, in general, by climatic conditions, where the rainfall rate directly influences the vegetation cover in the area.

The dynamics of the variables shown in Figure 7 are strongly influenced by the seasonality of rainfall and, hence by soil moisture conditions, which is a determining factor for the seasonality of leaf cover for each land use and land cover. Over the tim-series, we observed a marked positive trend in $CO_2$Flux for the areas where the soil was exposed or in vegetation senescence. This positive trend is due to the vegetation's efficiency of the carbon sequestration process, as already evidenced in previous studies (DELLA-SILVA et al., 2022; ROSSI et al., 2022). Rainfall and soil moisture dynamics in the study area affect phenology, stomatal conductance seasonality, and photosynthesis (MARQUES et al., 2020; MENDES et al., 2017). It is essential to point out that photosynthesis decreases with the closing of the stomas due to the reduction of $CO_2$ absorption in the dry season (BAI et al., 2017; PINHO-PESSOA et al., 2018; ZHANG et al., 2014), which leads to leaf loss (senescence) under drought stress conditions. Besides the senescence of leaf tissue, there is a severe reduction of remaining leaves due to soil moisture deficits or soybean defoliation, resulting in lower EVI and LAI values. These findings indicate different plant-environment interactions affecting the variables in the study areas.

The variables Ms and Ts are important for the $CO_2$ emission process during the time-series, directly influencing the decomposition of organic matter and the microbial and root activities (SILVA-OLAYA et al., 2013a). Ms and Ts are always on opposite axes of the PCA (Figure 7) and are, therefore, negatively correlated (Figure 8). On the other hand, no high-magnitude correlation was found between Ts and Ms with $FCO_2$, $CO_2$Flux, and the LULCs, possibly due to the low variation over the time-series period (MOITINHO et al., 2021). The effect of Ms may partially hide the effects of Ts on $FCO_2$, as these are interdependent variables and commonly change simultaneously (DING et al., 2010).

The contribution of soil $FCO_2$ obtained during the experimental period will increase, due to the increased activity of the soil microbiota (CHEN et al., 2014; STRUECKER; DYCKMANS; JOERGENSEN, 2017) and *priming* effect (SHAHBAZ et al., 2018). The concentration of $FCO_2$ values for the LULC are different. For the native forest, the high values come from the higher amount of roots (NICHOLS et al., 2016) and the intense rotation of soil organic matter (CHEN et al., 2016; CRAIG et al., 2022). The increased soil $FCO_2$ occurs as a function of carbon inputs into the soil, either from roots of cover crops, autotrophic respiration (FERREIRA et al., 2018; HU et al., 2018; WENCHEN et al., 2017) or by the decomposition of residues deposited on the soil surface. Aerobic conditions favor the decomposition of soil organic carbon (JAIN et al., 2016).

## 2.5 CONCLUSIONS

The link among land use and land cover to soil $CO_2$ emissions were high in our assessment, and closely related to biotic pool of carbon. In descending order, in the native forest, degraded pasture, productive pasture, high-yield potential soybean, and low-yield potential soybean areas are listed in order of greatest $FCO_2$ value, which means that these values may have been affected by the increased stock of soil organic matter and roots within the chamber.

The positive values of $CO_2$ flux model suggest carbon loss towards atmosphere due to plant respiration in the soybean areas and lower in the native forest area, even in a landscape with abrupt changes of phytophysiognomy, i.e., land use and land cover. Thus, areas with large forest areas had lower concentrations of carbon dioxide, mitigating climate change. Furthermore, future works comparing the variables considered in our study for other landscapes may contribute to the carbon dynamics comprehension.

# CHAPTER 3 – RELATION BETWEEN SOIL RESPIRATION AND MULTIPLE VARIABLES ON EUCALYPTUS SPECIES CROP IN SOUTHWESTERN BRAZILIAN CERRADO

**ABSTRACT –** Vegetation indices (VIs) are spectral models that allow the measurement of chlorophyll content, crop health, predict dry biomass, allowing a priori decision making. An important factor in planted areas is the soil $CO_2$ emission, also known as soil respiration, which is the result of the decay of labile organic matter and root respiration and is related to species, temperature, and soil moisture. This study aims to verify if soil carbon dioxide ($CO_2$) flux ($FCO_2$) and VIs obtained via airborne remote sensor over a eucalyptus species area (*E*. *camaldulensis*, *E*. *uroplylla*, *E*. *saligna*, *E*. *grandis*, *E*. *urograndis* and *Corymbria citriodora*). A multispectral imagery based the VIs estimation (green, red-edge and near infrared) from the Parrot Sequoia sensor, and on the same day $FCO_2$, soil moisture and temperature were collected. The six species of eucalyptus were randomly arranged in blocks with four repetitions and each block repetition divided into four zones, totaling 96 samples that were compared by statistical metrics to the data estimated by the. Soil moisture has a negative and significant correlation compared to $FCO_2$ ($p < 0.05$), proved to be one of the main factors that controls soil respiration. The vegetation indices NDRE (Normalized Difference Red-Edge Index), NDVI (Normalized Difference Vegetation Index), SAVI (Soil-Adjusted Vegetation Index) and MSAVI (Modified Soil Adjusted Vegetation Index) showed higher negative correlation to $FCO_2$, for *E*. *camaldulensis*, *E*. *saligna* and *E*. *uroplylla* species. Multivariate Analysis of Variance showed significance ($p < 0.01$) for the species factor, which indicates there are differences when considering all variables simultaneously. Results achieved in this study allow us to differentiate $FCO_2$ among eucalyptus species using sensors attached to remotely piloted aircraft. This relation relies on the contribution of roots, soil organic matter, plant residues, canopy spectral response and the chlorophyll content of eucalyptus species.

**Keywords:** Carbon Dioxide; Remote Sensor; Sustainability

## 3.1 INTRODUCTION

The increasing demand for timber over the last few years has led to land use for the rapid growth of tree crops. (VIERA; RODRÍGUEZ-SOALLEIRO, 2019). In Brazil, the total forestry area is about 9.5 million of hectares (ha), of which 76.9% are eucalyptus (*Eucalyptus* spp.) cash crops (IBGE, 2022). This genus is distinguished for cultivars availability adapted to the different Brazilian biomes and edaphoclimatic conditions (COSTA; CAMPANHA; GONTIJO NETO, 2022). Eucalyptus monoculture fields are distributed over tropics and subtropics, notably in Brazil (BOOTH, 2013). Mato Grosso do Sul state has been the eucalyptus expansion head, presenting a significant increase of cellulose production in the last five years, making this state as the leading exporter in the first four months of 2020 (MACHADO; RAYMUNDO, 2021).

According to La Scala et al. (2012), eucalyptus has the potential to stock atmospheric carbon as aboveground biomass and in the soil, mostly when combined with pasture and agricultural land cover. Thus, forest crops plays an important role on global carbon cycle, especially on greenhouse effect reduction as well as stocking atmospheric $CO_2$ (DU et al., 2015). The monitoring of $CO_2$ amount emitted from soil over forest areas may dispose important data for cultivation, in view of forest management and taking the human action affects the carbon emission, as well as climatic variation, since soil had the second biggest $CO_2$ efflux source ($FCO_2$) (DARENOVA; ČATER, 2020). Drake et al. (2018) suggests that soil $FCO_2$ on eucalyptus crops are affected by environmental factors, such as soil temperature, water content and precipitation variations.

Throughout the carbon cycle, $CO_2$ is based on plant (autotrophic) and microbial respiration (heterotrophic). Soil respiration is the sum of autotrophic respiration below the soil surface, where plant roots are the main responsible for it, and heterotrophic respiration of microorganisms during the decomposition of organic matter (GUTIÉRREZ DEL ARROYO; WOOD, 2021; MA et al., 2019; ZENG et al., 2016).

The challenges of forest management are related to reliable, accurate, and cost-effective methods for properly dating forest dynamics, seeking the growing carbon market (e.g., reducing emissions from deforestation and forest degradation) determines this need (SHI et al., 2022). In this sense, mechanisms generated by remote sensing may assist the carbon dynamics comprehension, taking the role of greenhouse gases (GHGs) in the soil-atmosphere interface, through multispectral image analysis that enables in loco measurements, monitoring, mapping, and application of vegetation cover (HATFIELD et al., 2008; MARCELINO DO NASCIMENTO et al., 2022).

Considering the advancement on big data, geoprocessing, and informatics technologies (DE OLIVEIRA et al., 2021), significant changes have occurred in forestry activities management, as the use of remotely piloted aircrafts that use images for crop mapping, evaluation of cultivated areas, disease detection, and soil mapping (Zás et al., 2017). Thus, image analysis tools through spectral indices are presented as alternatives for further research and decision-making in a more objective way.

It can be stated that there is a relationship between the amount of cumulative $CO_2$ efflux ($FCO_2$) and the growth of eucalyptus trees, since these plants need the nutrients released into the soil after decomposition of the existing organic material (VERSINI et al., 2013). Vegetation indices are also related to several factors related to eucalyptus plants, such as the amount of water in the leaf (VILLACRÉS et al., 2021), provide information about the plant's leaf area index (HIRIGOYEN et al., 2022), and recognize different species by reflectance and growth (DE OLIVEIRA et al., 2021).

Given this, the hypothesis of this study was that eucalyptus species have differences in $FCO_2$ and spectral variables. This research objective is to evaluate the relation between soil carbon dioxide flux and multispectral indices of vegetation in a monoculture system of eucalyptus species.

## 3.2 MATERIAL AND METHODS

### 3.2.1 Study area

This study is based in the experimental field of eucalyptus crop at Universidade Federal de Mato Grosso do Sul, Chapadão do Sul campus. The municipality of Chapadão do Sul has an area 3,252.327 $km^2$ of area and an estimated population of 26,499 (IBGE, 2021) (Figure 1). According to Köppen, the region is classified as tropical monsoon climate (Am), with two well defined seasons, being the dry season from April to September and other wet season from October to March (ALVARES et al., 2013). The annual temperature varies from 13°C to 28°C and presents pluviometric precipitation varying from 750 to 1,850 mm (CUNHA; MAGALHÃES; CASTRO, 2013). The soil in this region is classified as dystrophic red oxisol (SANTOS et al., 2011).

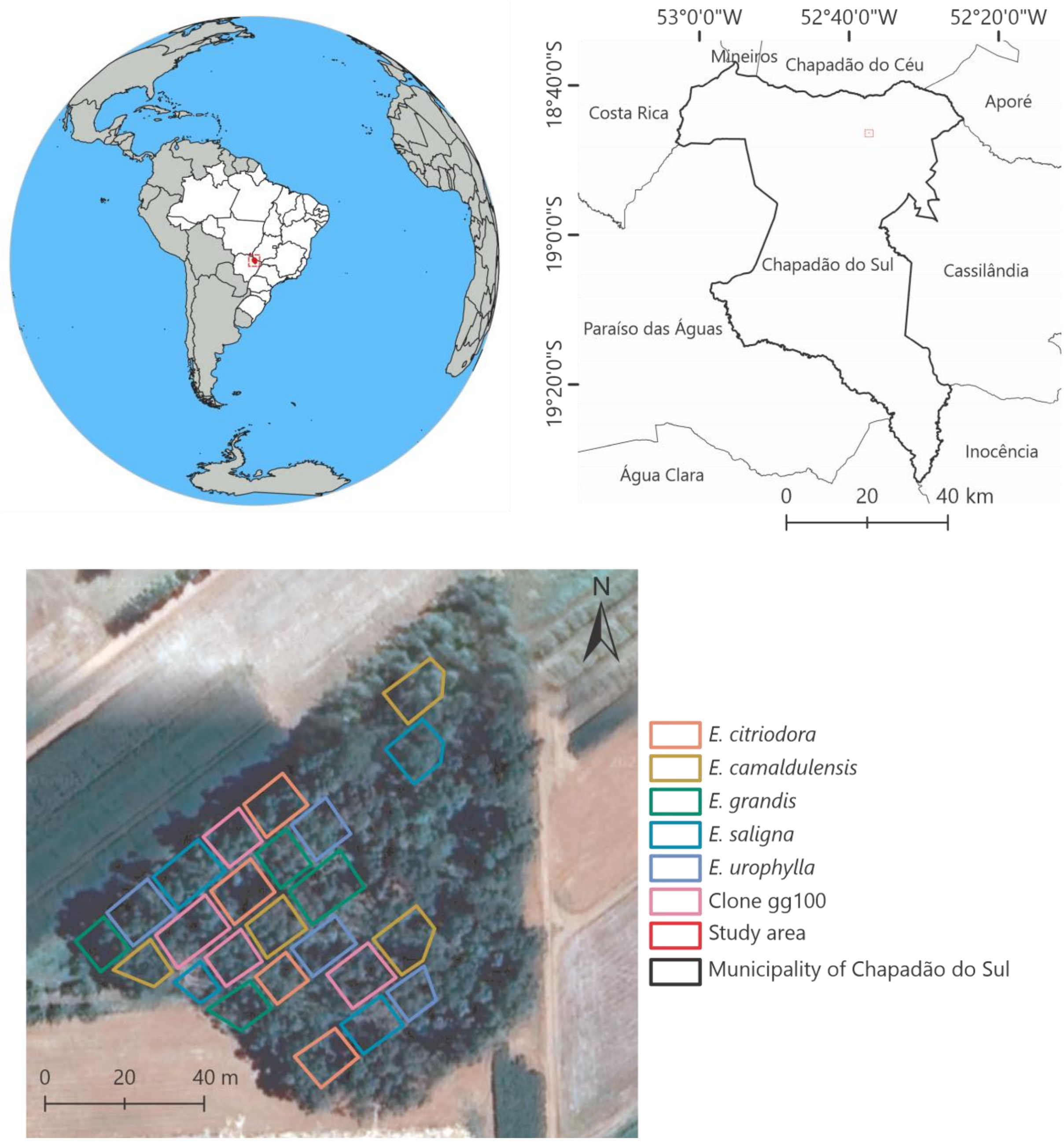


**Figure 1.** Study area at the Universidade Federal de Mato Grosso do Sul, Chapadão do Sul campus. An area composed by five eucalyptus species: *E. camaldulensis, E. uroplylla, E. saligna, E. grandis, E. urograndis* and *Corymbria citriodora*.

### 3.2.2 *In loco* performance of experiment

The experiment was conducted in January 2014, and every fertilization requirement was determined from the chemical analysis of the soil. The following results were found: pH ($CaCl_2$): 4.9; organic matter: 31.5 g $dm^{-3}$; phosphor: 13.6 m g $dm^{-3}$; hydrogen + aluminum (H + Al): 5.4; potassium: 0.29 $cmol_c$ $dm^{-3}$; calcium: 2.8 $cmol_c$ $dm^{-3}$; magnesium: 0.5 $cmol_c$ $dm^{-3}$; cation exchange capacity (CEC): 9.0 $cmol_c$ $dm^{-3}$; base saturation: 39.9%. The proportions of clay, sand and silt were 46%, 46%

and 8%, respectively. Crowning, weeding, ant control and herbicide application (glyphosate) were performed when necessary.

The experimental design consisted of randomized blocks with four replications, with 20 plants in each experimental plot. The treatments consisted of six species of eucalyptus: *E. camaldulensis*, *E. uroplylla*, *E. saligna*, *E. grandis e E. urograndis* e *Corymbria citriodora* (Figure 2).

**Figure 9.** Experimental local of the six eucalyptus species.

To evaluate the carbon dioxide ($CO_2$) efflux from the soil ($FCO_2$), we used the LI-COR portable system, model LI-8100 (Figure 3a), which monitors the $CO_2$ concentration variations inside the soil respiration chamber (Figure 3b) using optical absorption spectroscopy in the infrared spectral region. The soil breathing chamber is a closed system with internal volume of 854.2 $cm^3$ and circular contact area of 83.7 $cm^2$, being coupled over the PVC collars that were previously inserted into the soil 24 h before collection. This procedure results from the fact that the direct insertion of the chamber over the soil can cause disturbances causing additional $CO_2$ emissions from the soil.


**Figure 3.** LI-COR model LI-8100 portable system (a) connected to the soil chamber (b), soil moisture sensor (c) and soil temperature sensor (d).

*In loco* measurements were performed in each block of the repetitions of the eucalyptus species and each block of repetitions was divided into four zones, for installation of PVC in the centroid of each zone, thus having four measurements in each block, taken in the morning period, from 8 am to 10 am in each species of eucalyptus. The $FCO_2$ was evaluated at each point by an adjustment of the $CO_2$ concentration of the air inside the chamber as a function of a parabolic regression in the time after its closure. The measurement mode for the determination of soil CO2 emission took 90 seconds at each of the sample points and the $CO_2$ concentration inside the chamber was determined every 2.5 seconds, approximately (SÁ et al., 2019).

The soil temperature (Ts) was monitored using a Digital Spit-Type Thermometer (DELLT DT-625) (Figure 3d). It consists of a 20 cm rod that is inserted into the soil at 5 cm from the location where the PVC collars were previously installed for the evaluation of soil $CO_2$ emission. Similarly, the Soil Moisture (Ms) was recorded using a TDR – Time Domain Reflectometry (Hydrosense TM, Campbell Scientific, Australia) (Figure 3c) device, consisting of a probe with two 12 cm rods that were inserted inside the soil, perpendicular to the surface, also at 5 cm from the PVC collars. The soil moisture value is derived from the time it takes for an electric current to travel the distance of 32 mm from one rod to the other. The soil temperature and soil moisture assessments were carried out concomitantly with the assessments of soil $CO_2$ emission.

### 3.2.3 Multispectral airborne images acquisition and vegetation indices

The characteristics related to high-throughput phenotyping were obtained on the same dates. In addition, flights were conducted with remotely piloted fixed-wing aircraft Sensefly eBee RTK, with autonomous flight control (Figure 4). The eBee airborned the Parrot Sequoia multispectral sensor. This sensor is a multispectral camera for agricultural applications which uses the sunlight sensor and an additional 16 Mpx RGB camera for recognition. Yet, the sensor has horizontal field of view (HFOV) of 61.9°, vertical field of view (VFOV) of 48.5° and diagonal field of view (DFOV) of 73.7°. The multispectral images were acquired over the green (550 nm ± 40 nm), red (660 nm ± 40 nm), red-edge (735 nm ± 10 nm) and near-infrared (790 nm ± 40 nm) wavelengths (λ). The flight altitude over the study site was 100 m, involving a spatial resolution of 0.10 m.


**Figure 4.** Remotely Piloted Fixed-Wing Aircraft Sensefly eBee RTK loaded with Sensefly Sequoia sensor.

Overflights were performed with an image overlap of 80% lateral and 85% longitudinal, and the same area was imaged twice using perpendicular flight lines. The increase in overlap between images was necessary to obtain a greater number of scenes containing the same control points, enabling greater accuracy in the mosaicing of images using Pix4Dmapper software. This need occurs because of the height of the eucalyptus plants, which are at the mercy of stem oscillations due to the winds, because no matter how small their speed may be, they interfere in the mosaicing process. The overflights were performed near the zenith in order to minimize shadows on the trees, at 11 am local time, because the multispectral sensor is of the passive type, i.e., dependent on sunlight.

The data from these wavelengths (λ) allowed the calculation of the vegetation indices, as shown in Table 1. The aerial survey was carried out by using RTK (Real Time Kinematics) technology, which in turn allows the estimation of the camera position in making it possible to estimate the position of the camera at the instant of image collection with an accuracy of 2.5 cm. The images were mosaic and orthorectified in the computer program Pix4Dmapper. This reflectance calibration plate is individualized for each device. It contains information about reflectance ratios for each wavelength measured by the multispectral sensor. The field calibration procedure is carried out immediately before the flight is carried out. The procedure to take the reference photo for field calibration is carried out by e-Motion software. As the flight had a maximum duration of 15 minutes, there was no need to repeat the calibration after the field flight. The positional accuracy of the orthoimages was verified with ground control points (GCP), based on GNSS RTK Emilid Reach.

**Table 1.** Vegetation indices over Parrot Sequoia imagery.

| Index | Equation |
|---|---|
| ARVI2 (Atmospherically Resistant Vegetation Index 2) | $-0.18 + 1.17 \cdot \left(\frac{R\lambda_{nir} - R\lambda_{red}}{R\lambda_{nir} + R\lambda_{red}}\right)$ |
| ATSAVI (Ajusted Transformed soil-ajusted VI) | $1.22 \cdot \left(\frac{R\lambda_{nir} - 1.22 \cdot - R\lambda_{red} - 0.03}{1.22 \times R\lambda_{nir} + R\lambda_{red} - 0.03 + 0.08(1 + 1.22^2)}\right)$ |
| BWDRVI (Blue-wide dynamic range vegetation index) | $0.1 \times (R\lambda_{nir} + R\lambda_{red})$ |
| CCCI (Canopy Chlorophyll Content Index) | $\frac{(R\lambda_{nir} - R\lambda_{rededge})/(R\lambda_{nir} + R\lambda_{rededge})}{(R\lambda_{nir} - R\lambda_{red})/(R\lambda_{nir} + R\lambda_{red})}$ |
| CIgreen (Chlorophyll Index Green) | $(R\lambda_{nir} \ / \ R\lambda_{green}) - 1$ |
| CIrededge (Chlorophyll Index RedEdge) | $(R\lambda_{nir} \ / \ R\lambda_{rededge}) - 1$ |
| CVI (Chlorophyll Vegetation Index) | $R\lambda_{nir} \cdot (R\lambda_{red} \ / \ R\lambda_{green}{}^2)$ |
| DVI (Difference Vegetation Index) | $R\lambda_{nir} \ / \ R\lambda_{red}$ |
| EVEI2 (Enhanced Vegetation Index 2) | $2.5 \cdot (R\lambda_{nir} - R\lambda_{red}) / \ (R\lambda_{nir} + 2.4 \cdot R\lambda_{red} + 1)$ |
| GDVI (Difference NIR/Green Difference Vegetation Index) | $R\lambda_{nir} - \ R\lambda_{green}$ |
| GEMI (Global Environment Monitoring Index) | $2 \cdot (1 - 0.25 \cdot 2) - ((R\lambda_{red} - 0.125) \ / \ (1 - R\lambda_{red}))$ |
| GNDVI (Green Normalized Difference Vegetation Index) | $(R\lambda_{nir} - R\lambda_{green}) \ / \ (R\lambda_{nir} + R\lambda_{green})$ |
| GRNDVI (Green-Red NDVI) | $(R\lambda_{nir} - (R\lambda_{green} + R\lambda_{red})) \ / \ (R\lambda_{nir} + (R\lambda_{green} + R\lambda_{red}))$ |

| | |
|---|---|
| GRVI (Green-Red Vegetation Index) | $(R\lambda_{green} - R\lambda_{red}) \,/\, (R\lambda_{green} + R\lambda_{red})$ |
| GSAVI (Green Soil Adjusted Vegetation Index) | $((R\lambda_{nir} - R\lambda_{green}) \,/\, (R\lambda_{nir} + R\lambda_{green} + 0.5)) \cdot 1.5$ |
| GTVI (Green Triangle Vegetation Index) | $(NDVI + 0.5) / \,(NDVI + 0.5) \cdot (\sqrt{NDVI} + 0.5)$ |
| IPVI (Infrared Percentage Vegetation Index) | $R\lambda_{nir} \,/\, ((R\lambda_{nir} + R\lambda_{red}) \,/\, 2) \cdot (NDVI + 1)$ |
| LogR (Log Ratio) | $\log(R\lambda_{nir} \,/\, R\lambda_{red})$ |
| MSAVI (Modified Soil Adjusted Vegetation Index) | $(2 \cdot R\lambda_{nir} + 1 - \sqrt{(2 \cdot R\lambda_{nir} + 1)^2 - 8 \cdot (R\lambda_{nir} - R\lambda_{red})}) \,/\, 2$ |
| MSRNir_Red (Modified Simple Ratio NIR/RED) | $(R\lambda_{nir} \,/\, R\lambda_{red} - 1) \,/\, \sqrt{R\lambda_{nir} \,/\, R\lambda_{red} + 1}$ |
| NDRE (Normalized Difference Red-Edge Index) | $(R\lambda_{nir} - R\lambda_{rededge}) \,/\, R\lambda_{nir} + R\lambda_{rededge}$ |
| NDVI (Normalized Difference Vegetation Index) | $(R\lambda_{nir} - R\lambda_{red}) \,/\, (R\lambda_{nir} + R\lambda_{red})$ |
| NGRDI (Normalized Green-Red Difference Index) | $(R\lambda_{green} - R\lambda_{red}) \,/\, R\lambda_{green} \,/\, (R\lambda_{nir} + R\lambda_{red} + R\lambda_{green})$ |
| NormR1 (Normalized G) | $R\lambda_{green} \,/\, (R\lambda_{nir} + R\lambda_{red} + R\lambda_{green})$ |
| NormR2 (Normalized NIR) | $R\lambda_{nir} \,/\, (R\lambda_{nir} + R\lambda_{red} + R\lambda_{green})$ |
| NormR3 (Normalized R) | $R\lambda_{red} \,/\, (R\lambda_{nir} + R\lambda_{red} + R\lambda_{green})$ |
| RGR (Red Green Ratio Index) | $R\lambda_{red} \,/\, R\lambda_{green}$ |
| RI (Redness Index) | $R\lambda_{red} - R\lambda_{green} \,/\, R\lambda_{red} + R\lambda_{green}$ |
| RRI 1 | $R\lambda_{nir} \,/\, R\lambda_{rededge}$ |
| SAVI (Soil-Adjusted Vegetation Index) II | $(1 + 0.5) \cdot (R\lambda_{nir} - R\lambda_{red}) \,/\, (R\lambda_{nir} + R\lambda_{red} + 0.5)$ |
| SRQT_IR_R | $\sqrt{R\lambda_{nir} \,/\, R\lambda_{red}}$ |
| SRRed_NIR | $R\lambda_{red} \,/\, R\lambda_{nir}$ |
| WDRVI (Wide Dynamic Range Vegetation Index) | $(0.1 \cdot R\lambda_{nir} - R\lambda_{red}) \,/\, (0.1 \cdot R\lambda_{nir} + R\lambda_{red})$ |

For each vegetation index derived from the spectral bands, the average of the total pixels in each zone of the repetition blocks of eucalyptus species was calculated. In order to remove the border effect between the repetition blocks, an internal buffer of one meter was removed from the borders of each block.

### 3.2.4 Statistical analysis

First, a Pearson correlation network was constructed owing to the large number of variables. Variables with positive correlations presents green connection lines, meanwhile negative correlations among variables are red lines. The line thickness is proportional to the correlation magnitude. The analyses were based on “qgraph” pack (EPSKAMP et al., 2012), on R 3.6.3 (R CORE TEAM, 2022) software.

Thereafter, the main spectral indices results were based on multivariate analysis of variance and canonical variables analysis, in view of the interrelation among eucalyptus species. For this purpose, the “candisc” package was used (FRIENDLY; FOX, 2021).

Finally, a further examination of the main spectral and $CO_2$ flux-related variables was performed using Pearson correlation (by using “GGally” package) (SCHLOERKE et al., 2021), in order to construct a scatterplot and dispersion of variables related to eucalyptus species.

## 3.3 RESULTS

The correlation network (Figure 5) was high and positive between the features derived from the aggregated photosynthetic processes. The *green, red-edge* and NIR (near infrared) spectral bands had a negative linear correlation with carbon dioxide efflux ($CO_2$) of soil ($FCO_2$). The NDRE (Normalized Difference Red-Edge Index), NDVI (Normalized Difference Vegetation Index), SAVI (Soil-Adjusted Vegetation Index) e MSAVI (Modified Soil Adjusted Vegetation Index) indices showed the highest correlation with the characteristics soil $CO_2$ efflux ($FCO_2$). The $FCO_2$ variable showed links with all variables, but no variable was clearly associated.

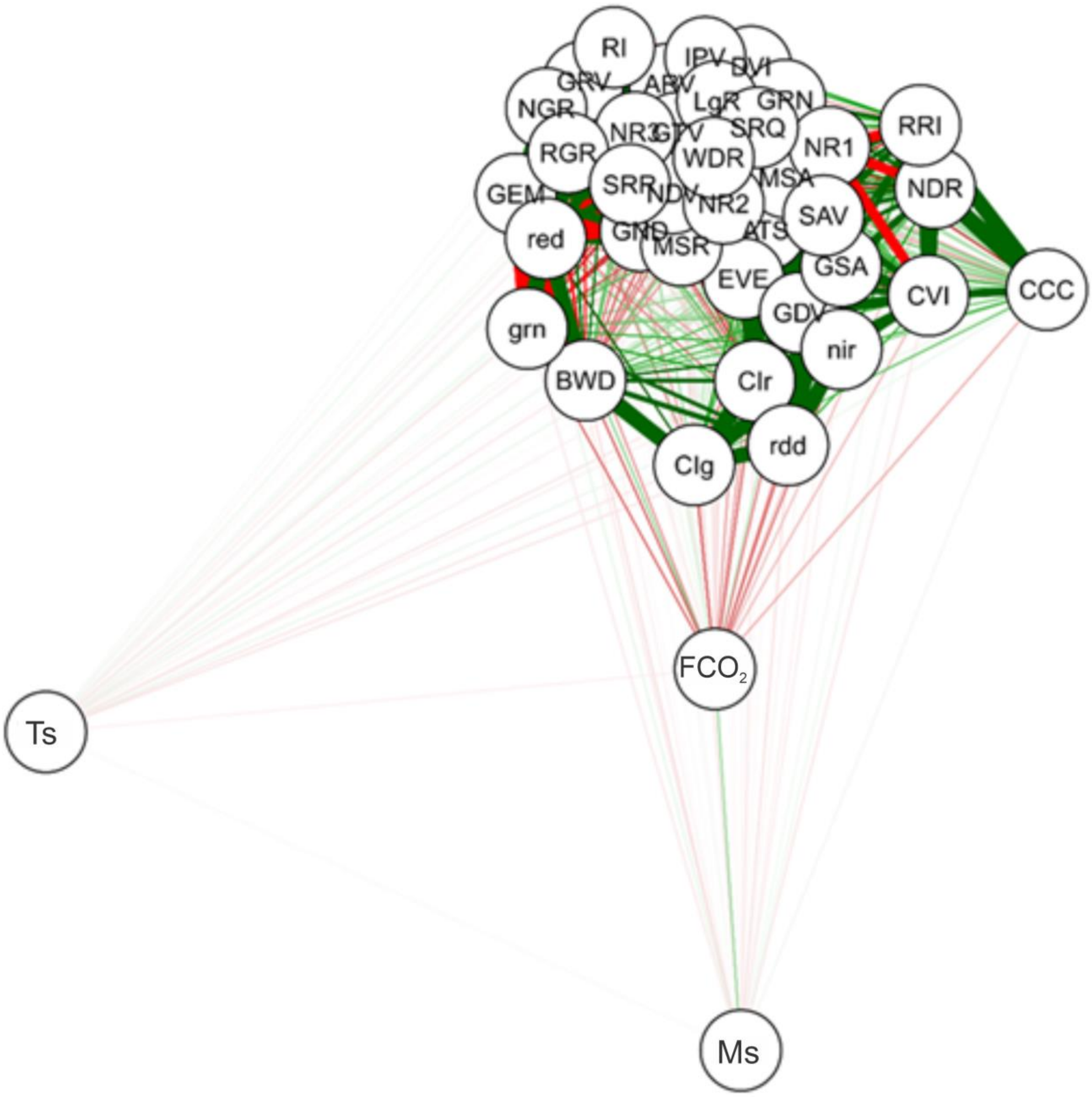


**Figure 5.** Pearson correlation network among the analyzed variables. Each point represents an index and the lines between the points are correlations between the indices, with thicker lines indicating a correlation greater than 0.6 and the red and green color indicating negative and positive correlation respectively.

Considering the large number of variables acquired via remote sensing and assigned in loco to the eucalyptus species applied in the Pearson correlation network, the variables NDRE, NDVI, SAVI, and MSAVI were selected, which had the highest correlations with soil $CO_2$ efflux ($FCO_2$).

Table 2 shows the multivariate analysis of variance for eucalyptus species. The variables soil moisture, soil temperature, the spectral bands (green, red, infrared and red edge) and vegetation indices (NDRE, NDVI, SAVI and MSAVI) were used to test the hypothesis of the difference between the eucalypt species in relation to the variable $FCO_2$. The significance level for the species in the test was ρ = < 0.00 for Pillai's test, showing that the null hypothesis is rejected, as there are differences between eucalypt species considering all variables simultaneously.

**Table 2.** Multivariate analysis of variance considering eucalyptus species and the variables $FCO_2$, soil temperature and moisture, spectral bands (green, red, infrared, and red edge), and vegetation indices (NDRE, NDVI, SAVI, and MSAVI).

| **Source of variation**† | **Degrees of freedom** | **Pillai's test** | **p-value** |
|---|---|---|---|
| Intercepto | 1 | 1.00 | <0.00*** |
| Espécies | 5 | 0.91 | <0.00** |
| Resíduos | 90 | | |

† Considered statistical significance of p ≤ 0.05 by * e p ≤ 0.01 by **

The canonical analysis considering the eucalyptus species and the variables with a higher correlation to $FCO_2$ is shown in Figure 5. The ratio of the variance accumulated in the first two canonical variables was higher than 65%. The variables NDRE, $FCO_2$, Soil moisture, red-edge, NIR, SAVI, NDVI, and MSAVI were most important in distinguishing between eucalypt species in Can1, while part red, green and soil temperature ratio were the most relevant variables in Can2. This finding reveals that a significant portion of the variability of the eucalypt species in relation to the variables evaluated in each species can be summarized in two linear combinations, named Can1 and Can2.

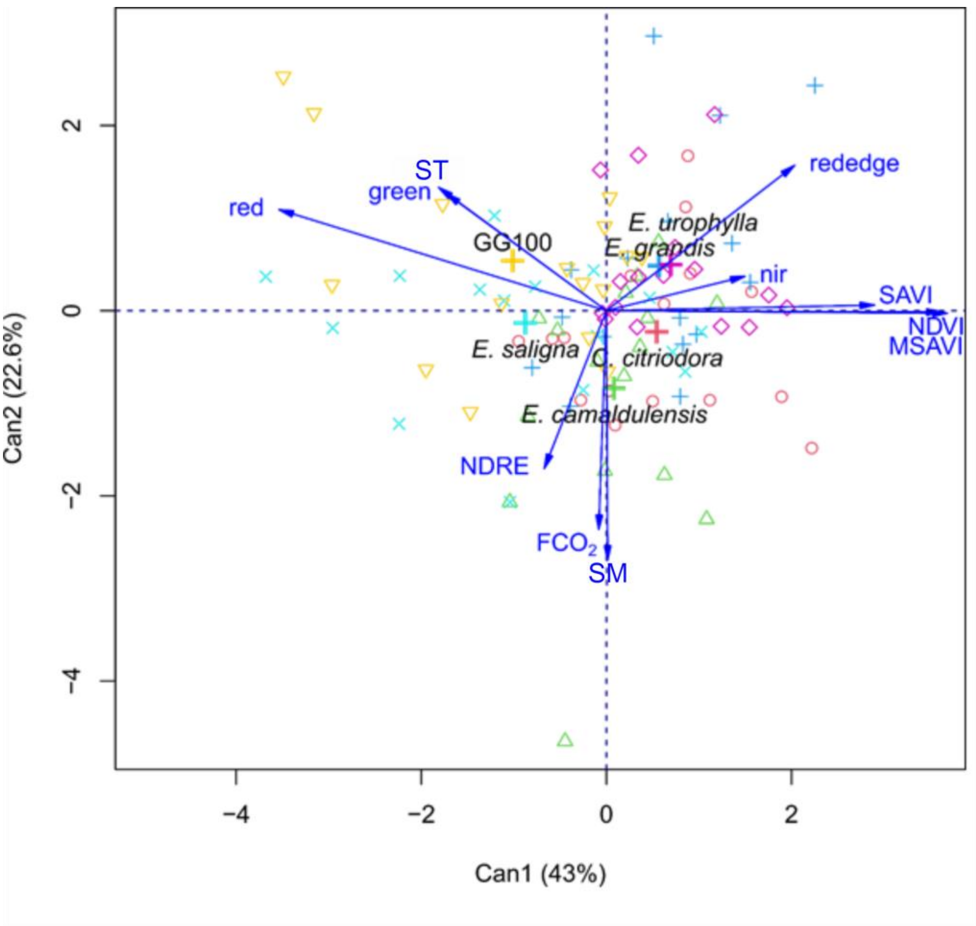


**Figure 6.** Canonical variable analysis considering eucalyptus species and $FCO_2$, soil moisture (Ms) and temperature (Ts), spectral bands (green, red, NIR, and red-edge), and vegetation indices (NDRE, NDVI, SAVI, and MSAVI).

From the analyzed variables in Figure 6, it can be observed that red, Soil Moisture (Ms), NDVI, and MSAVI presented the greatest variability, which can be proven by the module of their vectors. The variables NDRE, $FCO_2$ and Soil Moisture were those that contributed most to the discrimination of the species *E. camaldulensis* and the variables red, green and Soil temperature were those that contributed most to the discrimination of the clone GG100. On the other hand, the species *E. uroplylla* and *E. grandis* were more similar in the canonical variables analysis.

The spatialization of NDRE, NDVI, SAVI, and MSAVI variables is presented in Figure 5, considering that the canonical variable analysis among the eucalyptus species correlated significantly with $FCO_2$. Maximum values of 0.45, 0.88, 0.70, 0.99 and minimum values of -0.24, 0.31, 0.13 and -0.24 were observed for NDRE, NDVI, SAVI and MSAVI, respectively, among *E. camaldulensis*, *E. uroplylla* and *E. saligna*.

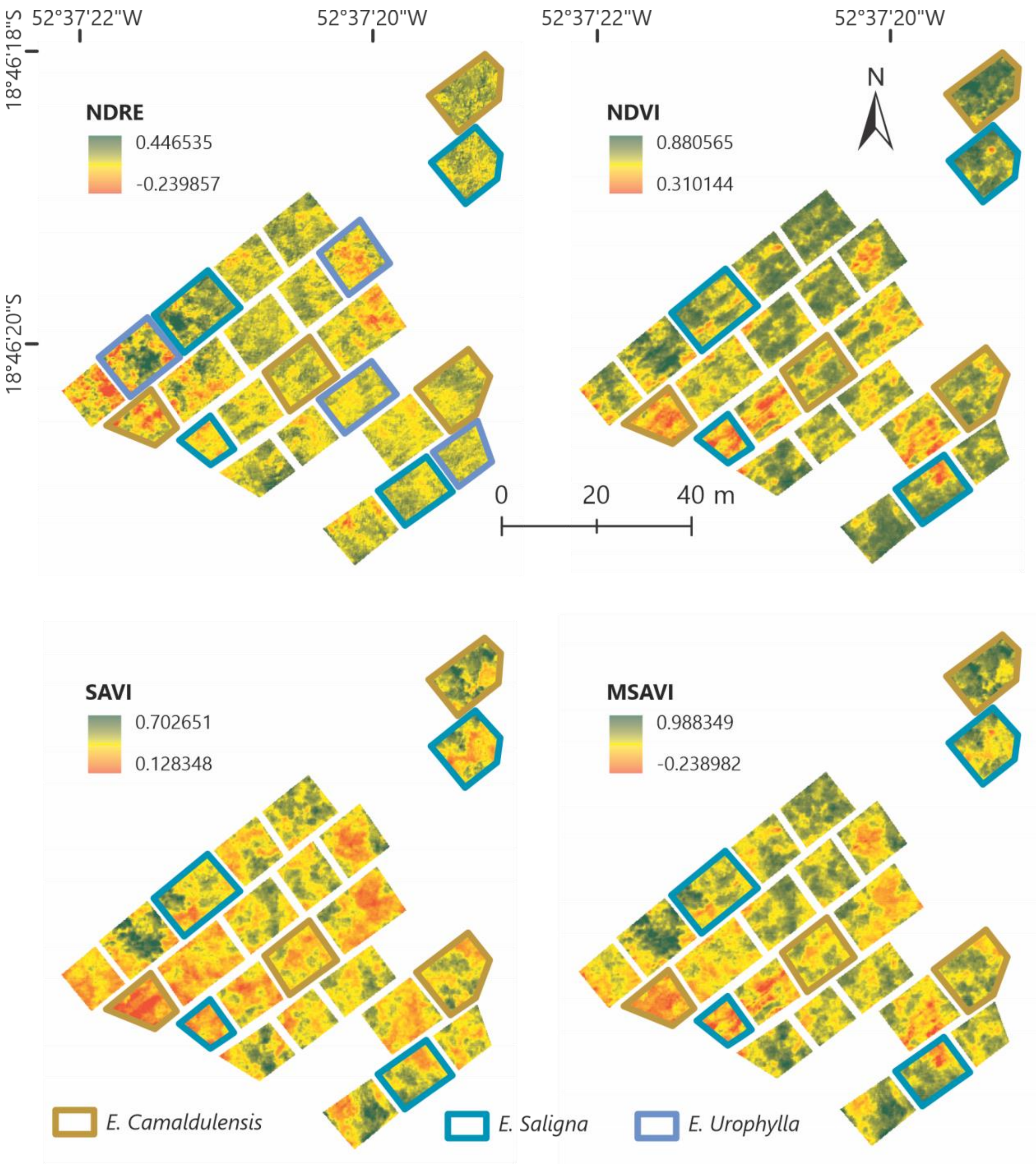


**Figure 7.** The spatialization of the vegetation indices that best correlated significantly with $FCO_2$ among the eucalyptus species, NDRE, NDVI, SAVI, and MSAVI.

In Figure 6, it can be seen that not only the correlation between the variables but also that the eucalyptus species showed specific correlations with $FCO_2$. The $FCO_2$ correlation to soil moisture (0.243*), red (-0.260*) and SAVI (-0.233*) were significant at 95%, with correlation among *E. camaldulensis* (0.514*) and *E. grandis* (0.487*); *E. saligna* (-0.861***), *E. uroplylla* (-0.514*) and GG100 clone (-0.638**); *E. camaldulensis* (-0.736**) and *E. saligna* (0,723**) respectively. For the variables green

(-0.374***), nir (-0.335***) and red-edge (-0.352***) had significance >99%, with correlation among *E. saligna* (-0.885***), *E. uroplylla* (-0.505*) and GG100 clone (-0.676**); *E. camaldulensis* (-0.636**), *E. uroplylla* (-0.517*) and GG100 clone (-0.697**); *E. camaldulensis* (-0.506*), *E. saligna* (0.528*) and GG100 clone (-0.674**) respectively.

Soil temperature (-0.032), NDRE (-0.148), NDVI (-0.067) and MSAVI (-0.150) presented showed a negligible and non-significant correlation, though among *E. camaldulensis* (-0.526*) and *E. grandis* (-0.477*); *E. camaldulensis* (-0.774***), *E. saligna* (-0.736**) and *E. uroplylla* (-0.632**); *E. camaldulensis* (-0.727**) and *E. saligna* (-0.836***); *E. camaldulensis* (-0.736**) and *E. saligna* (-0.723**) respectively, had significative correlation.

*C. citriodora* had no significance for the correlation to $FCO_2$ in the entire set of variables. The species most often correlated significantly with $FCO_2$ were *E. camaldulensis* and *E. saligna*.

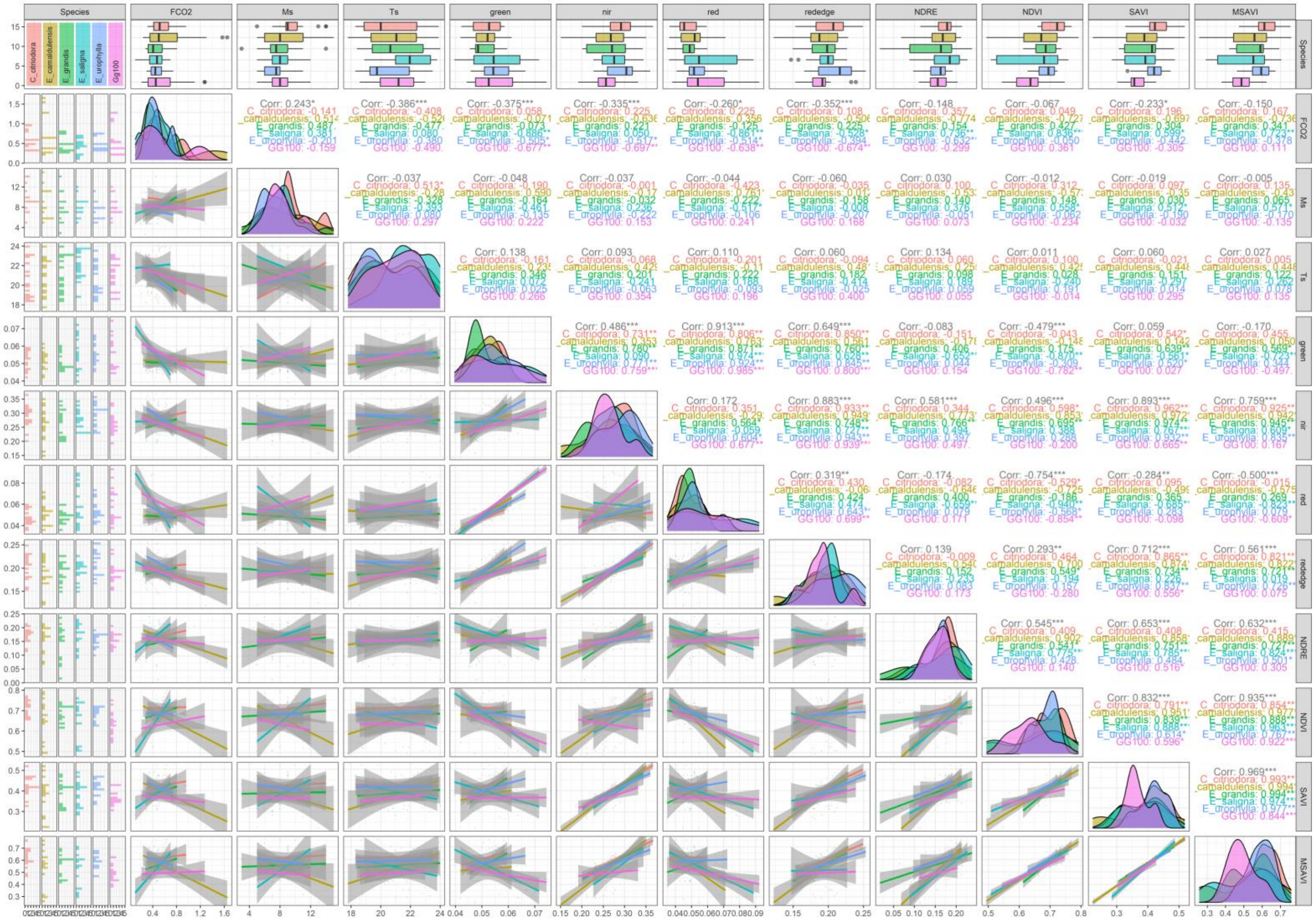


**Figure 8.** Scatterplot of Pearson correlations and variables ($FCO_2$, soil temperature and moisture, spectral bands, and vegetation indices) and the distribution of variables according to the canonical variable analysis modeling considering the eucalyptus species.

## 3.4 DISCUSSION

This study showed an absence of strong and significant correlations between soil $CO_2$ emission ($FCO_2$) and the rest of the variables in a general set with eucalyptus species (Figure 5). However, differences were identified among the Eucalyptus species while simultaneously considering the soil variables with the main VIs (Table 2). Total soil respiration comprises autotrophic and heterotrophic respiration (BOND-LAMBERTY; WANG; GOWER, 2004; SUN et al., 2014), which are directly and indirectly related to biotic and abiotic factors (REN et al., 2016; WANG et al., 2014) for components regulation.

The behavior of autotrophic respiration is strongly correlated with photosynthesis (FERNÁNDEZ-MARTÍNEZ et al., 2014; PEÑUELAS et al., 2013) and is mediated by phenological dynamics throughout the plant cycle (JANSSENS et al., 2010; MO et al., 2008). Heterotrophic respiration from the mineralization of organic matter by the decomposer community is highly affected by soil carbon availability, moisture and temperature (LI et al., 2013; PENG et al., 2017).

Soil moisture (Ms) and temperature (Ts) are important for the respiration process of soils and directly influence the decomposition of organic matter and microbial and root activities (SILVA-OLAYA et al., 2013a; WANG et al., 2015). Thus, Ms showed a positive correlation and Ts showed a negative correlation with $FCO_2$. However, this low-magnitude correlation between Ms and Ts with $FCO_2$ can be explained by the low variation over the time series period (MOITINHO et al., 2021). The effects of Ts on $FCO_2$ may be partially hidden by the effect of Ms, because these are interdependent variables and commonly change simultaneously (DING et al., 2010).

The results obtained by Almeida et al. (2018), Dossou-Yovo et al. (2016) and Pires et al. (2017), show showedthe transport of carbon dioxide ($CO_2$) and among gases from soil tthe o atmospthe here is dependent on porosity, moisture content, and the coions for all soil biota. These conditions in the ecosystem are at the same time very favorable for the activity of microorganisms, which can positively influence respiration rates (GONZÁLEZ-UBIERNA; LAI, 2019). In addition, management practices will influence the behavior of carbon storage capacity and the loss of $CO_2$ from the soil to the atmosphere (BASHAR; ZHOU, 2015).

In the case of data obtained via passive remote sensors, the spectral bands green, nir, red, and red were negatively correlated and of low magnitude with $FCO_2$, but with significance in *E. camaldulensis*, *E. saligna*, and *C. citriodora* (Figure 6). The low association between spectral bands and $FCO_2$ is directly associated with the green vegetative canopy and also related to the stage of development of the eucalypt species that influences leaf thickness, water content and response of leaf chlorophyll contents. The chlorophyll a and b pigmentations are the ones that most influence the electromagnetic radiation in the visible region, with two absorption peaks, the higher in the red band and the lower in the blue band, respectively (LIMA et al., 2011; SILVA JUNIOR et al., 2021), favoring a better result for the classifier that used the red (R) and blue (B) spectral bands. From Silva et al. (2014), the green wavelength response is entirely associated with the potential of photosynthetic activity, and this relation is directly related to the utilization of available radiation by these chlorophyll pigments. The process of $CO_2$ absorption from the atmosphere by the leaves occurs when the pores of the stomas open, allowing the carbon dioxide to enter the leaf, mainly located in the lower epidermis (BUNCE, 2004; FAN et al., 2020).

The use of the red and near-infrared (NIR) spectral bands in the composition of vegetation indices is because these wavelengths are inversely proportional to leaf reflectance, with greater than 90% sensitivity on the spectral behavior of a vegetation canopy (BARET; GUYOT; MAJOR, 1989). The NDVI uses red and NIR spectral reflectance to measure the density and greenness of vegetation, showing a specific negative and positive correlation with *E. camaldulensis* and *E. saligna*, respectively. The red spectral band is strongly absorbed by the top of the plant canopy, the lower levels of the canopy do not contribute to reflectance and scattering of electromagnetic radiation, which impairs the correlation of NDVI with $FCO_2$.

The absorption of the red radiation is by the photosynthesizing pigments of the leaves, which are the chlorophyll "a", while in the near infrared the absorption is almost zero, and the reflectance and transmittance are high, due to the internal cellular structures of the leaves and the effect of the multiple reflectances (PONZONI; DISPERATI, 2001). To capture variations in the amount of chlorophyll not only in the upper canopy but also throughout the foliage, the NDRE index was calculated using a combination of the NIR and red-edge bands. A negative, positive, and specific negative correlation with *E. camaldulensis*, *E. saligna*, and *E. uroplylla*, respectively, differed from the correlations of the NDVI index, which can be explained by the low values of chlorophyll content.

SAVI and MSAVI use a soil brightness correction factor (L) applied to maximize the reduction of soil effects on the vegetation signal and showed negative and positive correlations with $FCO_2$ for *E. camaldulensis* and *E. saligna*, respectively. However, the presence of straw on the soil surface decreased the effect of precipitation on $FCO_2$ since straw forms a physical barrier against the abrupt entry of water into the soil.

The results of the present study allow the management of differentiation among eucalyptus species using sensors coupled to remotely piloted aircraft and $FCO_2$, thus integrating new assumptions in this line of research. The reflectance of eucalyptus species acquired by remotely piloted aircraft makes it possible to obtain data about them in a fast, non-destructive, and accurate way. Measuring $CO_2$ provides important information about the carbon emissions in areas of eucalyptus. Both pieces of information contribute to the improvement of forest management. It is important to emphasize that the study was conducted in places with different soil and climate conditions than the current research.

## 3.5 CONCLUSIONS

The results obtained in this study present that there is a good correlation between the spectral response of the canopy and the chlorophyll content in eucalyptus species, with the most important spectral regions being green (550 nm ± 40 nm), red-edge (735 nm ± 10 nm), and near-infrared (790 nm ± 40 nm).

There was a specific correlation between the soil carbon dioxide efflux data and the eucalyptus species, providing a distinction of values among the species in the statistical data. Based on different combinations of bands and vegetation indices from remotely sensed multispectral cameras, it is possible to distinguish between eucalyptus species.

Further research should consider the seasonality of eucalyptus species, since this may affect the contribution of autotrophic and heterotrophic respiration to total soil respiration.

# CHAPTER 4 – CARBON DIOXIDE SPATIAL VARIABILITY AND DYNAMICS FOR CONTRASTING LAND USES IN CENTRAL BRAZIL AGRICULTURAL FRONTIER FROM REMOTE SENSING DATA[5]

**ABSTRACT -** Greenhouse gas (GHG) sources and sinks are an important global concern. Monitoring the spatiotemporal variations of GHG concentrations, particularly carbon dioxide ($CO_2$), is crucial for identifying potential sources and sinks and moving toward a sustainable future. Therefore, via a time-series of remote data and multispectral images, this study evaluates the $CO_2$ spatiotemporal dynamics and related factors during 2015 – 2018 in one of the world's main agricultural frontier areas, the state of Mato Grosso (SMT), Brazil, which is both experiencing continued deforestation and attempting to achieve sustainable food production. In this study, data was obtained from the measurement of column-averaged carbon dioxide ($CO_2$) dry air mole fraction in the atmosphere, set as $X_{CO2}$ from Orbiting Carbon Observatory-2 satellite from January 2015 to December 2018. The enhanced vegetation index data were obtained from the Moderate-Resolution Imaging Spectroradiometer (MODIS) sensor, and rainfall data were obtained from the Climate Hazards Group InfraRed Precipitation with Station dataset. From a series of Landsat-8 satellite images, it was possible to distinguish land use and land cover classes and estimate the $CO_2$ flux in the SMT. The results showed that the temporal variability of $CO_2$ flux is correlated positively with rainfall, while $X_{CO2}$ is negatively correlated with rainfall. Regarding spatial variability, we observed that forest areas that were converted to other land uses resulted in higher values that characterize with sources, and that the highest and lowest average concentrations of $CO_2$ occurred in the dry and rainy months, respectively, for $X_{CO2}$, which might be the result of differences in the vertical resolution of the $CO_2$ column and scale. In contrast, areas with large continuous forest areas tended to have lower values and contribute positively to the carbon balance as sinks, thereby mitigating climate change impacts. Therefore, not only $X_{CO2}$ but also $CO_2$ flux are directly related to changes in land use and land cover (LULC) in complex systems that are affected by climatic variables and processes, such as photosynthesis and soil respiration.

**Keywords:** Environmental degradation; emission; climate change; orbital sensor

---

[5] This chapter corresponds to the scientific article published in the Journal of South American Earth Sciences https://doi.org/10.1016/j.jsames.2022.103809.

## 4.1 INTRODUCTION

The sustainable expansion of the world economy is directly linked to greenhouse gas (GHG) sources and sinks in production systems (WASTI; ZAIDI, 2020). Agricultural activities areas respond to 24% of total global emissions (WAHEED et al., 2018). In particular, the agricultural sector accounts for 20% of carbon dioxide ($CO_2$), 70% of methane ($CH_4$), and 90% of nitrogen oxide ($N_2O$) of global emissions (The World Bank, 2016; Luo et al. 2017). The high rates of GHG emissions related to agriculture result from the inappropriate use of soil and water resources, the excessive use of agrochemicals, such as fertilizers (ISMAEL; SROUJI; BOUTABBA, 2018), deforestation, and the use of fire for pasture management, renewal and expansion of areas, and farming activities (BACCINI et al., 2012; CAÚLA et al., 2015). Changes in land use and land cover (LULC) due to anthropogenic activity affect both the global carbon cycle and the climate (QUESADA et al., 2018). Specifically, the atmospheric $CO_2$ concentration has increased by more than 30 ppm in the last 17 years (LINDSEY R, 2020). In 2018, the average $CO_2$ was approximately 407 ppm (Lindsey R, 2020), for which the $CO_2$ released from LULC was estimated to be approximately 1 Pg C year$^{-1}$ (ARNETH et al., 2017; HOUGHTON et al., 2012; LE QUÉRÉ et al., 2015; PAN et al., 2011). LULC is rising as the world's demand for food, biofuels, and fibers increases, especially the increase in global demand for animal protein, which requires increases in livestock growth (FEARNSIDE, 2001; NAYLOR et al., 2005; NEPSTAD; STICKLER; ALMEIDA, 2006).

LULC for commodity production is one of Brazil's main GHG sources, making the country responsible for 2.8% of global emissions (Pereira et al. 2020). Among its producing regions, the state of Mato Grosso (SMT), which is located in the western center of the country, is the country's leading agricultural frontier as its largest producer of commodities (KASTENS et al., 2017; PICOLI et al., 2018). In particular, the SMT leads national production in soybeans and beef, which are main drivers of

---

Greenhouse gas, GHG; state of Mato Grosso, SMT; land use and land cover, LULC; enhanced vegetation index, EVI; linear spectral mixture model, LSMM; normalized difference fraction index, NDFI; healthy vegetation, HV; standardized precipitation index, SPI; probability density function, PDF; Climate Hazards Group InfraRed Precipitation with Station, CHIRPS; photosynthetic vegetation index, PRI.

deforestation, accounting for 22 Mha of pastures and 10.2 Mha of areas cultivated with soybean in 2018 (Silva Junior and Lima 2018).

Although there has been a 2.30 $km^2$ increase in soybean cultivation area in the last two harvest years in the SMT (SojaMaps 2020), deforestation has increased in recent years, increasing from 757 $km^2$ (the lowest level) in 2012 to 1,702 $km^2$ in 2019 (INPE, 2020). Further, certain measures, such as the Soy Moratorium (Gibbs H K et al. 2015) and Cattle Agreement (Gibbs et al. 2016; Alix-Garcia and Gibbs 2017), have not been sufficient to contain deforestation, contributing significant GHG emissions to the atmosphere, especially $CO_2$, that does not return to the atmosphere at the production site because of export or consumption in another region. Since 2013, approximately 1 Mha of land has been deforested in the SMT (INPE, 2020), which is contradictory to the efforts of those in the soybean chain, who desire sustainable soybean production, as per programs such as the Soy Moratorium and Soja Plus (ABIMILHO, 2021). This deforestation is attributed to the degradation of pastures caused by the "Sudden Death of Pastures" syndrome (SILVA et al., 2018), in which an increasing atmospheric $CO_2$ concentration has forced cattle ranchers to renew their pastures. Renewed pastures imply an increase in the stocking rate, a decrease in the age at which cattle can be slaughtered, a lower carbon cost/kg of meat produced, mitigation of gas emissions in degraded pastures, and, theoretically, lower pressure on the forest to open new areas (Silva et al. 2018; Eri et al. 2020).

Given this fact, it is interesting to highlight the importance of estimating biophysical parameters of vegetations and correlating $CO_2$ concentrations through geotechnologies. For the generation of objective information in near-real time, remote sensing is a tool that provides and contributes to the distinction and characterization of forests, agriculture, climate, among others (ALMEIDA et al., 2019; LIU et al., 2020a; WEST; QUINN; HORSWELL, 2019). The use of this tool through various sensors has enabled studies on understanding carbon dynamics (GAO et al., 2020; HE et al., 2020).

The hypothesis of this research is that remote sensing responds the dynamics of $CO_2$ dry air mole fraction ($X_{CO2}$) in the atmosphere and $CO_2$ fluxes are related to the seasonality of climate variables and LULC classes. Therefore, the objective of this study was to use remote sensing to evaluate the spatiotemporal dynamics of $CO_2$ from 2015 to 2018 in the SMT, which is the main agricultural frontier of Brazil.

## 4.2 MATERIAL AND METHODS

### 4.2.1 Study area

The study area comprises the SMT, located in the central-western region of Brazil (Figure 1), with a territorial area of 903,207.047 km$^2$, and an estimated population of 3,567,234 people (IBGE, 2021). The SMT has a predominantly tropical climate, with air temperatures between 24 °C and 40 °C and an annual average rainfall of 1500 mm (ALVARES et al., 2013). Its conversion from natural forest to agriculture (annual crops and pasture) been intense since the 2000s, making it the basis of studies considering the alteration of ecotones in ecoregions (da Silva Junior et al. 2019; Santos et al. 2015). In addition, the SMT is the largest producer of soybeans in Brazil (SOJAMAPS 2020).

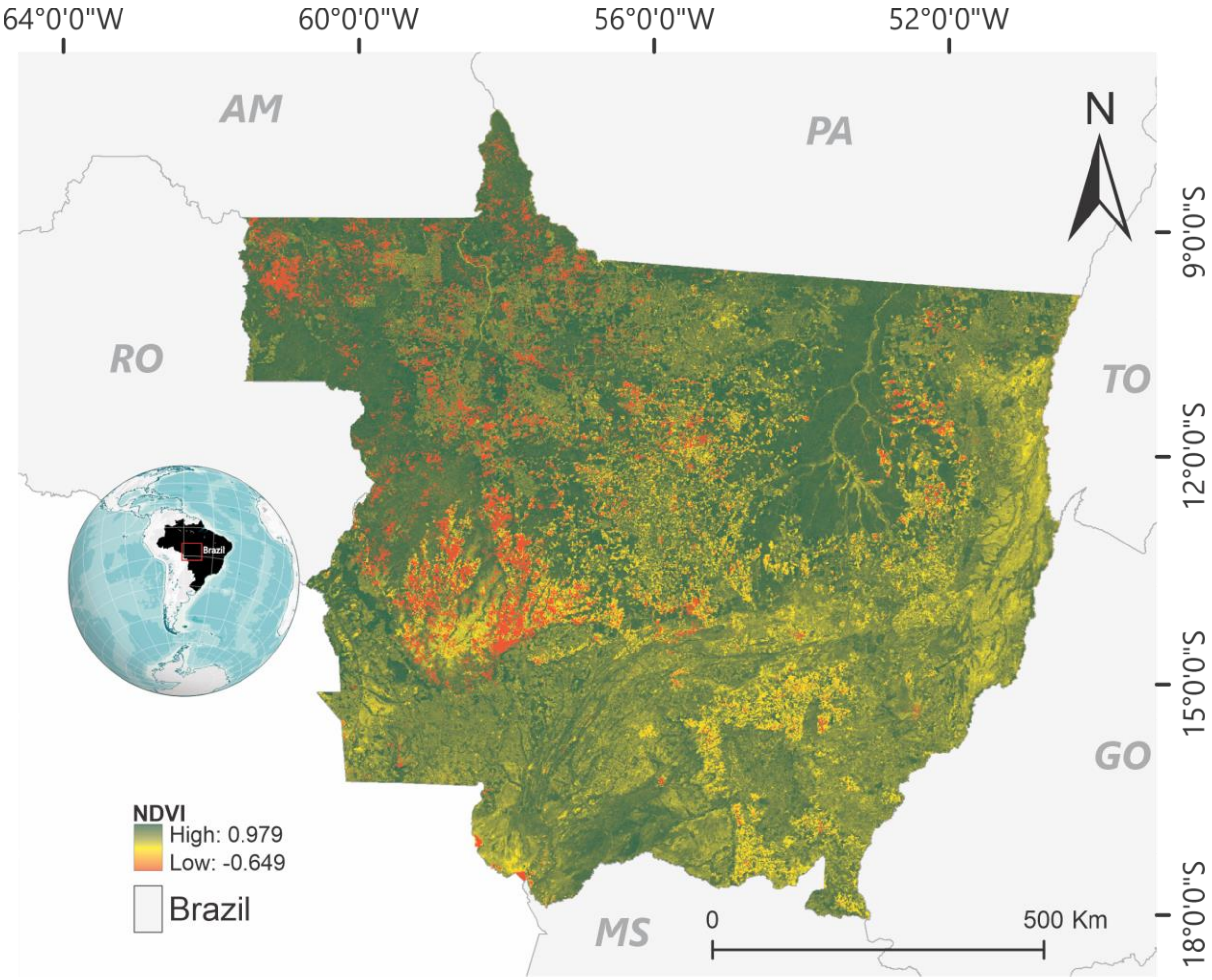


**Figure 1.** Location of study area in central-western Brazil, Mato Grosso State based on the average Normalized Difference Vegetation Index (NDVI) for March 2018.

### 4.2.2 Orbiting Carbon Observatory-2

The primary product delivered by the Orbiting Carbon Observatory-2 (OCO-2) consists of spatially resolved estimates of the column-averaged dry air mole fraction. This quantity, called $X_{CO2}$ by members of the atmospheric carbon science community, quantifies the average concentration of $CO_2$ in a column of dry air extending from the Earth's surface to the top of the atmosphere. The values of $X_{CO2}$ are estimate of are derived by taking the ratios of path-integrated $O_2$ and $CO_2$ densities between the Sun, surface footprint, and OCO-2 satellite, followed by multiplication by of mole fraction of oxygen of 0.20935 and near uniform globally (ELDERING et al., 2015).

Quantification is made by a high-resolution three-band spectrometer which measures the absorption by $CO_2$ and $O_2$ in reflected sunlight in three independent wavelength bands: the $O_2$ A-band at around 0.765 µm, the weak $CO_2$ band at around 1.61 µm, and the strong $CO_2$ band at around 2.06 µm. OCO-2 it has a precision of <0.3% (1 ppm) (WUNCH et al., 2017) and spatial resolution (≤1.29 × 2.25 $km^2$) observations at nadir with a 16-day repeat cycle along a swath width of ≤10 km (CRISP et al., 2017). The OCO-2 mission provides four different levels of data products for the user community, supplying comprehensive mission data results (CRISP et al., 2012).

We obtained $X_{CO2}$ data from the OCO-2 Lite version (V8r), which has a spatial grid resolution from the OCO-2 data archive that is maintained at National Aeronautics and Space Administration (NASA) (https://co2.jpl.nasa.gov/#mission=OCO-2). Data with an alert level less than or equal to 11, and data that passed through the cloud screens and converged (xco2_quality_flag = 0) (WUNCH et al., 2017). Alerts above 12 for nadir and glint modes, may contain significantly larger errors than the a posteriori uncertainty stated about the $X_{CO2}$ values (MANDRAKE et al., 2015). A temporal trend adjustment of the $X_{CO2}$ data was made using the regression method (y = 00000.7x + 394.9) (Gujarati and Porter 2011).

### 4.2.3 Enhanced Vegetation Index time-series

Vegetation indices have been developed to highlight the combinations of surface reflectance at two or more wavelengths designed to highlight a particular property of vegetation in order to exclude soil and other terrestrial targets. The numerical values of these indices can vary between -1 and 1, in which vegetation is commonly indicated by positive values, as there is greater reflectance in the near-infrared wavelength than in the red (HUETE et al., 2002; SOLANO et al., 2010). Some targets, such as water and snow, exhibit higher reflectance at the red (600 – 750 nm) wavelength region, as compared with the near-infrared (750 – 1100 nm) region, and present negative NDVI values. With the emergence of the Moderate-Resolution Imaging Spectroradiometer (MODIS) sensor, Huete et al. (1997) proposed an enhanced vegetation index (EVI) that minimizes the effects of soil and atmosphere by considering the blue spectral band.

In this study, MODIS sensor images were used and applied a tolerable cloud mask of maximum 20% percent clouds per pixel, in which the EVI values (Equation 1) of the MOD13Q1 product collection 6.0 of the 16-day MODIS images (HUETE et al., 2002) from the TERRA orbital platform with a spatial resolution of 250 m were obtained from the Google Earth Engine derived from a temporal series from January 1, 2015 to December, 31, 2018 via ee.ImageCollection ("MODIS/006/MOD13Q1").

$$EVI = g\frac{\rho_{IVP} - \rho_V}{\rho_{IVP} + (c_1 \cdot \rho_V) - (c_2 \cdot \rho_A) + L} \quad (1)$$

where $\rho_{IVP}$, $\rho_V$, and $\rho_A$ are the reflectances in the spectral ranges of near-infrared, red, and blue, respectively; $g$ is the gain factor (2.5); $c_1$ and $c_2$ are the correction coefficients for red (6) and blue (7.5) atmospheric effects, respectively; and $L$ is the correction factor for soil interference (1). The coefficients adopted in the EVI equation according to (HUETE; JUSTICE; LIU, 1994; HUETE et al., 1997).

#### 4.2.4 Detection of Land Use via Normalized Difference Fraction Index

To evaluate the potential of the spectro-temporal information derived from the Landsat-8 series (OLI sensor) and to distinguish the LULC classes in the SMT, 53 scenarios were used each year, totaling 212 scenes. The images were converted to top of atmosphere reflectance using metadata values by converting the digital level values to reflectance factor (0 and 1) and a tolerable cloud mask of maximum 20% percent clouds per pixel was applied.

After treatments in the images were performed on the images, the linear spectral mixture model (LSMM) was applied (Equation 2). This model aims to estimate the proportion of components, such as soil, vegetation, and shade, of each pixel based on the spectral responses in several Operational Land Imager (OLI) sensor bands in order to generate fraction images (SHIMABUKURO; SMITH, 1991). These image components were extracted from the reference reflectance image. Shade was assigned zero percent reflectance at all wavelengths (SOUZA; ROBERTS; COCHRANE, 2005; SOUZA; ROBERTS; MONTEIRO, 2005).

$$ri = a_{li}.V + a_{2i}.P + a_{3i}.C + ei \quad (2)$$

where $ri$ is the spectral response of the pixel in the i-th band, $a_{li.}$ is the response of the V *endmember* in the i-th band, $a_{2i.}$ is the response of the P *endmember* in the i-th band, $a_{3i.}$ is the response of the C *endmember* in the i-th band, *V* is the estimated proportion of the V component in the pixel, *P* is the estimated proportion of the P component in the pixel, *C* is the estimated proportion of the C component in the pixel, and $ei$ is the error associated with the i-th spectral band in the pixel.

The model was then applied to each image of each spectral band according to the sensor bands, as well as the selected endmembers in the images themselves. Fraction images were obtained to calculate the normalized difference fraction index (NDFI).

The NDFI improves canopy damage detection, as compared with existing techniques, and can be used in combination with other algorithms to unambiguously map forest canopy damage caused by selective cutting and burning (SOUZA; ROBERTS; COCHRANE, 2005). Further, this index can be integrated into existing image processing methods to classify damaged forest cover areas into degradation subclasses.

Thus, the LSMM was applied both to each image in each spectral band using the aforementioned sensor bands and the selected endmembers in the images (Equation 3), as described by Souza Jr et al. (2005). The results were used as a basis for interpreting the orbital images.

$$NDFI = \frac{HV_{Shade} - (PNV + Soil)}{HV_{Shade} + PNV + Soil} \quad (3)$$

where *PNV* is the photosynthetically inactive vegetation and $HV_{Shade}$ is the fraction of healthy vegetation (HV) normalized by the shade given by Equation 4.

$$HV_{Shade} = \frac{HV}{100 - Shade} \quad (4)$$

NDFI values range from -1 to 1 and variable was rescaled to 0–200 to classifying regions deforestation and forest degradation (SOUZA et al., 2013b), wherein intact forests have high values (close to 1) because of their high HV (i.e., high HV content and canopy shade) and low PNV and soil values. As the forest is degraded, the PNV and soil fractions increase because of a decrease in canopy cover, thereby producing low NDFI values (SOUZA et al., 2013b). Based on the thresholds proposed by Souza Jr et al. (2005), the uses of forest, anthropic action, exposed soil, and watercourses were mapped.

#### 4.2.5 Rainfall data and Standardized Precipitation index

We used a spatial and temporal dynamics analysis to compare the observed rainfall dataset Climate Hazards Group InfraRed Precipitation with Station (CHIRPS) with the other study variables. This methodology has been widely used in assessing rainfall estimated by remote sensing (BAEZ-VILLANUEVA et al., 2018; CAVALCANTE et al., 2020; DE OLIVEIRA-JÚNIOR et al., 2021; PAREDES-TREJO; BARBOSA; LAKSHMI KUMAR, 2017).

For classification, a CHIRPS dataset developed by the U.S. Geological Survey and the Climate Hazards Group at the University of California, Santa Barbara, was used. This dataset combines pentadal precipitation climatology, near-global geostationary TIR satellite observations from the CPC and National Climatic Data Center (Knapp et al., 2011), precipitation fields from the NOAA Climate Forecast System (CFSv2) atmospheric model (Saha et al., 2010), and in situ rainfall observations (Toté et al., 2015). These products were used because of the lack of temporal data from in situ stations in the SMT (de Oliveira-Júnior et al., 2021). Further, the data are available from 1981 to the present at a spatial resolution of 0.05° (±5.3 km), providing monthly, pentadal, and decadal temporal global resolutions (Funk et al., 2014).

The standardized precipitation index (SPI) was developed by Mckee et al. (1993), and quantifies the rainfall deficit or excess at different time scales. The SPI was calculated on the annual (SPI-12) and monthly (SPI-1) scales for the SMT from 2015 to 2018 to identify dry and wet periods. The SPI calculation is determined from the total accumulated rainfall records over 20 years fitted to a probability distribution function, which is then transformed into a normal probability distribution function, allowing users to adjust the average SPI for a given location and period to zero (Mckee, et al., 1993; Teodoro et al., 2015).

To determine the SPI, we initially calculated the gamma distribution, which is defined by the probability density function (PDF) as follows:

$$f(x) = \frac{1}{\Gamma(a)\beta^{a}} x^{a-1} e^{-\frac{x}{\beta}} \quad (5)$$

where $\alpha$ is the shape parameter (dimensionless), β is the scale parameter (mm), $x$ is the total rainfall (mm), and $\Gamma(a) = \int_0^\infty x^{a-1} e^{-x} dx$.

All the parameters and the gamma PDF were fitted to the frequency distribution of accumulated rainfall using remote sensing data at the cited scale. Using the maximum likelihood method, α and β were estimated, which is the most appropriate approach, according to Gois et al. (2015). To determine the cumulative probability of an observed rainfall event for the adopted scale, the α and β parameters were calculated. The cumulative probability is given by Equation 6.

$$F(x) = \int_0^x f(x)dx = \frac{1}{\Gamma(\mathrm{a})\beta^{a}} \int_0^x x^{a-1} e^{-\frac{x}{\beta}} dx \quad (6)$$

According to the annual SPI values for the SMT, the SPI was classified according to (Mckee et al. (1993) the wet and dry periods as follows: extremely wet (≥ 2.00), very wet (1.5 to 1.99), moderately wet (1.00 to 1.49), close to normal (0.99 to -

0.99), moderately dry (-1.00 to -1.49), very dry (-1.50 to -1.99), and extremely dry (≤ -2.00).

### 4.2.6 $CO_2$ Model Data

The OLI/Landsat-8 sensor system was used to monitor land use efficiencies and $CO_2$ flux in the SMT. For this, we used the corrected orbital reflectance images and the best composition mosaic with at most 20% percent clouds per pixel tiles using the Google Earth Engine platform (GORELICK et al., 2017) over the study period.

The $CO_2$ flux index was used (RAHMAN et al., 2001) to measure the efficiency of the vegetation-related carbon sequestration process, which is the photosynthesis rate derived from photosynthetic processes. For this, the photochemical reflectance index (PRI) (Equation 7) was calculated (GAMON; SERRANO; SURFUS, 1997) using the green and blue spectral bands. The PRI estimates the amount of carotenoid pigments in leaves, which indicate the $CO_2$ storage rate in the leaves (BARNES et al., 2017; RAHMAN et al., 2001).

$$PRI = \frac{A - Ve}{A + Ve} \tag{7}$$

where *A* is the blue spectral band reflectance and *Ve* is the green spectral band reflectance.

However, the PRI results must be repeated for reliability, resulting in positive values. Therefore, it is necessary to generate the sPRI (Equation 8) (MARTINS; BAPTISTA, 2013).

$$sPRI = \frac{PRI + 1}{2} \tag{8}$$

Thus, the $CO_2$ flux ($\mu mol\ m^{-2}\ s^{-1}$) is the multiplied result of the NDVI and sPRI. There is a relationship where it may be possible to capture the carbon sequestration absorptions using the PRI index, which indicates the efficient use of light during photosynthesis, and the NDVI, which demonstrates the vigor of the photosynthetically active vegetation (RAHMAN et al., 2001). For more coherent estimates of CO2Flux in Brazil, the fitting of flux data associated with the CO2Flux model with direct measurement of CO2 fluxes by Turbulent Vortex Covariance (Eddy Covariance) (Goulden et al., 1996) was applied. Santos, (2017) determined a coefficient of R2 = 0, 8182 and the regression model y = -66.207x + 11.406 between the direct measurement of CO2 fluxes and the CO2Flux model, the best correlation is given in Equation (9).

$$CO2FLUX = 13.63 - (66.207 \cdot (NDVI \cdot sPRI)) \quad (9)$$

### 4.2.7 Statistical analysis

To study the temporal variation of the variables, scatter plots and boxplots were constructed for the time series evaluated. Furthermore, a heat-map containing Pearson's correlations between variables was constructed. The analyses were performed using R software (SOMANATHAN et al., 2004).

## 4.3 RESULTS

### 4.3.1 Temporal Dynamics

The temporal dynamics of $X_{CO2}$ are shown in Figure 2. Overall, the daily and monthly observations of $X_{CO2}$ (Figure 2 A, C) presented significant temporal variability, with an increasing $CO_2$ concentration in the dry season, from May to October, followed by lower values in other months. For the evaluated period (2015 – 2018), the highest averages (maximum values) were observed in October 2015 (395.76 ± 0.20 ppm), 2016 (396.63 ± 0.17 ppm), 2017 (396.44 ± 0.17 ppm), and September 2018 (398.98 ± 0.10 ppm). Meanwhile, the lowest means varied over the study period, especially from December to March, which is the rainy season. Differences of 4.87% (2015), 4.89% (2016), 2.98% (2017), and 5.76% (2018) between the maximum and minimum values were observed.

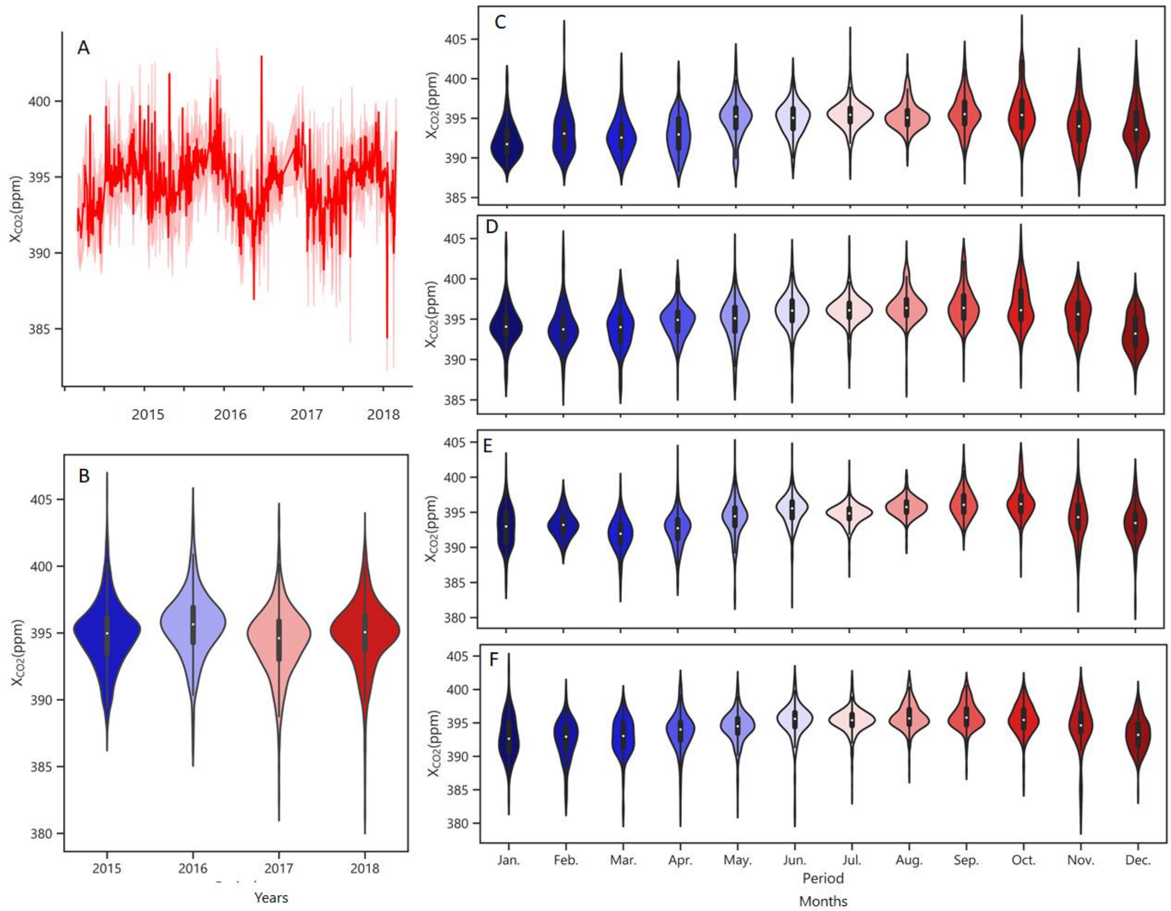


**Figure 2.** Temporal series of $X_{CO2}$ (ppm), including (A) daily observations, (B) annual averages, and monthly averages for (C) 2015, (D) 2016, (E) 2017, and (F) 2018 for the State of Mato Grosso, Brazil.

Despite the seasonality observed for one year, when analyzing different years, the mean values revealed small differences, in which there was only a 1.2 ppm different among the year with the highest mean (2016; 395.57 ± 0.04 ppm) and that with the lowest (2017; 394.37 ± 0.04 ppm). On this basis, a monthly scale temporal variability analysis of $X_{CO2}$ was performed and the results were compared with the SPI (SPI-1), rainfall, $CO_2$ flux, and the EVI for each year studied (Figure 3). Note that all the studied variables presented annual variability with a quasi-parabolic shape, revealing either a maximum or a minimum value throughout the year. The SPI is widely used to characterize dry and wet periods for time scales ranging from 1 to 24 months. In this study, the maximum value for SPI-1 was 1.91, occurring in February 2018, and a minimum value of -2.2 was observed in both July 2016 and July 2017. The highest rainfall volumes occurred between November and March, whereas June and July had the lowest accumulated rainfall values. Moreover, the highest and lowest rainfall values were observed in February 2018 (362.60 mm) and July 2017 (1.90 mm), respectively, which is consistent with the SPI results.

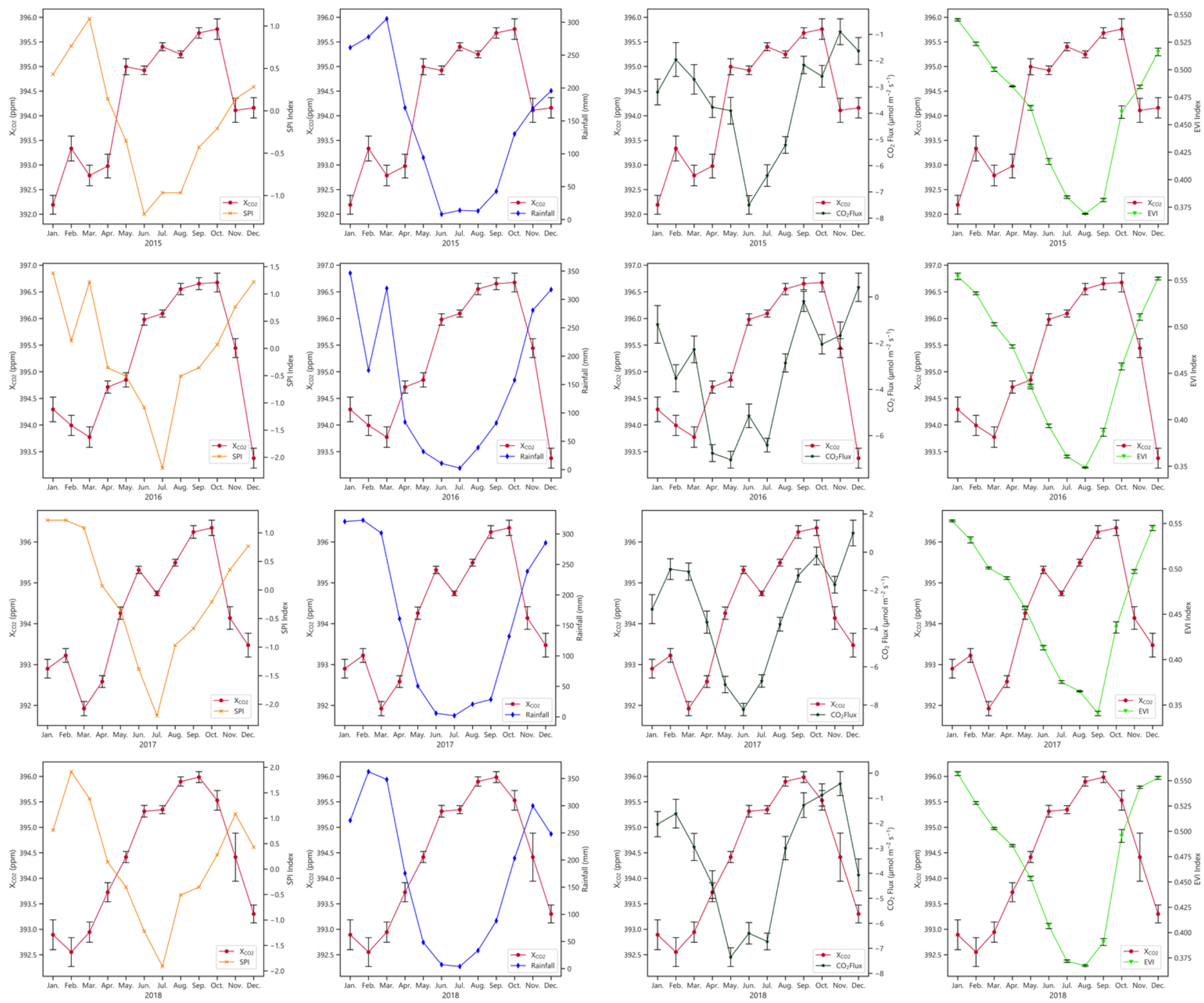


**Figure 3.** Seasonal variability of atmospheric $X_{CO2}$ with (a,b,c,d) the standardized precipitation index (SPI), (e,f,g,h) rainfall (i,j,k,l) $CO_2$ flux, and (m,n,o,p) the enhanced vegetation index (EVI) for the State of Mato Grosso, Brazil.

Regarding $CO_2$ flux, December (1 ± 0.67 µmol $m^{-2}$ $s^{-1}$) and June (-8.23 ± 0.32 µmol $m^{-2}$ $s^{-1}$) of 2017 achieved the highest and lowest averages among the studied years, respectively. Specifically, negative values of $CO_2$ flux were estimated from May and June, and positive values were estimated between November and December. The EVI generally showed lower values in August, and the months with the highest positive values were December and January. Further, $CO_2$ flux was directly related to the highest and lowest means for the EVI, which were observed in January 2018 (0.55 ±

0.001) and September 2016 (0.38 ± 0.004), respectively. The monthly average $CO_2$ flux shown in Figure 3 (i, j, k, and l) for the SMT in the dry season indicates a net absorption of carbon and, for the rainy season, a net loss of carbon to the atmosphere.

The seasonal variation of $X_{CO2}$ has an inflection between the months of February/March and September/October that is clear for each study year. An increase in $X_{CO2}$ and a decrease in the SPI-1 were consistently observed from June to July, whereas an increase in the SPI and a decrease in $X_{CO2}$ occurred around October. Specifically, the intercept between the decrease in $X_{CO2}$ and the increase in SPI-1 was observed in November. For rainfall, these intercepts were concentrated in April and November, respectively, and for $CO_2$ flux and the EVI, the intercepts were observed between April and May, whereas November, as is consistent for the other studies variables, was the predominant month in the intercept between the decrease in $X_{CO2}$ and increases in $CO_2$ flux and EVI.

The EVI had the highest negative correlation with $X_{CO2}$ (Figure 5), and was also significantly correlated with $CO_2$ flux. Hence, the EVI was used as a proxy in the temporal variation analysis to compare LULC in the SMT (Figure 4). The results show that land use directly influences temporal EVI dynamics, which are inversely correlated with $X_{CO2}$ and directly correlated with $CO_2$ flux. A smaller variability in the EVI values was observed in forested areas, whereas in areas of anthropic use, a significant reduction in the EVI was observed. In forest areas, the critical period was concentrated between May and August, whereas for areas with anthropic use, the critical period occurred between June and October. In areas with watercourses, the critical period was between February and September.

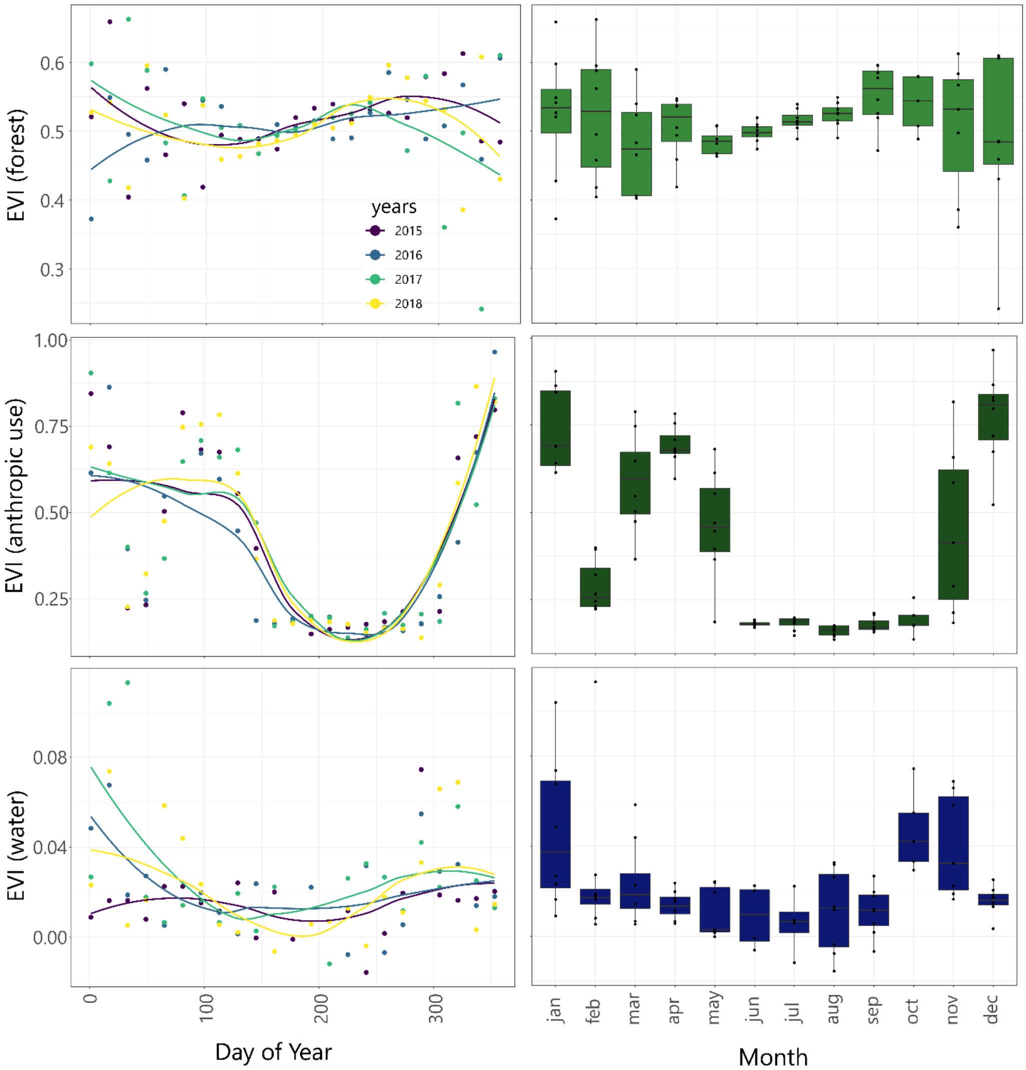


**Figure 4.** Temporal series of land use according to the enhanced vegetation index (EVI) for the State of Mato Grosso, Brazil.

A Pearson's correlation analysis was applied to relate $X_{CO2}$ to the other variables (Figure 5). As expected, $X_{CO2}$ showed a significant negative linear relationship ($p < 0.05$) with rainfall, SPI-12, and the EVI. The correlation coefficients between $X_{CO2}$ and these variables were -0.71, -0.65, and -0.76, respectively.

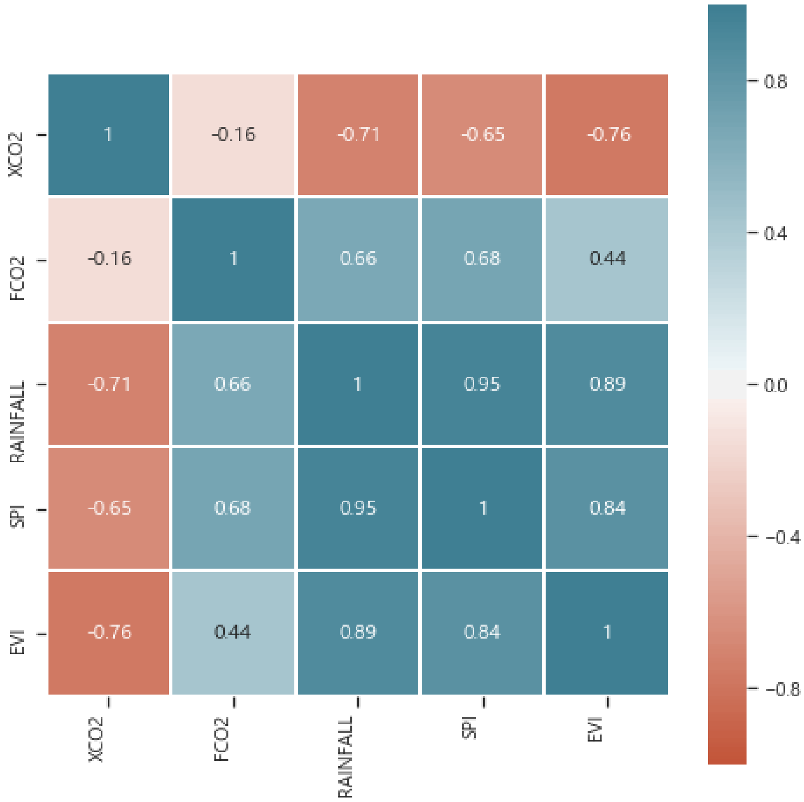


**Figure 5.** Heat-map of Pearson's correlation matrix for $X_{CO2}$ with $CO_2$ flux ($FCO_2$), rainfall, and standardized precipitation index (SPI-12) for the State of Mato Grosso, Brazil.

The $CO_2$ flux (Figure 5) exhibited positive correlations (r = 0.66, 0.68, and 0.44, respectively) with rainfall, SPI, and the EVI, which may be because it demonstrates the vigor of photosynthetically active vegetation, allowing it to capture the absorption from carbon sequestration in the process of photosynthesis and loss through respiration.

#### 4.3.2. Spatial dynamics

The NDFI (Figure 6) showed an expansion in variations in land cover from the exposed soil area (bare soil) to the anthropization area in the southeastern region of the SMT between 2016 and 2017. Meanwhile, in the northeastern region, soybean crop areas were replaced with exposed soil.

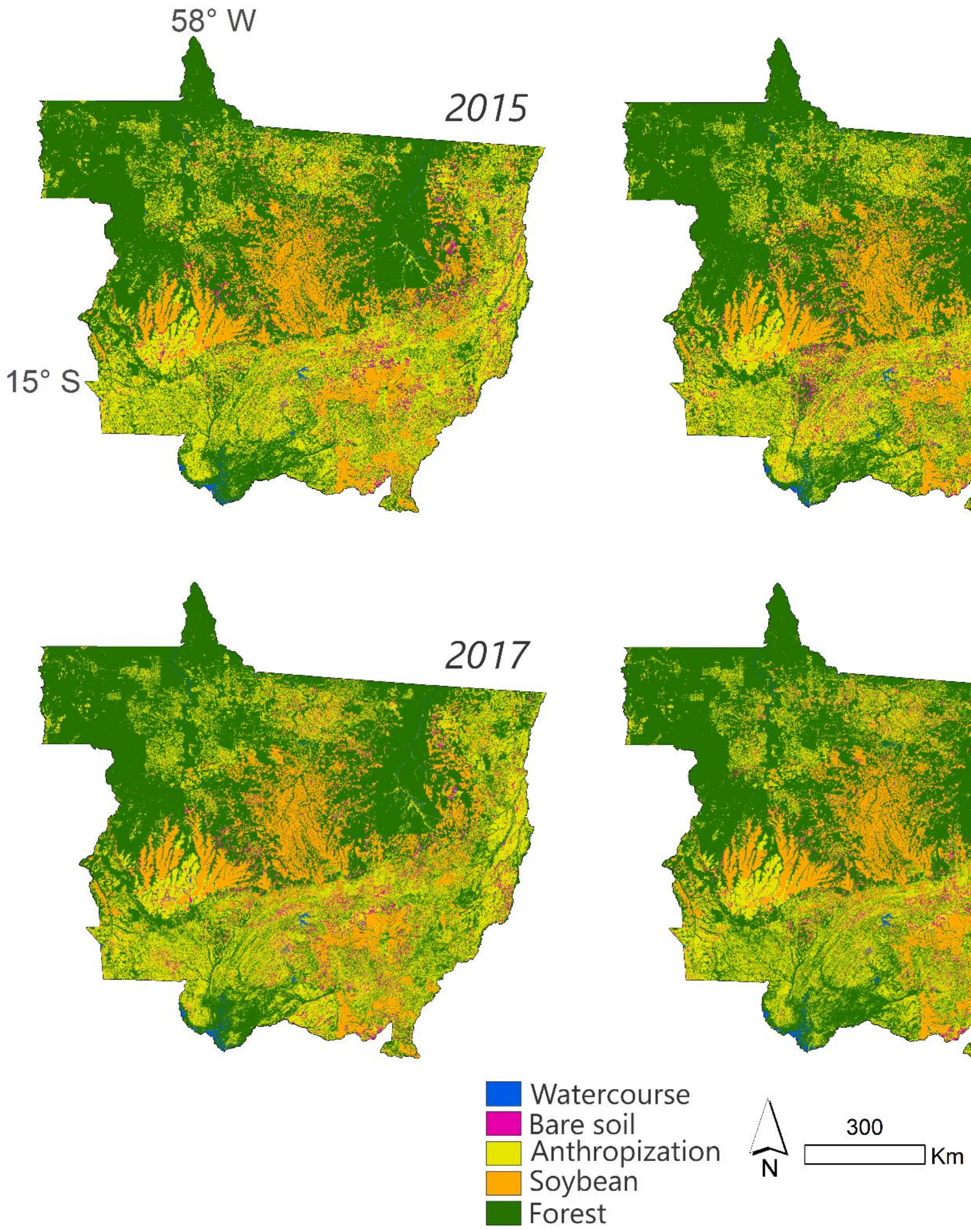


**Figure 6.** Land use in the State of Mato Grosso, Brazil during 2015, 2016, 2017, and 2018.

In addition, the forest areas underwent significant changes in the southern part of the state, wherein 2015 and 2017 showed a more concentrated distribution of forest than 2016 and 2018. In the northern part of the state, there was an increase in soybean production areas (Figure 6) as a result of direct forest replacement and forest/grassland succession.

The annual average rainfall in 2015 (Figure 7) was the highest in the northwest region, but gradually shifted to the center and north by 2018. According to the rainfall spatialization throughout the SMT, 2015 had the worst distribution, 2016 and 2018 had an equal distribution, and 2018 had the highest distribution and volume of rainfall.

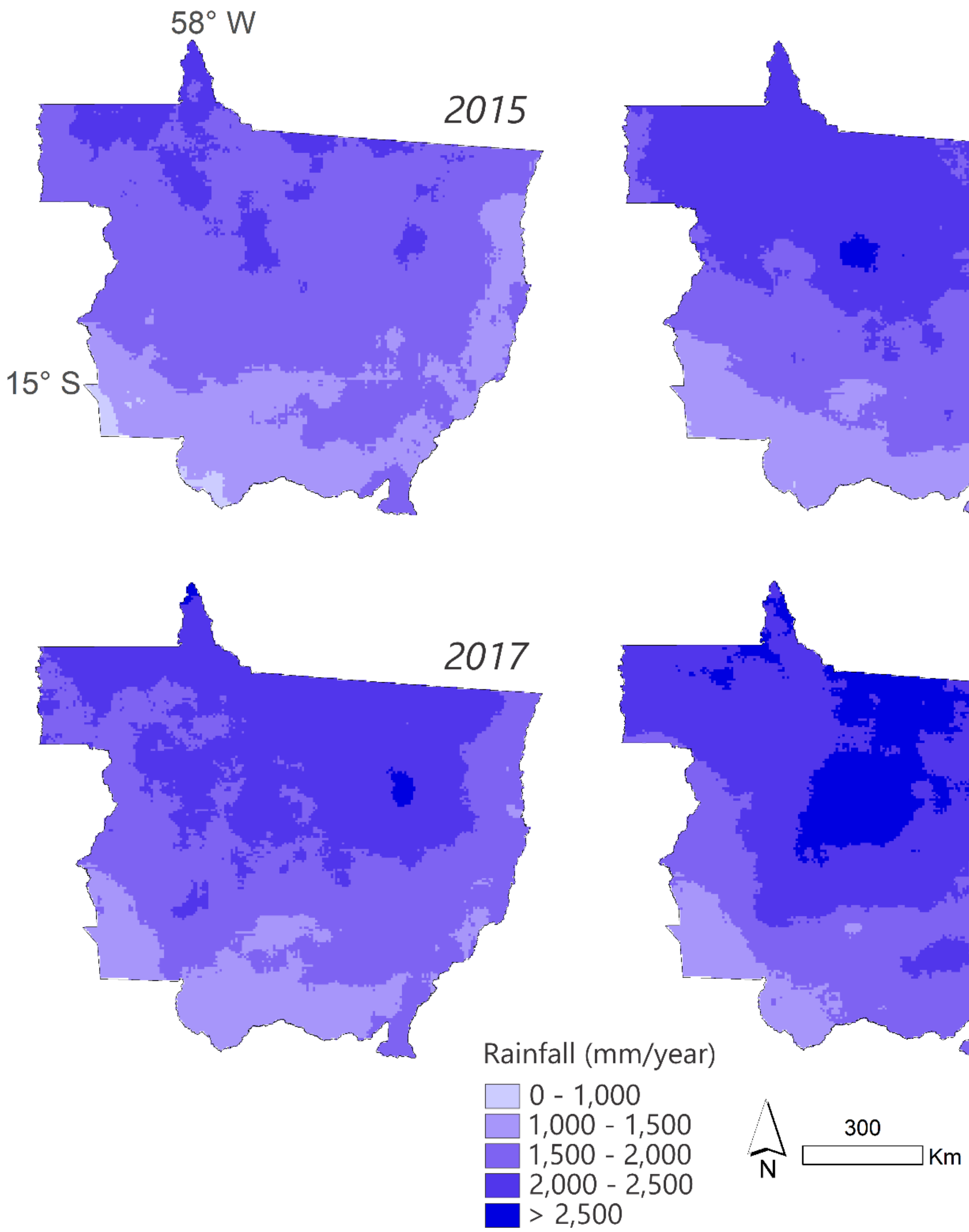


**Figure 7.** Average annual rainfall for the State of Mato Grosso, Brazil via Climate Hazards Group InfraRed Precipitation with Station (CHIRPS) data for 2015, 2016, 2017, and 2018.

The SPI-12 shows varying drought conditions in the SMT during the study period (Figure 8). In particular, the average annual results showed that among the years evaluated, 2015 experienced the most severe drought, while 2018 was the wettest year. The northeast, north, northwest, west, and southwest regions (Figure 8) in 2015 presented drought records associated with extreme to moderate droughts, revealing the highest annual drought spatialization, as compared with 2016, 2017, and 2018. Further, 2018 had the lowest total average annual drought.

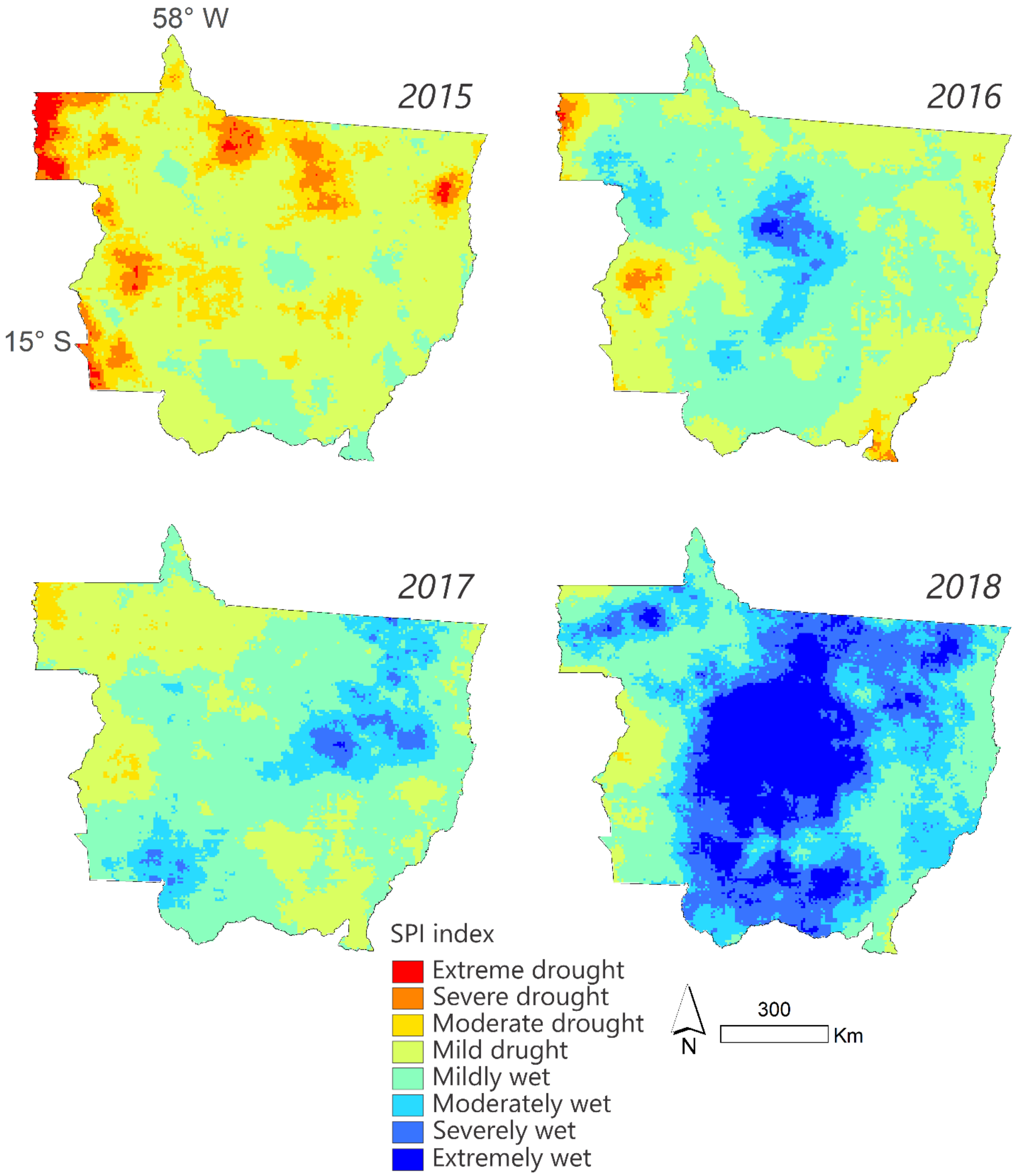


**Figure 8.** Standardized precipitation index (SPI-12) values for the State of Mato Grosso, Brazil via Climate Hazards Group InfraRed Precipitation with Station (CHIRPS) data for 2015, 2016, 2017, and 2018.

The $CO_2$ flux results showed that the amount of $CO_2$ was minimal in the northwest and northeast regions, which was consistent for all study years. Note that these regions are characterized by the highest percentages of forest vegetation areas

(Figure 9). Conversely, in the mid-north regions, the $CO_2$ flux exhibited opposite behavior, revealing higher amounts and positive values for $CO_2$. Note that this region is a major soybean producing area in the state, consisting of municipalities such as Sorriso, Sapezal, and Sinop (Figure 9).

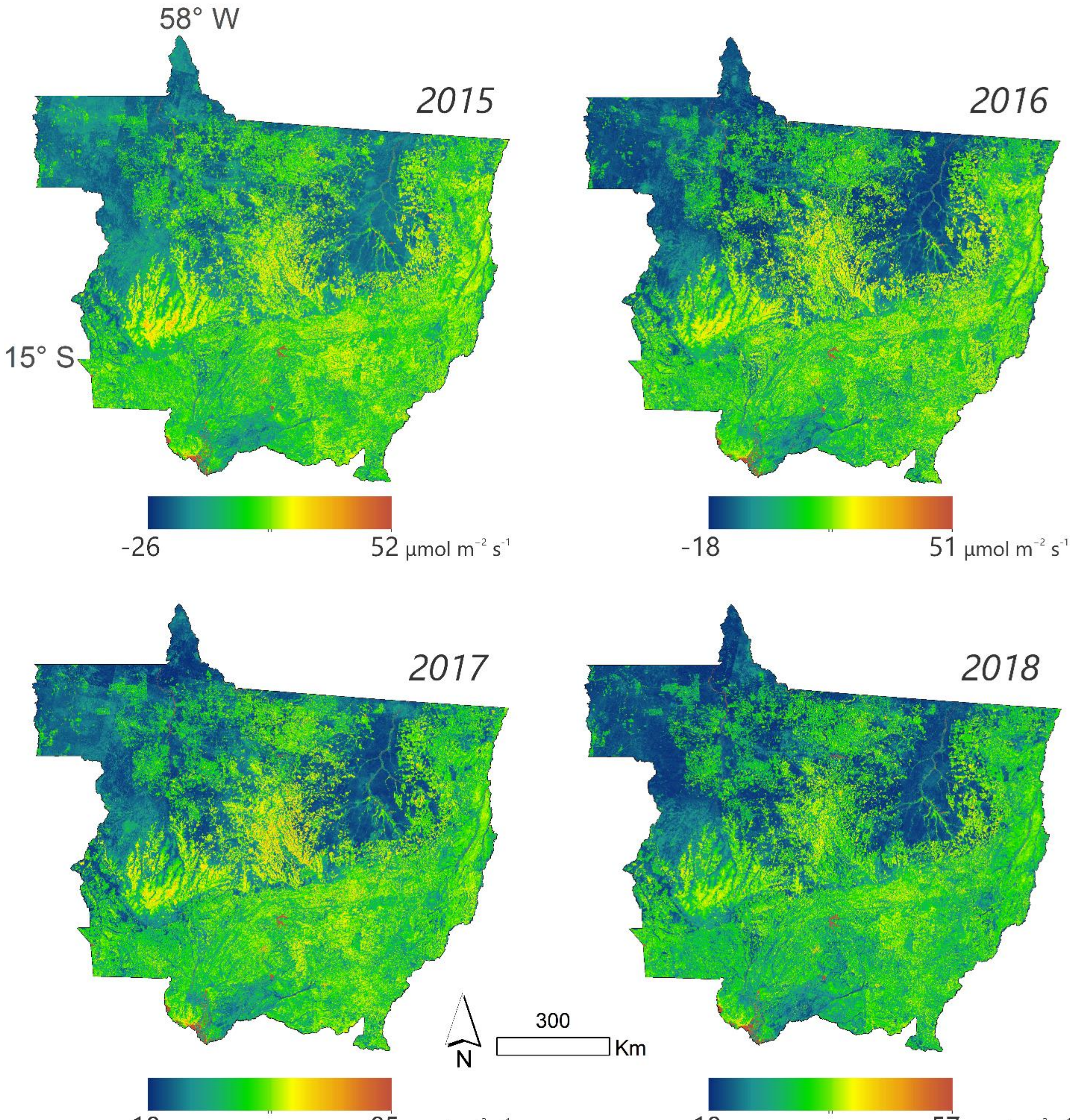


**Figure 9.** $CO_2$ flux for the State of Mato Grosso, Brazil for 2015, 2016, 2017, and 2018.

The spatial pattern results of the atmospheric concentration of annual averages of $X_{CO2}$ revealed that the maximum observed values were 402 ppm to 405 ppm over the study period (Figure 10). In the mid-north regions, hotspots were observed in 2015 and 2016. Note that 2015 and 2016 had higher atmospheric spatial patterns of $X_{CO2}$ concentration (ppm) than 2017 and 2018. Further, in the northwest and northeast regions, we observed higher atmospheric spatial concentrations of $X_{CO2}$. Therefore, the hotspots had lower values in 2018 than the other years, showing a 0.7% reduction in the annual averages of $X_{CO2}$ concentration (ppm), as compared with that of 2015 (Figure 10).

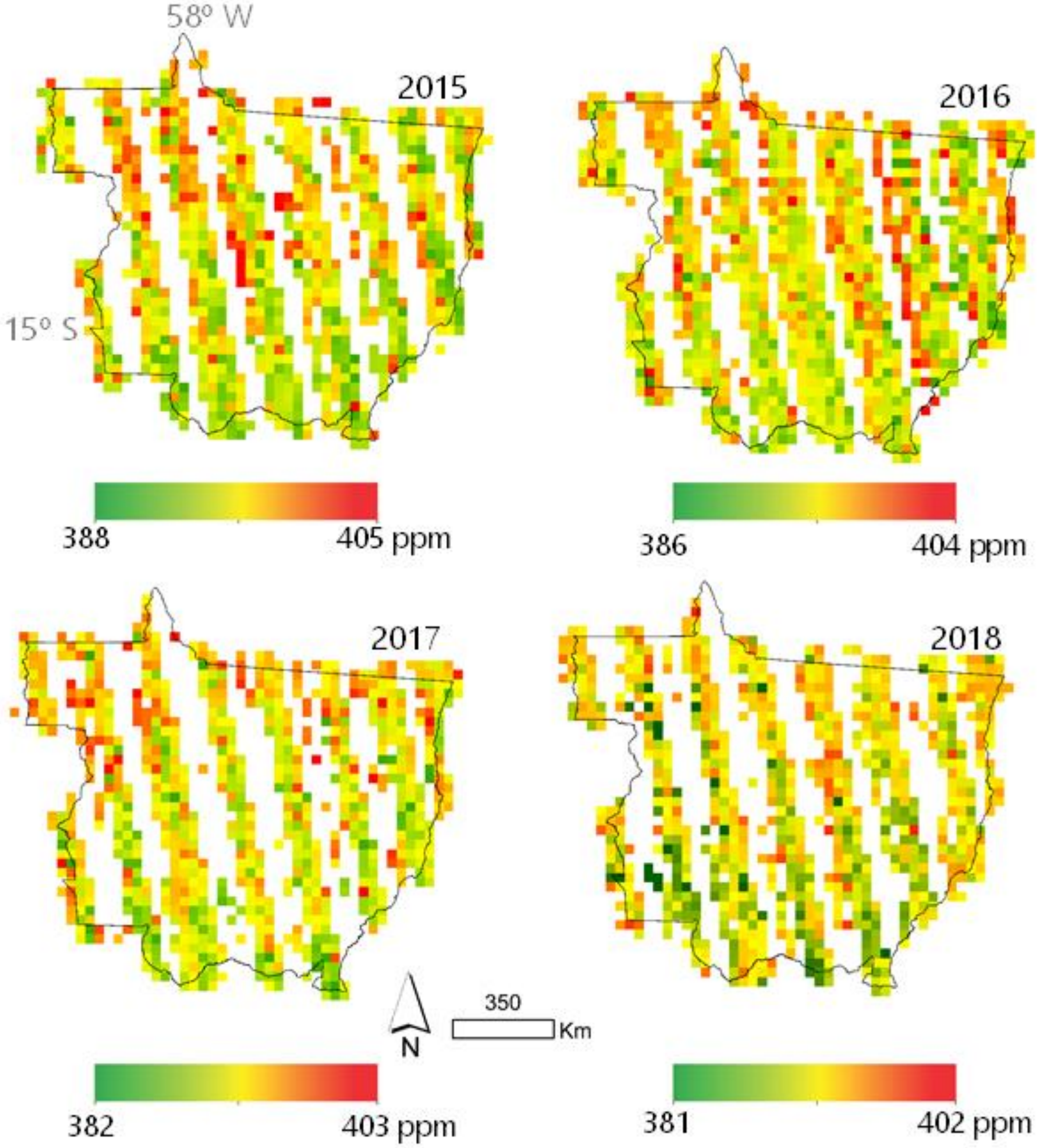


**Figure 10.** Spatial patterns of atmospheric XCO2 concentration for the State of Mato Grosso, Brazil for 2015, 2016, 2017, and 2018.

## 4.4 DISCUSSION

### 4.4.1 Temporal Dynamics

The regional oscillating atmospheric $CO_2$ concentrations presented in the Keeling Curve (KEELING; BACASTOW; BAINBRIDGE, 1976) from observations at Mauna Loa, Hawaii, USA, which are directly related to seasonal fluctuations, are similar to those observed in this study (Figure 3) (PILI; VIOLANDA, 2020). Jiang and

Yung (2019) found that the temporal variability of atmospheric $CO_2$ may present, in addition to annual and semiannual cycles, inter-seasonal and inter-annual cycles.

In this study, we observed the annual variability of the carbon cycle in the SMT, in which there were smaller $X_{CO2}$ values in the rainy season (from November to March), which coincides with the results of Parazoo et al. (2013) and de Oliveira-Júnior et al. (2021). Rossi and Santos (2020) also observed that the variation in carbon assimilation (gross primary production) by biomes in the SMT is strongly seasonal and related to rainfall. Specifically, in the rainy season, the $CO_2$ flux showed positive average values, indicating a transfer of carbon to the atmosphere in the form of $CO_2$, because the values analyzed were not classified for different land uses, such as pasture, forest, agriculture, city, and exposed soil.

The interaction between the biosphere and atmosphere in contrasting biomas has been presented in several studies as a critical aspect in determining the inter-annual variability of atmospheric $CO_2$ (BUERMANN et al., 2007; SHIA et al., 2006). However, several factors regulate this relationship. Jiang and Yung (2019) identified that the Madden-Julian Oscillation, sudden stratospheric warming, the El Niño-Southern Oscillation, the tropospheric biennial oscillation, annular modes, and regional aspects, such as severe droughts, are potential drivers of atmospheric $CO_2$ oscillations.

Some studies have shown the effects of El Niño (CHATTERJEE et al., 2017; ELDERING et al., 2017; FAN et al., 2019) and severe droughts (LIU et al., 2018; NOGUEIRA et al., 2015) on the atmospheric $CO_2$ concentration in the southern hemisphere. For example, Morais Filho et al. (2021) evaluated the temporal variability of $X_{CO2}$ over three main agricultural crops (soy, pasture, and sugarcane) in Brazil, and observed an increase in $X_{CO2}$ in the rainy seasons and a reduction in the dry period. Other researches, shows that the low rate of photosynthesis and the gradual increase in temperature, along with the increase in the rate of decomposition and respiratory activity we have the increases the atmospheric $CO_2$ concentration (FALAHATKAR; MOUSAVI; FARAJZADEH, 2017; SCRIPPS OCEANOGRAPHY, 2022; SIABI; FALAHATKAR; ALAVI, 2019). Our results showed a strong correlation of $X_{CO2}$ with the drought index (SPI), rainfall, and vegetation, which were the main factors controlling the temporal variability of $X_{CO2}$ over the SMT.

The EVI detects vegetation conditions by isolating the soil effect (HUETE et al., 2002). In this study, our results revealed strong correlations between the EVI and the SPI and rainfall in regard to their effect on atmospheric $CO_2$ concentration. Overall, these correlations express the sensitivity of $X_{CO2}$ to land cover and photosynthesis processes.

A negative relationship between $X_{CO2}$ and rainfall was also observed by Chhabra and Gohel (2020) and Golkar et al. (2020). Note that the relationship between atmospheric $CO_2$ concentration and rainfall will always be negative, as reported by Wang, Zeng, and Wang (2016), because the sensitivity of the vegetation cover to rainfall affects the dynamics of $CO_2$ in the atmosphere by increasing capture via photosynthesis.

The positive or negative correlations of $X_{CO2}$ with the other variables may be directly correlated to combination effects, such as spatial and temporal resolutions.

**4.4.2 Spatial Dynamics**

LULC changes are driving factors of the carbon cycle. Specifically, different land uses influence $CO_2$ absorption and $CO_2$ flux to the atmosphere (SIABI; FALAHATKAR; ALAVI, 2019). For example, forested areas tend to sequester $CO_2$ from the atmosphere (CASTRO-MAGNANI et al., 2021; MARCOS-MARTINEZ et al., 2019), incorporate carbon into their biomass, and split it into the soil. Studies have shown that the carbon sinks of intact African and Amazonian rainforests have peaked (BRIENEN et al., 2015; GATTI et al., 2014; HUBAU et al., 2020). Chhabra and Gohel (2020) highlighted the importance of vegetation and ground cover in controlling atmospheric $CO_2$ emissions, as supported by the lower $CO_2$ fluxes observed in the northwestern and northeastern regions of the SMT.

Note that the areas in the mid-north of the SMT had a concentration of positive values of the highest annual averages of $CO_2$ flux, indicating carbon loss to the atmosphere via respiration. Also note that this region has intense farming (Silva Junior et al. 2020). Land use change (BACCINI et al., 2017; BRANDT et al., 2018) can explain the higher observations of $CO_2$ fluxes in these areas. In particular, net carbon fluxes from LULC changes accounted for 12.5% of anthropogenic carbon emissions over the last decade (HOUGHTON et al., 2012).

Increase of 3 ppm and 2 ppm in 2015 and 2016, respectively, in the observed maximum annual atmospheric $X_{CO2}$ concentration, as compared with that of 2018, can be attributed to influence of El Niño (CHATTERJEE et al., 2017; DE OLIVEIRA-JÚNIOR et al., 2018; GATTI et al., 2014; LIU et al., 2017), which contributes to a global increase in atmospheric $CO_2$ as a response of the terrestrial carbon cycle induced by changing weather patterns (CHHABRA; GOHEL, 2019). Based on the observations from the OCO-2 satellite, an increase in atmospheric $CO_2$ concentrations over the tropical Pacific Ocean was observed during 2015 – 2016, confirming the influence of El Niño (CHATTERJEE et al., 2017).

The severe drought observed in 2015 was also the result of El Niño events (DE OLIVEIRA-JÚNIOR et al., 2018). Meanwhile, 2018 was an extremely wet year in the central region of the SMT, which ultimately resulted in lower $X_{CO2}$ values. Chhabra and Gohel (2020) mentioned that high rainfall contributes to vegetation growth and development and increases photosynthetic activity, thus reducing the atmospheric $CO_2$ concentration. Thus, monthly $CO_2$ concentration fluctuations can be linked to water vapor content, rainfall, and vegetation cover (TIWARI; REVADEKAR; RAVI KUMAR, 2013; WANG; ZENG; WANG, 2016).

Figure 8 and 9 show the direct links between changes in atmospheric radiative forcing and the distribution of atmospheric heating by maintaining heat concentration, which causes changes in the hydrologic cycle and atmospheric moisture content (RICHTER; XIE, 2008), ultimately affecting rainfall (HELD; SODEN, 2006).

## 4.5 CONCLUSIONS

The temporal variability of $X_{CO2}$ is inversely related to rainfall events, with peak concentrations occurring in drier periods, from May to October, throughout the SMT. Variations in land surface temperature related to land-use changes increase $CO_2$ concentrations and result in more $CO_2$ in the atmosphere, especially in years of low rainfall.

Regarding spatial variability, converting forests into other land uses caused increased $CO_2$ concentrations in the SMT. Similarly, areas with large forest ranges presented lower $CO_2$ concentrations, mitigating climate change.

Therefore, not only $X_{CO2}$ but also $CO_2$ concentrations are directly related to LULC in complex systems that are affected by climatic variables and processes, such as photosynthesis and soil respiration.

Thus, we conclude that, Remote Sensing is an important resource in monitoring the spatio-temporal dynamics of $CO_2$ and detecting possible changes with time series in the SMT.

## CHAPTER 5 – GENERAL CONCLUSIONS

Monitoring the Earth's surface and the dynamics of its vegetation studies using remote sensing techniques are essential to the environment. With the advent of automatics and programming technologies, it is possible to monitor the entire Brazilian territory using remote sensing techniques. These tools provide and contributes to the distinction and characterization of forests, agriculture, weather, and $CO_2$ flow. Sensors on board environmental satellites provide data that help to understand the global distribution of vegetation types, as well as their biophysical and structural properties and spatial-temporal variations.

Land use and land cover change is currently one of the biggest impacts caused to the environment and having several consequences, as the loss of local biodiversity and C (carbon) emission. This data survey is essential to report on the achievement of the targets signed with the civil society and international organizations, besides being important in the elaboration of strategies for the improvement of public policies. Thus, the land use and cover change survey in a timely and objective way contribute to action strategies for commercialization establishment, regulation of strategic stocks, and growth of new areas in a controlled manner, which makes it economically and environmentally important for a country.

The results found in this study present an important contribution to a better understanding of greenhouse gases dynamics in the states of Mato Grosso and Mato Grosso do Sul. Thus, in this study the total soil respiration and the multispectral vegetation indices used to evaluate the spatial-temporal dynamics in areas with contrasting land use with soybean cultivation in the state of Mato Grosso and in a monoculture system of eucalyptus species in the state of Mato Grosso do Sul, show that in areas of native forest there are higher emissions of $FCO_2$ and lower values for $CO_2$Flux compared to soybean areas in the northern region of the state of Mato Grosso. When we applied remote sensing to assess the spatial-temporal dynamics of $CO_2$ across the state of Mato Grosso, we detected that not only $X_{CO2}$, but also $CO_2$ flux are directly related to land use and land cover change (LULC) in complex systems that are affected by climatic variables and processes, such as photosynthesis and soil respiration. For the state of Mato Grosso do Sul the results show that there is a strong correlation between canopy spectral response and chlorophyll content in eucalypt species, with the most important spectral regions being green and near infrared. The results make it possible to differentiate $FCO_2$ among eucalypt species using sensors airborne to unmanned aerial vehicle. This relation depends on the contribution of roots, soil organic matter, plant residues, canopy spectral response, and chlorophyll content of the eucalypt species.

Therefore, in order to collaborate with sustainable production, reduction of C emissions and contribute to the 17 Sustainable Development Goals (SDGs), to take urgent action to combat climate change and its impacts, we suggest that the information obtained in this work can be used to support new research in decision making by society, over the effects of climate change through technical strategies, but also for agencies seeking solid strategies for environmental conservation and sustainable development.

In this sense, strategies such as agricultural inventories considering $CO_2$ emissions from the soil estimates over integrated agricultural systems, which include arboreal plants as an element of the agroecosystems, soil management, such as no-till farming practices, and crop rotation, can and should play an important role in mitigating deforestation and $CO_2$ emissions at the soil-atmosphere interface.

**References**

ABIMILHO. **Associação Brasileira das Indústrias do Milho**. 2021. Disponível em: <https://www.abimilho.com.br/estatisticas>.

ABREU, E. S. De; FEIO, P. H. B. Impactos resultantes da expansão das monoculturas de soja e eucalipto entre 2010 a 2019 na bacia do rio Macacoari, Estado do Amapá--AP. [s. l.], 2021.

ALIX-GARCIA, J.; GIBBS, H. K. Forest conservation effects of Brazil's zero deforestation cattle agreements undermined by leakage. **Global Environmental Change**, [s. l.], v. 47, p. 201–217, 2017.

ALLEN, R. G.; TASUMI, M.; TREZZA, R.; WATERS, R.; BASTIAANSSEN, W. SEBAL (Surface Energy Balance Algorithms for Land)—Advanced Training and Users Manual—Idaho Implementation (Version 1.0). **The Idaho Department of Water Resources: Boise, ID, USA**, [s. l.], 2002.

ALMEIDA, C. A.; VIEIRA, I. C. G. Expansão territorial da monocultura do eucalipto na Amazônia oriental. **Novos Cadernos NAEA**, [s. l.], v. 25, n. 3, 2022. Disponível em: <https://periodicos.ufpa.br/index.php/ncn/article/view/10501>

ALMEIDA, D. R. A.; STARK, S. C.; CHAZDON, R.; NELSON, B. W.; CESAR, R. G.; MELI, P.; GORGENS, E. B.; DUARTE, M. M.; VALBUENA, R.; MORENO, V. S.; MENDES, A. F.; AMAZONAS, N.; GONÇALVES, N. B.; SILVA, C. A.; SCHIETTI, J.; BRANCALION, P. H. S. The effectiveness of lidar remote sensing for monitoring forest cover attributes and landscape restoration. **Forest Ecology and Management**, [s. l.], v. 438, p. 34–43, 2019. Disponível em: <https://www.sciencedirect.com/science/article/pii/S037811271831819X>

ALMEIDA, R. F.; DE BORTOLI TEIXEIRA, D.; MONTANARI, R.; BOLONHEZI, A. C.; TEIXEIRA, E. B.; MOITINHO, M. R.; PANOSSO, A. R.; SPOKAS, K. A.; JÚNIOR, N. L. S. Ratio of CO2 and O2 as index for categorising soil biological activity in sugarcane areas under contrasting straw management regimes. **Soil Research**, [s. l.], v. 56, n. 4, p. 373–381, 2018.

ALMEIDA, R. F.; SANCHES, B. C. Disponibilidade de carbono orgânico nos solos do cerrado brasileiro. **Scientia Agraria Paranaensis**, [s. l.], v. 13, n. 4, p. 259–264, 2014.

ALVARES, C. A.; STAPE, J. L.; SENTELHAS, P. C.; DE MORAES GONÇALVES, J. L.; SPAROVEK, G. Köppen's climate classification map for Brazil. **Meteorologische Zeitschrift**, [s. l.], v. 22, n. 6, p. 711–728, 2013.

ARNETH, A.; SITCH, S.; PONGRATZ, J.; STOCKER, B. D.; CIAIS, P.; POULTER, B.; BAYER, A. D.; BONDEAU, A.; CALLE, L.; CHINI, L. P.; GASSER, T.; FADER, M.; FRIEDLINGSTEIN, P.; KATO, E.; LI, W.; LINDESKOG, M.; NABEL, J. E. M. S.; PUGH, T. A. M.; ROBERTSON, E.; VIOVY, N.; YUE, C.; ZAEHLE, S. Historical carbon dioxide emissions caused by land-use changes are possibly larger than assumed. **Nature Geoscience**, [s. l.], v. 10, n. 2, p. 79–84, 2017.

AWUCHI, C.; AWUCHI, C.; UKPE, A.; ASOEGWU, C.; UYO, C.; NGOKA, K. Environmental Impacts of Food and Agricultural Production: A Systematic Review. **European Academic Research**, [s. l.], v. 8, p. 1120–1135, 2020.

BACCINI, A.; GOETZ, S. J.; WALKER, W. S.; LAPORTE, N. T.; SUN, M.; SULLA-MENASHE, D.; HACKLER, J.; BECK, P. S. A.; DUBAYAH, R.; FRIEDL, M. A.; SAMANTA, S.; HOUGHTON, R. A. Estimated carbon dioxide emissions from tropical deforestation improved by carbon-density maps. **Nature Climate Change**, [s. l.], v. 2, n. 3, p. 182–185, 2012.

BACCINI, A.; WALKER, W.; CARVALHO, L.; FARINA, M.; SULLA-MENASHE, D.; HOUGHTON, R. A. Tropical forests are a net carbon source based on aboveground measurements of gain and loss. **Science**, United States, v. 358, n. 6360, p. 230–234, 2017.

BAEZ-VILLANUEVA, O. M.; ZAMBRANO-BIGIARINI, M.; RIBBE, L.; NAUDITT, A.; GIRALDO-OSORIO, J. D.; THINH, N. X. Temporal and spatial evaluation of satellite rainfall estimates over different regions in Latin-America. **Atmospheric Research**, [s. l.], v. 213, p. 34–50, 2018.

BAI, B.; PEVIANI, A.; VAN DER HORST, S.; GAMM, M.; SNEL, B.; BENTSINK, L.; HANSON, J. Extensive translational regulation during seed germination revealed by polysomal profiling. **New Phytologist**, [s. l.], v. 214, n. 1, p. 233–244, 2017.

BARBOSA, V. **A última gota**. [s.l.] : Editora Planeta do Brasil, 2015.

BARET, F.; GUYOT, G.; MAJOR, D. J. Crop biomass evaluation using radiometric measurements. **Photogrammetria**, [s. l.], v. 43, n. 5, p. 241–256, 1989. Disponível em: <https://www.sciencedirect.com/science/article/pii/003186638990001X>

BARNES, M. L.; BRESHEARS, D. D.; LAW, D. J.; VAN LEEUWEN, W. J. D.; MONSON, R. K.; FOJTIK, A. C.; BARRON-GAFFORD, G. A.; MOORE, D. J. P. Beyond greenness: Detecting temporal changes in photosynthetic capacity with hyperspectral reflectance data. **PLoS ONE**, [s. l.], v. 12, n. 12, p. 1–17, 2017.

BASHAR, M.; ZHOU, Y. li Jun,"Effect of Soil Strength and Soil Physical Properties on Performance of Tillage Machines". **Journal of Earth Science and Engineering**, [s. l.], p. 251–255, 2015.

BASTIAANSSEN, W. G. M.; MENENTI, M.; FEDDES, R. A.; HOLTSLAG, A. A. M. A remote sensing surface energy balance algorithm for land (SEBAL). 1. Formulation. **Journal of Hydrology**, [s. l.], v. 212–213, p. 198–212, 1998. a. Disponível em: <https://linkinghub.elsevier.com/retrieve/pii/S0022169498002534>

BASTIAANSSEN, W. G. M.; PELGRUM, H.; WANG, J.; MA, Y.; MORENO, J. F.; ROERINK, G. J.; VAN DER WAL, T. A remote sensing surface energy balance algorithm for land (SEBAL). **Journal of Hydrology**, [s. l.], v. 212–213, p. 213–229, 1998. b. Disponível em: <https://linkinghub.elsevier.com/retrieve/pii/S0022169498002546>

BATISTA FARIAS, A. Contexto sócio-histórico e econômico no Norte de Mato Grosso (caso de Sinop): a expansão da fronteira agrícola. **Em Tempo de Histórias**, [s. l.], n. 31, 2018.

BATJES, N. H. **Management options for reducing CO2-concentrations in the atmosphere by increasing carbon sequestration in the soil**. [s.l.] : International Soil Reference and Information Centre Wageningen, 1999.

BERENGUER, E.; FERREIRA, J.; GARDNER, T. A.; ARAGÃO, L. E. O. C.; DE CAMARGO, P. B.; CERRI, C. E.; DURIGAN, M.; OLIVEIRA, R. C. De; VIEIRA, I. C. G.; BARLOW, J. A large-scale field assessment of carbon stocks in human-modified tropical forests. **Global Change Biology**, [s. l.], v. 20, n. 12, p. 3713–3726, 2014. Disponível em: <https://onlinelibrary.wiley.com/doi/10.1111/gcb.12627>

BERNOUX, M.; DA CONCEIÇÃO SANTANA CARVALHO, M.; VOLKOFF, B.; CERRI, C. C. Brazil's Soil Carbon Stocks. **Soil Science Society of America Journal**, [s. l.], v. 66, n. 3, p. 888–896, 2002. Disponível em: <http://doi.wiley.com/10.2136/sssaj2002.8880>

BONAN, G. B. Forests and Climate Change: Forcings, Feedbacks, and the Climate Benefits of Forests. **Science**, [s. l.], v. 320, n. 5882, p. 1444–1449, 2008. Disponível em: <https://www.science.org/doi/10.1126/science.1155121>

BOND-LAMBERTY, B.; THOMSON, A. Temperature-associated increases in the global soil respiration record. **Nature**, [s. l.], v. 464, n. 7288, p. 579–582, 2010. Disponível em: <https://doi.org/10.1038/nature08930>

BOND-LAMBERTY, B.; WANG, C.; GOWER, S. T. A global relationship between the heterotrophic and autotrophic components of soil respiration? **Global Change Biology**, [s. l.], v. 10, n. 10, p. 1756–1766, 2004. Disponível em: <https://onlinelibrary.wiley.com/doi/10.1111/j.1365-2486.2004.00816.x>

BOOTH, T. H. Eucalypt plantations and climate change. **Forest Ecology and Management**, [s. l.], v. 301, p. 28–34, 2013. Disponível em: <https://linkinghub.elsevier.com/retrieve/pii/S0378112712002125>

BRANDT, M.; WIGNERON, J. P.; CHAVE, J.; TAGESSON, T.; PENUELAS, J.; CIAIS, P.; RASMUSSEN, K.; TIAN, F.; MBOW, C.; AL-YAARI, A.; RODRIGUEZ-FERNANDEZ, N.; SCHURGERS, G.; ZHANG, W.; CHANG, J.; KERR, Y.; VERGER, A.; TUCKER, C.; MIALON, A.; RASMUSSEN, L. V.; FAN, L.; FENSHOLT, R. Satellite passive microwaves reveal recent climate-induced carbon losses in African drylands. **Nature Ecology and Evolution**, [s. l.], v. 2, n. 5, p. 827–835, 2018.

BRIENEN, R. J. W. et al. Long-term decline of the Amazon carbon sink. **Nature**, [s. l.], v. 519, n. 7543, p. 344–348, 2015. Disponível em: <https://doi.org/10.1038/nature14283>

BRUHWILER, L.; BASU, S.; BUTLER, J. H.; CHATTERJEE, A.; DLUGOKENCKY, E.; KENNEY, M. A.; MCCOMISKEY, A.; MONTZKA, S. A.; STANITSKI, D. Observations of greenhouse gases as climate indicators. **Climatic Change**, [s. l.], v. 165, n. 1–2, p. 12, 2021. Disponível em: <https://link.springer.com/10.1007/s10584-021-03001-7>

BUERMANN, W.; LINTNER, B. R.; KOVEN, C. D.; ANGERT, A.; PINZON, J. E.; TUCKER, C. J.; FUNG, I. Y. The changing carbon cycle at Mauna Loa Observatory. **Proceedings of the National Academy of Sciences of the United States of America**, [s. l.], v. 104, n. 11, p. 4249–4254, 2007.

BUNCE, J. A. Carbon dioxide effects on stomatal responses to the environment and water use by crops under field conditions. **Oecologia**, [s. l.], v. 140, n. 1, p. 1–10, 2004. Disponível em: <http://link.springer.com/10.1007/s00442-003-1401-6>

BYERS, E.; KREY, V.; KRIEGLER, E.; RIAHI, K.; SCHAEFFER, R.; KIKSTRA, J.; LAMBOLL, R.; NICHOLLS, Z.; SANDSTAD, M.; SMITH, C.; VAN DER WIJST, K.; LECOCQ, F.; PORTUGAL-PEREIRA, J.; SAHEB, Y.; STROMANN, A.; WINKLER, H.; AUER, C.; BRUTSCHIN, E.; LEPAULT, C.; MULLER-CASSERES, E.; GIDDEN, M.; HUPPMANN, D.; KOLP, P.; MARANGONI, G.; WERNING, M.; CALVIN, K.; GUIVARCH, C.; HASEGAWA, T.; PETERS, G.; STEINBERGER, J.; TAVONI, M.; VAN VUUREN, D.; AL -KHOURDAJIE, A.; FORSTER, P.; LEWIS, J.; MEINSHAUSEN, M.; ROGELJ, J.; SAMSET, B.; SKEIE, R. **AR6 Scenarios Database**, Intergovernmental Panel on Climate Change, 2022. Disponível em: <https://pure.iiasa.ac.at/id/eprint/18399/>

CASTRO-MAGNANI, M.; SANCHEZ-AZOFEIFA, A.; METTERNICHT, G.; LAAKSO, K. Integration of remote-sensing based metrics and econometric models to assess the socio-economic contributions of carbon sequestration in unmanaged tropical dry forests. **Environmental and Sustainability Indicators**, [s. l.], v. 9, p. 100100, 2021. Disponível em: <https://www.sciencedirect.com/science/article/pii/S2665972721000015>

CAÚLA, R. H.; OLIVEIRA-JÚNIOR, J. F.; LYRA, G. B.; DELGADO, R. C.; HEILBRON FILHO, P. F. L. Overview of fire foci causes and locations in Brazil based on meteorological satellite data from 1998 to 2011. **Environmental Earth Sciences**, [s. l.], v. 74, n. 2, p. 1497–1508, 2015.

CAVALCANTE, R. B. L.; FERREIRA, D. B. da S.; PONTES, P. R. M.; TEDESCHI, R. G.; DA COSTA, C. P. W.; DE SOUZA, E. B. Evaluation of extreme rainfall indices from CHIRPS precipitation estimates over the Brazilian Amazonia. **Atmospheric Research**, [s. l.], v. 238, p. 104879, 2020. Disponível em: <https://www.sciencedirect.com/science/article/pii/S0169809519314073>

CHATTERJEE, A.; GIERACH, M. M.; SUTTON, A. J.; FEELY, R. A.; CRISP, D.;

ELDERING, A.; GUNSON, M. R.; O’DELL, C. W.; STEPHENS, B. B.; SCHIMEL, D. S. Influence of El Niño on atmospheric $CO_2$ over the tropical Pacific Ocean: Findings from NASA’s OCO-2 mission. **Science**, [s. l.], v. 358, n. 6360, 2017.

CHEN, G.; YANG, Y.; YANG, Z.; XIE, J.; GUO, J.; GAO, R.; YIN, Y.; ROBINSON, D. Accelerated soil carbon turnover under tree plantations limits soil carbon storage. **Scientific Reports**, [s. l.], v. 6, n. 1, p. 19693, 2016. Disponível em: <https://doi.org/10.1038/srep19693>

CHEN, R.; SENBAYRAM, M.; BLAGODATSKY, S.; MYACHINA, O.; DITTERT, K.; LIN, X.; BLAGODATSKAYA, E.; KUZYAKOV, Y. Soil C and N availability determine the priming effect: microbial N mining and stoichiometric decomposition theories. **Global change biology**, [s. l.], v. 20, n. 7, p. 2356–2367, 2014.

CHEN, Y.; XIN, Y. Implications of geoengineering under the 1.5 °C target: Analysis and policy suggestions. **Advances in Climate Change Research**, [s. l.], v. 8, n. 2, p. 123–129, 2017. Disponível em: <https://linkinghub.elsevier.com/retrieve/pii/S1674927817300400>

CHHABRA, A.; GOHEL, A. Dynamics of atmospheric carbon dioxide over different land cover types in India. **Environmental Monitoring and Assessment**, [s. l.], v. 191, n. 3, p. 799, 2019.

CHRISTENSEN, B. T. Carbon in primary and secondary organomineral complexes. In: **Structure and organic matter storage in agricultural soils**. [s.l.] : CRC Press, 2020. p. 97–165.

CIDIN, A. C. M. **Estoque de carbono em solos brasileiros e potencial de contribuição de mitigação de emissões de gases de efeito estufa. 2016. 76 f**. 2016. Dissertação (Mestrado em Agricultura e Ambiente)-Universidade Federal de São~…, [s. l.], 2016.

COLLALTI, A.; THORNTON, P. E.; CESCATTI, A.; RITA, A.; BORGHETTI, M.; NOLÈ, A.; TROTTA, C.; CIAIS, P.; MATTEUCCI, G. The sensitivity of the forest carbon budget shifts across processes along with stand development and climate change. **Ecological Applications**, [s. l.], v. 29, n. 2, 2019. Disponível em: <https://onlinelibrary.wiley.com/doi/10.1002/eap.1837>

COLTRI, P. P.; RAMIREZ, G. M.; WALTER, M. K. C.; JUNIOR, J. Z.; PINTO, H. S.; NASCIMENTO, C. R.; GONÇALVES, R. R. do V. Utilização de {\'\i}ndices de vegetação para estimativas não destrutivas da biomassa, estoque e sequestro de carbono do cafeeiro arábica. **XIV Simpósio Brasileiro de Sensoriamento Remoto. Natal**, [s. l.], p. 121–128, 2009.

COSTA, T. C. C.; CAMPANHA, M. M.; GONTIJO NETO, M. M. **Sequestro de $CO_2$ em Árvores de Eucalipto no Sistema ILPF**. 2022. Disponível em: <https://www.infoteca.cnptia.embrapa.br/infoteca/bitstream/doc/1149131/1/Boletim-244-Sequestro-de-CO2-em-arvores-de-eucalipto-no-sistema-ILPF.pdf>. Acesso em: 17 dez. 2022.

CRAIG, M. E.; GEYER, K. M.; BEIDLER, K. V; BRZOSTEK, E. R.; FREY, S. D.; STUART GRANDY, A.; LIANG, C.; PHILLIPS, R. P. Fast-decaying plant litter enhances soil carbon in temperate forests but not through microbial physiological traits. **Nature Communications**, [s. l.], v. 13, n. 1, p. 1229, 2022. Disponível em: <https://doi.org/10.1038/s41467-022-28715-9>

CRISP, D.; FISHER, B. M.; O'DELL, C.; FRANKENBERG, C.; BASILIO, R.; BÖSCH, H.; BROWN, L. R.; CASTANO, R.; CONNOR, B.; DEUTSCHER, N. M.; ELDERING, A.; GRIFFITH, D.; GUNSON, M.; KUZE, A.; MANDRAKE, L.; MCDUFFIE, J.; MESSERSCHMIDT, J.; MILLER, C. E.; MORINO, I.; NATRAJ, V.; NOTHOLT, J.; O'BRIEN, D. M.; OYAFUSO, F.; POLONSKY, I.; ROBINSON, J.; SALAWITCH, R.; SHERLOCK, V.; SMYTH, M.; SUTO, H.; TAYLOR, T. E.; THOMPSON, D. R.; WENNBERG, P. O.; WUNCH, D.; YUNG, Y. L. The ACOS CO 2 retrieval algorithm - Part II: Global X CO2 data characterization. **Atmospheric Measurement Techniques**, [s. l.], v. 5, n. 4, p. 687–707, 2012.

CRISP, D.; POLLOCK, H.; ROSENBERG, R.; CHAPSKY, L.; LEE, R.; OYAFUSO, F.; FRANKENBERG, C.; DELL, C.; BRUEGGE, C.; DORAN, G.; ELDERING, A.; FISHER, B.; FU, D.; GUNSON, M.; MANDRAKE, L.; OSTERMAN, G.; SCHWANDNER, F.; SUN, K.; TAYLOR, T.; WENNBERG, P.; WUNCH, D. The on-orbit performance of the Orbiting Carbon Observatory-2 (OCO-2) instrument and its radiometrically calibrated products. **Atmospheric Measurement Techniques**, [s. l.], v. 10, n. 1, p. 59–81, 2017.

CUNHA, F. F. Da; MAGALHÃES, F. F.; CASTRO, M. A. De. MÉTODOS PARA ESTIMATIVA DA EVAPOTRANSPIRAÇÃO DE REFERÊNCIA PARA CHAPADÃO DO SUL - MS. **Revista Engenharia na Agricultura - REVENG**, [s. l.], v. 21, n. 2 SE-Meteorologia Agrícola, p. 159–172, 2013. Disponível em: <https://periodicos.ufv.br/reveng/article/view/313>

DA SILVA, C. A.; NANNI, M. R.; TEODORO, P. E.; SILVA, G. F. C. Vegetation Indices for Discrimination of Soybean Areas: A New Approach. **Agronomy Journal**, [s. l.], v. 109, n. 4, p. 1331–1343, 2017. Disponível em: <https://doi.org/10.2134/agronj2017.01.0003>

DA SILVA JUNIOR, C. A.; NANNI, M. R.; SHAKIR, M.; TEODORO, P. E.; DE OLIVEIRA-JÚNIOR, J. F.; CEZAR, E.; DE GOIS, G.; LIMA, M.; WOJCIECHOWSKI, J. C.; SHIRATSUCHI, L. S. Soybean varieties discrimination using non-imaging hyperspectral sensor. **Infrared Physics & Technology**, [s. l.], v. 89, p. 338–350, 2018. Disponível em: <https://linkinghub.elsevier.com/retrieve/pii/S1350449517308186>

DAMASCENO, A. S. da S.; BOECHAT, C. L.; SOUZA, H. A. De; CAPRISTO-SILVA, G. F.; MENDES, W. de S.; TEODORO, P. E.; MORAIS, P. G. C.; OLIVEIRA, R. I. De; DELLA-SILVA, J. L.; SOUZA, I. A. M. De; SILVA JUNIOR, C. A. Da. Nutritional monitoring of boron in Eucalyptus spp. in the Brazilian cerrado by multispectral bands of the MSI sensor (Sentinel-2). **Remote Sensing Applications: Society and Environment**, [s. l.], v. 29, p. 100913, 2023. Disponível em:

<https://linkinghub.elsevier.com/retrieve/pii/S235293852200221X>

DANISH; ULUCAK, R.; KHAN, S. U.-D. Determinants of the ecological footprint: Role of renewable energy, natural resources, and urbanization. **Sustainable Cities and Society**, [s. l.], v. 54, p. 101996, 2020. Disponível em: <https://www.sciencedirect.com/science/article/pii/S2210670719335371>

DARENOVA, E.; ČATER, M. Effect of spatial scale and harvest on heterogeneity of forest floor $CO_2$ efflux in a sessile oak forest. **CATENA**, [s. l.], v. 188, p. 104455, 2020. Disponível em: <https://linkinghub.elsevier.com/retrieve/pii/S0341816220300047>

DE AREA LEÃO PEREIRA, E. J.; DE SANTANA RIBEIRO, L. C.; DA SILVA FREITAS, L. F.; DE BARROS PEREIRA, H. B. Brazilian policy and agribusiness damage the Amazon rainforest. **Land Use Policy**, [s. l.], v. 92, p. 104491, 2020.

DE BORTOLI TEIXEIRA, D.; PANOSSO, A. R.; CERRI, C. E. P.; PEREIRA, G. T.; LA SCALA, N. Soil $CO_2$ emission estimated by different interpolation techniques. **Plant and Soil**, [s. l.], v. 345, n. 1–2, p. 187–194, 2011. Disponível em: <http://link.springer.com/10.1007/s11104-011-0770-6>

DE CASTRO PEREIRA, L.; NUNES, A. B.; ROCHA, I. L.; DE OLIVEIRA, J. L.; BRANDÃO, M. L. S. M.; LEITE, L. F. C.; DE FREITAS IWATA, B. Fluxo de $CO_2$ e os {\'\i}ndices de vegetação do Parque Nacional das Nascentes do Rio Parna{\'\i}ba, Piau{\'\i}, Brasil. **Revista Brasileira de Geografia F{\'\i}sica**, [s. l.], v. 13, n. 07, p. 3585–3601, 2020.

DE FIGUEIREDO, E. B.; JAYASUNDARA, S.; DE OLIVEIRA BORDONAL, R.; BERCHIELLI, T. T.; REIS, R. A.; WAGNER-RIDDLE, C.; LA SCALA JR., N. Greenhouse gas balance and carbon footprint of beef cattle in three contrasting pasture-management systems in Brazil. **Journal of Cleaner Production**, [s. l.], v. 142, p. 420–431, 2017. Disponível em: <https://www.sciencedirect.com/science/article/pii/S0959652616302049>

DE GOIS, G.; DELGADO, R. C.; OLIVEIRA-JÚNIOR, J. F. Transitive theoretical models applied to the spatial interpolation of the standardized precipitation index (SPI) for episodeds of strong el nino in the tocantins state. **Irriga**, [s. l.], v. 20, n. 2, p. 371–387, 2015.

DE M. SÁ, J. C.; CERRI, C. C.; DICK, W. A.; LAL, R.; FILHO, S. P. V.; PICCOLO, M. C.; FEIGL, B. E. Organic Matter Dynamics and Carbon Sequestration Rates for a Tillage Chronosequence in a Brazilian Oxisol. **Soil Science Society of America Journal**, [s. l.], v. 65, n. 5, p. 1486–1499, 2001. Disponível em: <http://doi.wiley.com/10.2136/sssaj2001.6551486x>

DE OLIVEIRA-JÚNIOR, J. F.; DA SILVA JUNIOR, C. A.; TEODORO, P. E.; ROSSI, F. S.; BLANCO, C. J. C.; LIMA, M.; DE GOIS, G.; CORREIA FILHO, W. L. F.; DE BARROS SANTIAGO, D.; DOS SANTOS VANDERLEY, M. H. G. Confronting CHIRPS dataset and in situ stations in the detection of wet and drought conditions in the Brazilian Midwest. **International Journal of Climatology**, [s. l.], v. 41, n. 9, p. 4478–4493, 2021.

DE OLIVEIRA-JÚNIOR, J. F.; DE GOIS, G.; DE BODAS TERASSI, P. M.; DA SILVA JUNIOR, C. A.; BLANCO, C. J. C.; SOBRAL, B. S.; GASPARINI, K. A. C. Drought severity based on the SPI index and its relation to the ENSO and PDO climatic variability modes in the regions North and Northwest of the State of Rio de Janeiro - Brazil. **Atmospheric Research**, [s. l.], v. 212, p. 91–105, 2018.

DE OLIVEIRA, B. R.; DA SILVA, A. A. P.; TEODORO, L. P. R.; DE AZEVEDO, G. B.; AZEVEDO, G. T. de O. S.; BAIO, F. H. R.; SOBRINHO, R. L.; DA SILVA JUNIOR, C. A.; TEODORO, P. E. Eucalyptus growth recognition using machine learning methods and spectral variables. **Forest Ecology and Management**, [s. l.], v. 497, p. 119496, 2021. Disponível em: <https://linkinghub.elsevier.com/retrieve/pii/S0378112721005867>

DELLA-SILVA, J. L.; DA SILVA JUNIOR, C. A.; LIMA, M.; TEODORO, P. E.; NANNI, M. R.; SHIRATSUCHI, L. S.; TEODORO, L. P. R.; CAPRISTO-SILVA, G. F.; BAIO, F. H. R.; DE OLIVEIRA, G.; DE OLIVEIRA-JÚNIOR, J. F.; ROSSI, F. S. CO2Flux Model Assessment and Comparison between an Airborne Hyperspectral Sensor and Orbital Multispectral Imagery in Southern Amazonia. **Sustainability**, [s. l.], v. 14, n. 9, 2022. Disponível em: <https://www.mdpi.com/2071-1050/14/9/5458>

DENG, Z.; ZHU, X.; HE, Q.; TANG, L. Land use/land cover classification using time series Landsat 8 images in a heavily urbanized area. **Advances in Space Research**, [s. l.], v. 63, n. 7, p. 2144–2154, 2019. Disponível em: <https://linkinghub.elsevier.com/retrieve/pii/S0273117718309037>

DIDAN, K.; MUNOZ, A. B.; SOLANO, R.; HUETE, A. MODIS vegetation index user's guide (MOD13 series). **University of Arizona: Vegetation Index and Phenology Lab**, [s. l.], 2015.

DING, W.; YU, H.; CAI, Z.; HAN, F.; XU, Z. Responses of soil respiration to N fertilization in a loamy soil under maize cultivation. **Geoderma**, [s. l.], v. 155, n. 3–4, p. 381–389, 2010.

DOSSOU-YOVO, E. R.; BRÜGGEMANN, N.; JESSE, N.; HUAT, J.; AGO, E. E.; AGBOSSOU, E. K. Reducing soil CO2 emission and improving upland rice yield with no-tillage, straw mulch and nitrogen fertilization in northern Benin. **Soil and Tillage Research**, [s. l.], v. 156, p. 44–53, 2016. Disponível em: <https://www.sciencedirect.com/science/article/pii/S0167198715300386>

DRAKE, J. E.; MACDONALD, C. A.; TJOELKER, M. G.; REICH, P. B.; SINGH, B. K.; ANDERSON, I. C.; ELLSWORTH, D. S. Three years of soil respiration in a mature eucalypt woodland exposed to atmospheric CO2 enrichment. **Biogeochemistry**, [s. l.], v. 139, n. 1, p. 85–101, 2018. Disponível em: <http://link.springer.com/10.1007/s10533-018-0457-7>

DU, H.; ZENG, F.; PENG, W.; WANG, K.; ZHANG, H.; LIU, L.; SONG, T. Carbon Storage in a Eucalyptus Plantation Chronosequence in Southern China. **Forests**, [s. l.], v. 6, n. 12, p. 1763–1778, 2015. Disponível em: <http://www.mdpi.com/1999-4907/6/6/1763>

ELDERING, A.; POLLOCK, R.; LEE, R.; ROSENBERG, R.; OYAFUSO, F.; CRISP, D.; CHAPSKY, L.; GRANAT, R. **Orbiting Carbon Observatory (OCO)--2 Level 1B Theoretical Basis Document**, Tech. Rep. D-55206, NASA Jet Propulsion Laboratory, California Institute of~…, 2015.

ELDERING, A.; WENNBERG, P. O.; CRISP, D.; SCHIMEL, D. S.; GUNSON, M. R.; CHATTERJEE, A.; LIU, J.; SCHWANDNER, F. M.; SUN, Y.; O'DELL, C. W.; FRANKENBERG, C.; TAYLOR, T.; FISHER, B.; OSTERMAN, G. B.; WUNCH, D.; HAKKARAINEN, J.; TAMMINEN, J.; WEIR, B. The Orbiting Carbon Observatory-2 early science investigations of regional carbon dioxide fluxes. **Science**, [s. l.], v. 358, n. 6360, 2017.

EMBRAPA_SOLOS. **Mapa de solos do Brasil — geoinfo.cnps.embrapa.br**. 2020. Disponível em: <http://geoinfo.cnps.embrapa.br/layers/geonode%3Abrasil_solos_5m_20201104#more>. Acesso em: 3 jul. 2022.

EMBRAPA. **Sistemas brasileiro de classificação de solos**. 5. ed. [s.l: s.n.].

EPRON, D.; BOSC, A.; BONAL, D.; FREYCON, V. Spatial variation of soil respiration across a topographic gradient in a tropical rain forest in French Guiana. **Journal of Tropical Ecology**, [s. l.], v. 22, n. 5, p. 565–574, 2006. Disponível em: <https://www.cambridge.org/core/product/identifier/S0266467406003415/type/journal_article>

EPSKAMP, S.; CRAMER, A. O. J.; WALDORP, L. J.; SCHMITTMANN, V. D.; BORSBOOM, D. {qgraph}: Network Visualizations of Relationships in Psychometric Data. **Journal of Statistical Software**, [s. l.], v. 48, n. 4, p. 1–18, 2012.

ERI, M.; SILVA JUNIOR, C. A. Da; LIMA, M.; LA SCALA JÚNIOR, N.; OLIVEIRA-JÚNIOR, J. F. De; TEODORO, P. E.; CAPRISTO-SILVA, G. F.; CAIONE, G.; PERES, C. A. Capitalizing on opportunities provided by pasture sudden death to enhance livestock sustainable management in Brazilian Amazonia. **Environmental Development**, [s. l.], v. 33, p. 100499, 2020.

FALAHATKAR, S.; MOUSAVI, S. M.; FARAJZADEH, M. Spatial and temporal distribution of carbon dioxide gas using GOSAT data over IRAN. **Environmental Monitoring and Assessment**, [s. l.], v. 189, n. 12, p. 627, 2017. Disponível em: <https://doi.org/10.1007/s10661-017-6285-8>

FAN, L.; WIGNERON, J. P.; CIAIS, P.; CHAVE, J.; BRANDT, M.; FENSHOLT, R.; SAATCHI, S. S.; BASTOS, A.; AL-YAARI, A.; HUFKENS, K.; QIN, Y.; XIAO, X.; CHEN, C.; MYNENI, R. B.; FERNANDEZ-MORAN, R.; MIALON, A.;

RODRIGUEZ-FERNANDEZ, N. J.; KERR, Y.; TIAN, F.; PEÑUELAS, J. Satellite-observed pantropical carbon dynamics. **Nature Plants**, [s. l.], v. 5, n. 9, p. 944–951, 2019.

FAN, X.; CAO, X.; ZHOU, H.; HAO, L.; DONG, W.; HE, C.; XU, M.; WU, H.; WANG, L.; CHANG, Z.; ZHENG, Y. Carbon dioxide fertilization effect on plant growth under soil water stress associates with changes in stomatal traits, leaf photosynthesis, and foliar nitrogen of bell pepper (Capsicum annuum L.). **Environmental and Experimental Botany**, [s. l.], v. 179, p. 104203, 2020. Disponível em: <https://linkinghub.elsevier.com/retrieve/pii/S009884722030229X>

FAOSTAT. **No Title**. [s.d.]. Disponível em: <http://www.fao.org/faostat/en/#data/QC>. Acesso em: 29 abr. 2022.

FEARNSIDE, P. M. Soybean cultivation as a threat to the environment in Brazil. **Environmental Conservation**, [s. l.], v. 28, v. 2002/05/10, n. 1, p. 23–38, 2001.

FERNANDES, F. A.; FERNANDES, A. Cálculo dos estoques de carbono do solo sob diferentes condições de manejo. **Embrapa Pantanal-Comunicado Técnico (INFOTECA-E)**, [s. l.], 2008.

FERNÁNDEZ-MARTÍNEZ, M.; VICCA, S.; JANSSENS, I. A.; SARDANS, J.; LUYSSAERT, S.; CAMPIOLI, M.; CHAPIN III, F. S.; CIAIS, P.; MALHI, Y.; OBERSTEINER, M.; PAPALE, D.; PIAO, S. L.; REICHSTEIN, M.; RODÀ, F.; PEÑUELAS, J. Nutrient availability as the key regulator of global forest carbon balance. **Nature Climate Change**, [s. l.], v. 4, n. 6, p. 471–476, 2014. Disponível em: <http://www.nature.com/articles/nclimate2177>

FERREIRA, C. R. P. C.; ANTONINO, A. C. D.; SAMPAIO, E. V. de S. B.; CORREIA, K. G.; LIMA, J. R. de S.; SOARES, W. de A.; MENEZES, R. S. C. Soil CO 2 efflux measurements by alkali absorption and infrared gas analyzer in the Brazilian semiarid region. **Revista Brasileira de Ciência do Solo**, [s. l.], v. 42, 2018.

FERREIRA, E. B.; CAVALCANTI, P. P.; NOGUEIRA, D. A. **ExpDes.pt: Pacote Experimental Designs (Portugues)**, 2021. Disponível em: <https://cran.r-project.org/package=ExpDes.pt>

FIELD, C. B.; RANDERSON, J. T.; MALMSTRÖM, C. M. Global net primary production: Combining ecology and remote sensing. **Remote Sensing of Environment**, [s. l.], v. 51, n. 1, p. 74–88, 1995. Disponível em: <https://www.sciencedirect.com/science/article/pii/003442579400066V>

FRIENDLY, M.; FOX, J. **candisc: Visualizing Generalized Canonical Discriminant and Canonical Correlation Analysis**, 2021. Disponível em: <https://cran.r-project.org/package=heplots>

FRONTISTIS, Z. New Trends in Environmental Catalytic Technologies for Water Remediation. **Water**, [s. l.], v. 13, n. 4, 2021. Disponível em:

<https://www.mdpi.com/2073-4441/13/4/571>

FU, L.; ZHAO, Y.; XU, Z.; WU, B. Spatial and temporal dynamics of forest aboveground carbon stocks in response to climate and environmental changes. **Journal of Soils and Sediments**, [s. l.], v. 15, n. 2, p. 249–259, 2015. Disponível em: <http://link.springer.com/10.1007/s11368-014-1050-x>

GAMON, J. A.; SERRANO, L.; SURFUS, J. S. The photochemical reflectance index: An optical indicator of photosynthetic radiation use efficiency across species, functional types, and nutrient levels. **Oecologia**, [s. l.], v. 112, n. 4, p. 492–501, 1997.

GAO, Y.; WANG, S.; GUAN, K.; WOLANIN, A.; YOU, L.; JU, W.; ZHANG, Y. **The Ability of Sun-Induced Chlorophyll Fluorescence From OCO-2 and MODIS-EVI to Monitor Spatial Variations of Soybean and Maize Yields in the Midwestern USA**, 2020.

GATTI, L. V.; GLOOR, M.; MILLER, J. B.; DOUGHTY, C. E.; MALHI, Y.; DOMINGUES, L. G.; BASSO, L. S.; MARTINEWSKI, A.; CORREIA, C. S. C.; BORGES, V. F.; FREITAS, S.; BRAZ, R.; ANDERSON, L. O.; ROCHA, H.; GRACE, J.; PHILLIPS, O. L.; LLOYD, J. Drought sensitivity of Amazonian carbon balance revealed by atmospheric measurements. **Nature**, [s. l.], v. 506, n. 7486, p. 76–80, 2014. Disponível em: <https://doi.org/10.1038/nature12957>

GIBBS, H. K.; MUNGER, J.; L'ROE, J.; BARRETO, P.; PEREIRA, R.; CHRISTIE, M.; AMARAL, T.; WALKER, N. F. Did Ranchers and Slaughterhouses Respond to Zero-Deforestation Agreements in the Brazilian Amazon? **Conservation Letters**, [s. l.], v. 9, n. 1, p. 32–42, 2016.

GIBBS, H. K.; RAUSCH, L.; MUNGER, J.; SCHELLY, I.; MORTON, D. C.; NOOJIPADY, P.; SOARES-FILHO, B.; BARRETO, P.; MICOL, L.; WALKER, N. F. Brazil's Soy Moratorium: Supply-chain governance is needed to avoid deforestation. **Science**, United States, v. 347, n. 6220, p. 377–378, 2015.

GITELSON, A. A.; VIÑA, A.; VERMA, S. B.; RUNDQUIST, D. C.; ARKEBAUER, T. J.; KEYDAN, G.; LEAVITT, B.; CIGANDA, V.; BURBA, G. G.; SUYKER, A. E. Relationship between gross primary production and chlorophyll content in crops: Implications for the synoptic monitoring of vegetation productivity. **Journal of Geophysical Research**, [s. l.], v. 111, n. D8, p. D08S11, 2006. Disponível em: <http://doi.wiley.com/10.1029/2005JD006017>

GITELSON, A.; ARKEBAUER, T.; VIÑA, A.; SKAKUN, S.; INOUE, Y. Evaluating plant photosynthetic traits via absorption coefficient in the photosynthetically active radiation region. **Remote Sensing of Environment**, [s. l.], v. 258, p. 112401, 2021. Disponível em: <https://linkinghub.elsevier.com/retrieve/pii/S003442572100119X>

GOLKAR, F.; AL-WARDY, M.; SAFFARI, S. F.; AL-AUFI, K.; AL-RAWAS, G. Using OCO-2 satellite data for investigating the variability of atmospheric CO2 concentration in relationship with precipitation, relative humidity, and vegetation over Oman. **Water (Switzerland)**, [s. l.], v. 12, n. 1, 2020.

GONZÁLEZ-UBIERNA, S.; LAI, R. Modelling the effects of climate factors on soil respiration across Mediterranean ecosystems. **Journal of Arid Environments**, [s. l.], v. 165, p. 46–54, 2019. Disponível em: <https://linkinghub.elsevier.com/retrieve/pii/S0140196318302246>

GORELICK, N.; HANCHER, M.; DIXON, M.; ILYUSHCHENKO, S.; THAU, D.; MOORE, R. Google Earth Engine: Planetary-scale geospatial analysis for everyone. **Remote Sensing of Environment**, [s. l.], v. 202, p. 18–27, 2017.

GOULDEN, M. L.; MUNGER, J. W.; FAN, S.-M.; DAUBE, B. C.; WOFSY, S. C. Measurements of carbon sequestration by long-term eddy covariance: methods and a critical evaluation of accuracy. **Global Change Biology**, [s. l.], v. 2, n. 3, p. 169–182, 1996. Disponível em: <https://onlinelibrary.wiley.com/doi/10.1111/j.1365-2486.1996.tb00070.x>

GOUVEIA, C.; TRIGO, R. M.; DACAMARA, C. C.; LIBONATI, R.; PEREIRA, J. M. C. The North Atlantic oscillation and European vegetation dynamics. **International Journal of Climatology: A Journal of the Royal Meteorological Society**, [s. l.], v. 28, n. 14, p. 1835–1847, 2008.

GUENET, B.; GABRIELLE, B.; CHENU, C.; ARROUAYS, D.; BALESDENT, J.; BERNOUX, M.; BRUNI, E.; CALIMAN, J.; CARDINAEL, R.; CHEN, S.; CIAIS, P.; DESBOIS, D.; FOUCHE, J.; FRANK, S.; HENAULT, C.; LUGATO, E.; NAIPAL, V.; NESME, T.; OBERSTEINER, M.; PELLERIN, S.; POWLSON, D. S.; RASSE, D. P.; REES, F.; SOUSSANA, J.; SU, Y.; TIAN, H.; VALIN, H.; ZHOU, F. Can N 2 O emissions offset the benefits from soil organic carbon storage? **Global Change Biology**, [s. l.], v. 27, n. 2, p. 237–256, 2021. Disponível em: <https://onlinelibrary.wiley.com/doi/10.1111/gcb.15342>

GUJARATI, DAMODAR N.; PORTER, D. C. **Econometria Básica**. 5 th Ed. ed. New York: Amgh Editora, 2011.

GUTIÉRREZ DEL ARROYO, O.; WOOD, T. E. Large seasonal variation of soil respiration in a secondary tropical moist forest in Puerto Rico. **Ecology and Evolution**, [s. l.], v. 11, n. 1, p. 263–272, 2021. Disponível em: <https://onlinelibrary.wiley.com/doi/10.1002/ece3.7021>

HATFIELD, J. L.; GITELSON, A. A.; SCHEPERS, J. S.; WALTHALL, C. L. Application of Spectral Remote Sensing for Agronomic Decisions. **Agronomy Journal**, [s. l.], v. 100, n. S3, 2008. Disponível em: <https://onlinelibrary.wiley.com/doi/10.2134/agronj2006.0370c>

HE, J.; ZHANG, P. Evaluation of carbon emissions associated with land use and cover change in Zhengzhou City of China. **Regional Sustainability**, [s. l.], v. 3, n. 1, p. 1–11, 2022. Disponível em: <https://www.sciencedirect.com/science/article/pii/S2666660X22000160>

HE, Z.; LEI, L.; ZENG, Z.-C.; SHENG, M.; WELP, L. R. **Evidence of Carbon Uptake Associated with Vegetation Greening Trends in Eastern China**, 2020.

HEINSCH, F. A. User's Guide, GPP and NPP (MOD17A2/A3) Products. **NASA MODIS land algorithm**, [s. l.], 2003.

HELD, I. M.; SODEN, B. J. Robust responses of the hydrological cycle to global warming. **Journal of Climate**, Boston MA, USA, v. 19, n. 21, p. 5686–5699, 2006.

HIRAKURI, M. H.; LAZZAROTTO, J. J. O agronegócio da soja nos contextos mundial e brasileiro. **Embrapa Soja-Documentos (INFOTECA-E)**, [s. l.], 2014.

HIRIGOYEN, A.; ACOSTA, C.; ARIZA, A.; VERO-MARTINEZ, M. A.; RACHID, C.; FRANCO, J.; NAVARA-CERRILLO, R. A machine learning approach to model leaf area index in Eucalyptus plantations using high-resolution satellite imagery and airborne laser scanner data. **Annals of Forest Research**, [s. l.], v. 64, n. 2, p. 165–183, 2022. Disponível em: <https://www.afrjournal.org/index.php/afr/article/viewFile/2073/1177>

HOUGHTON, J. T.; DING, Y.; GRIGGS, D. J.; NOGUER, M.; VAN DER LINDEN, P. J.; DAI, X.; MASKELL, K.; JOHNSON, C. A. **Climate change 2001: the scientific basis: contribution of Working Group I to the third assessment report of the Intergovernmental Panel on Climate Change**. [s.l.] : Cambridge university press, 2001.

HOUGHTON, R. A.; HOUSE, J. I.; PONGRATZ, J.; VAN DER WERF, G. R.; DEFRIES, R. S.; HANSEN, M. C.; LE QUÉRÉ, C.; RAMANKUTTY, N. Carbon emissions from land use and land-cover change. **Biogeosciences**, [s. l.], v. 9, n. 12, p. 5125–5142, 2012.

HOUGHTON, R. A.; UNRUH, J. D.; LEFEBVRE, P. A. Current land cover in the tropics and its potential for sequestering carbon. **Global Biogeochemical Cycles**, [s. l.], v. 7, n. 2, p. 305–320, 1993. Disponível em: <http://doi.wiley.com/10.1029/93GB00470>

HU, S.; LI, Y.; CHANG, S. X.; LI, Y.; YANG, W.; FU, W.; LIU, J.; JIANG, P.; LIN, Z. Soil autotrophic and heterotrophic respiration respond differently to land-use change and variations in environmental factors. **Agricultural and Forest Meteorology**, [s. l.], v. 250, p. 290–298, 2018.

HUBAU, W. et al. Asynchronous carbon sink saturation in African and Amazonian tropical forests. **Nature**, England, v. 579, n. 7797, p. 80–87, 2020.

HUETE, A.; DIDAN, K.; MIURA, T.; RODRIGUEZ, E. P.; GAO, X.; FERREIRA, L. G. Overview of the radiometric and biophysical performance of the MODIS vegetation indices. **Remote Sensing of Environment**, [s. l.], v. 83, n. 1–2, p. 195–213, 2002.

HUETE, A.; JUSTICE, C.; LIU, H. Development of vegetation and soil indices for MODIS-EOS. **Remote Sensing of Environment**, [s. l.], v. 49, n. 3, p. 224–234,

1994. Disponível em: <https://linkinghub.elsevier.com/retrieve/pii/0034425794900183>

HUETE, A. R. A soil-adjusted vegetation index (SAVI). **Remote Sensing of Environment**, [s. l.], v. 25, n. 3, p. 295–309, 1988. Disponível em: <https://www.sciencedirect.com/science/article/pii/003442578890106X>

HUETE, A. R.; LIU, H. Q.; BATCHILY, K.; VAN LEEUWEN, W. A comparison of vegetation indices over a global set of TM images for EOS-MODIS. **Remote Sensing of Environment**, [s. l.], v. 59, n. 3, p. 440–451, 1997. Disponível em: <https://www.sciencedirect.com/science/article/pii/S0034425796001125>

IBÁ. **Relatoria Anual IBÁ**. [s.l: s.n.]. Disponível em: <https://www.iba.org/datafiles/publicacoes/relatorios/relatorio-iba-2020.pdf>.

IBGE. **Ibge Cidades Conheça Cidades E Estados Do Brasil**. 2021. Disponível em: <https://cidades.ibge.gov.br/brasil>. Acesso em: 11 nov. 2022.

IBGE. **Instituto Brasileiro de Geografia e Estatística**. 2022. Disponível em: <https://agenciadenoticias.ibge.gov.br/agencia-noticias/2012-agencia-de-noticias/noticias/35056-valor-de-producao-da-silvicultura-e-da-extracao-vegetal-cresce-27-1-e-chega-ao-recorde-de-r-30-1-bilhoes>. Acesso em: 19 dez. 2022.

INPE. **Projeto PRODES: Monitoramento da floresta Amazônica Brasileira por satélite.** 2020. Disponível em: <http://terrabrasilis.dpi.inpe.br/app/dashboard/deforestation/biomes/legal_amazon/increments.>. Acesso em: 18 maio. 2020.

IPCC. **Climate Change 2013 – The Physical Science Basis: Working Group I Contribution to the Fifth Assessment Report of the Intergovernmental Panel on Climate Change**. Cambridge: Cambridge University Press, 2014. Disponível em: <https://www.cambridge.org/core/books/climate-change-2013-the-physical-science-basis/BE9453E500DEF3640B383BADDC332C3E>

IPCC. Methodology Report on Short-lived Climate Forcers. **Fourth Assessment Report of the Intergovernmental Panel on Climate Change**, [s. l.], 2020.

IPCC, A. R.; OTHERS. Climate change 2013: the physical science basis. **Contribution of working group I to the fifth assessment report of the intergovernmental panel on climate change**, [s. l.], v. 1535, 2013.

ISMAEL, M.; SROUJI, F.; BOUTABBA, M. A. Agricultural technologies and carbon emissions: evidence from Jordanian economy. **Environmental Science and Pollution Research**, Germany, v. 25, n. 11, p. 10867–10877, 2018.

ITAQUI, J. Quarta Colônia: inventários técnicos. **Santa Maria: Condesus Quarta Colônia**, [s. l.], 2002.

JAIN, N.; ARORA, P.; TOMER, R.; MISHRA, S. V.; BHATIA, A.; PATHAK, H.; CHAKRABORTY, D.; KUMAR, V.; DUBEY, D. S.; HARIT, R. C.; OTHERS.

Greenhouse gases emission from soils under major crops in Northwest India. **Science of the Total Environment**, [s. l.], v. 542, p. 551–561, 2016.

JANSSENS, I. A.; DIELEMAN, W.; LUYSSAERT, S.; SUBKE, J.-A.; REICHSTEIN, M.; CEULEMANS, R.; CIAIS, P.; DOLMAN, A. J.; GRACE, J.; MATTEUCCI, G.; PAPALE, D.; PIAO, S. L.; SCHULZE, E.-D.; TANG, J.; LAW, B. E. Reduction of forest soil respiration in response to nitrogen deposition. **Nature Geoscience**, [s. l.], v. 3, n. 5, p. 315–322, 2010. Disponível em: <http://www.nature.com/articles/ngeo844>

JARDIM, A. M. da R. F.; ARAÚJO JÚNIOR, G. do N.; SILVA, M. V. Da; SANTOS, A. Dos; SILVA, J. L. B. Da; PANDORFI, H.; OLIVEIRA-JÚNIOR, J. F. De; TEIXEIRA, A. H. de C.; TEODORO, P. E.; DE LIMA, J. L. M. P.; SILVA JUNIOR, C. A. Da; SOUZA, L. S. B. De; SILVA, E. A.; SILVA, T. G. F. Da. Using Remote Sensing to Quantify the Joint Effects of Climate and Land Use/Land Cover Changes on the Caatinga Biome of Northeast Brazilian. **Remote Sensing**, [s. l.], v. 14, n. 8, 2022. Disponível em: <https://www.mdpi.com/2072-4292/14/8/1911>

JIANG, X.; YUNG, Y. L. Global patterns of carbon dioxide variability from satellite observations. **Annual Review of Earth and Planetary Sciences**, [s. l.], v. 47, n. 1, p. 225–245, 2019.

KASSAMBARA, A.; MUNDT, F. Package ‘factoextra’: Extract and visualize the results of multivariate data analyses. **CRAN- R Package**, [s. l.], p. 84, 2020.

KASTENS, J. H.; BROWN, J. C.; COUTINHO, A. C.; BISHOP, C. R.; ESQUERDO, J. C. D. M. Soy moratorium impacts on soybean and deforestation dynamics in Mato Grosso, Brazil. **PLoS ONE**, [s. l.], v. 12, n. 4, p. 1–21, 2017.

KEELING, C. D.; BACASTOW, R. B.; BAINBRIDGE, A. E. Atmospheric carbon dioxide variations at Mauna Loa Observatory, Hawaii. **Tellus**, [s. l.], v. 28, n. 6, p. 538–551, 1976.

LA SCALA JÚNIOR, N.; DE FIGUEIREDO, E.; PANOSSO, A. A review on soil carbon accumulation due to the management change of major Brazilian agricultural activities. **Brazilian Journal of Biology**, [s. l.], v. 72, n. 3 suppl, p. 775–785, 2012. Disponível em: <http://www.scielo.br/scielo.php?script=sci_arttext&pid=S1519-69842012000400012&lng=en&tlng=en>

LA SCALA, N.; BOLONHEZI, D.; PEREIRA, G. T. Short-term soil $CO_2$ emission after conventional and reduced tillage of a no-till sugar cane area in southern Brazil. **Soil and Tillage Research**, [s. l.], v. 91, n. 1, p. 244–248, 2006. Disponível em: <https://www.sciencedirect.com/science/article/pii/S016719870500303X>

LAL, R. Residue management, conservation tillage and soil restoration for mitigating greenhouse effect by $CO_2$-enrichment. **Soil and Tillage Research**, [s. l.], v. 43, n. 1–2, p. 81–107, 1997. Disponível em: <https://linkinghub.elsevier.com/retrieve/pii/S0167198797000366>

LAL, R. Global Potential of Soil Carbon Sequestration to Mitigate the Greenhouse Effect. **Critical Reviews in Plant Sciences**, [s. l.], v. 22, n. 2, p. 151–184, 2003. Disponível em: <http://www.tandfonline.com/doi/abs/10.1080/713610854>

LAL, R.; NEGASSA, W.; LORENZ, K. Carbon sequestration in soil. **Current Opinion in Environmental Sustainability**, [s. l.], v. 15, p. 79–86, 2015. Disponível em: <https://linkinghub.elsevier.com/retrieve/pii/S1877343515001013>

LAMEIRA, A. M.; CANTO, O.; LIMA, R. Â.; FARIAS, A. Conflito socioambiental no cerrado: a monocultura da soja nos municípios de Itaubal e Macapá, Amapá. **Revista do Instituto Histórico e Geográfico do Pará**, [s. l.], v. 4, n. 1, p. 19–35, 2017.

LE QUÉRÉ, C. et al. Global Carbon Budget 2015. **Earth System Science Data**, [s. l.], v. 7, n. 2, p. 349–396, 2015.

LE QUÉRÉ, C. et al. Global Carbon Budget 2017. **Earth System Science Data**, [s. l.], v. 10, n. 1, p. 405–448, 2018. Disponível em: <https://essd.copernicus.org/articles/10/405/2018/>

LÊ, S.; JOSSE, J.; HUSSON, F. FactoMineR: An R Package for Multivariate Analysis. **Environment International**, [s. l.], v. 25, n. 1, p. 1–19, 2008.

LI, D.; ZHOU, X.; WU, L.; ZHOU, J.; LUO, Y. Contrasting responses of heterotrophic and autotrophic respiration to experimental warming in a winter annual-dominated prairie. **Global Change Biology**, [s. l.], p. n/a-n/a, 2013. Disponível em: <https://onlinelibrary.wiley.com/doi/10.1111/gcb.12273>

LIMA, L. G.; BARBOSA, J. L.; SANTOS, J. R.; LIMA, E. N. O deserto verde cresce em Alagoas: uma análise crítica da expansão do eucalipto no estado. **Caderno de Geografia**, [s. l.], v. 30, n. 63, p. 1210–1229, 2020.

LIMA, M. C.; AMARANTE, L. Do; MARIOT, M. P.; SERPA, R. Crescimento e produção de pigmentos fotossintéticos em Achillea millefolium L. cultivada sob diferentes níveis de sombreamento e doses de nitrogênio. **Ciência Rural**, [s. l.], v. 41, n. 1, p. 45–50, 2011. Disponível em: <http://www.scielo.br/scielo.php?script=sci_arttext&pid=S0103-84782011000100008&lng=pt&tlng=pt>

LIMA, M. S. B. Expansão da fronteira agrícola no Amazonas: uma analise das características da estrutura de governanta da cadeia da soja e suas relações com a cadeia de valor global. [s. l.], 2006.

LINDSEY R. **Climate Change: Atmospheric Carbon Dioxide**. 2020.

LIU, J.; BOWMAN, K.; PARAZOO, N. C.; BLOOM, A. A.; WUNCH, D.; JIANG, Z.; GURNEY, K. R.; SCHIMEL, D. Detecting drought impact on terrestrial biosphere carbon fluxes over contiguous US with satellite observations. **Environmental Research Letters**, [s. l.], v. 13, n. 9, p. 95003, 2018.

LIU, J.; BOWMAN, K. W.; SCHIMEL, D. S.; PARAZOO, N. C.; JIANG, Z.; LEE, M.; BLOOM, A. A.; WUNCH, D.; FRANKENBERG, C.; SUN, Y.; O'DELL, C. W.; GURNEY, K. R.; MENEMENLIS, D.; GIERACH, M.; CRISP, D.; ELDERING, A. Contrasting carbon cycle responses of the tropical continents to the 2015–2016 El Niño. **Science**, United States, v. 358, n. 6360, 2017.

LIU, J.; HUANG, R.; YU, K.; ZOU, B. How lime-sand islands in the South China Sea have responded to global warming over the last 30 years: Evidence from satellite remote sensing images. **Geomorphology**, [s. l.], v. 371, p. 107423, 2020. a. Disponível em: <https://www.sciencedirect.com/science/article/pii/S0169555X20303962>

LIU, W. T. H. **Aplicações de sensoriamento remoto**. [s.l.] : Oficina de Textos, 2015.

LIU, X.; ZHU, X.; ZHANG, Q.; YANG, T.; PAN, Y.; SUN, P. A remote sensing and artificial neural network-based integrated agricultural drought index: Index development and applications. **CATENA**, [s. l.], v. 186, p. 104394, 2020. b. Disponível em: <https://www.sciencedirect.com/science/article/pii/S0341816219305363>

LUO, Y.; LONG, X.; WU, C.; ZHANG, J. Decoupling CO2 emissions from economic growth in agricultural sector across 30 Chinese provinces from 1997 to 2014. **Journal of Cleaner Production**, [s. l.], v. 159, p. 220–228, 2017.

MA, M.; ZANG, Z.; XIE, Z.; CHEN, Q.; XU, W.; ZHAO, C.; SHEN, G. Soil respiration of four forests along elevation gradient in northern subtropical China. **Ecology and Evolution**, [s. l.], v. 9, n. 22, p. 12846–12857, 2019. Disponível em: <https://onlinelibrary.wiley.com/doi/10.1002/ece3.5762>

MACHADO, A. R.; RAYMUNDO, J. C. (EDS.). **Logística e Gestão da Cadeia de Suprimentos na Área Portuária – Volume 1**. [s.l.] : Editora Poisson, 2021. Disponível em: <https://www.poisson.com.br/livros/individuais/Logistica_Gestao_Portuaria/volume1/Logistica_Gestao_Portuaria_V1.pdf>

MANDRAKE, L.; O'DELL, C.; WUNCH, D.; WENNBERG, P. O.; FISHER, B.; OSTERMAN, G. B.; ELDERING, A. Orbiting Carbon Observatory–2 (OCO-2): Warn Level, Bias Correction, and Lite File Product Description. **Data Releases 7 and 7R**, [s. l.], p. 41, 2015.

MAPBIOMAS. **As transformações no território brasileiro nos últimos 36 anos**. 2021. Disponível em: <https://mapbiomasbr-site.s3.amazonaws.com/Fact_Sheet_Coleção_6 _ Agosto_2021_27082021_OK_ALTA.pdf>. Acesso em: 4 jan. 2023.

MARACAHIPES SANTOS, L.; LENZA, E.; DOS SANTOS, J. O.; MARIMON, B. S.; EISENLOHR, P. V.; MARIMON JUNIOR, B. H.; FELDPAUSCH, T. R. Diversity, floristic composition, and structure of the woody vegetation of the Cerrado in the

Cerrado–Amazon transition zone in Mato Grosso, Brazil. **Revista Brasileira de Botanica**, [s. l.], v. 38, n. 4, p. 877–887, 2015.

MARCELINO DO NASCIMENTO, D.; SALES, A. T.; SOUZA, R.; ALVES DA SILVA, A. S.; VALADARES DE SA BARRETTO SAMPAIO, E.; CEZAR MENEZES, R. S. Development of a methodological approach to estimate vegetation biomass using remote sensing in the Brazilian semiarid NE region. **Remote Sensing Applications: Society and Environment**, [s. l.], v. 27, p. 100771, 2022. Disponível em: <https://linkinghub.elsevier.com/retrieve/pii/S2352938522000799>

MARCOS-MARTINEZ, R.; BRYAN, B. A.; SCHWABE, K. A.; CONNOR, J. D.; LAW, E. A.; NOLAN, M.; SÁNCHEZ, J. J. Projected social costs of CO2 emissions from forest losses far exceed the sequestration benefits of forest gains under global change. **Ecosystem Services**, [s. l.], v. 37, p. 100935, 2019. Disponível em: <https://www.sciencedirect.com/science/article/pii/S2212041618300251>

MARÍN-SPIOTTA, E.; SHARMA, S. Carbon storage in successional and plantation forest soils: a tropical analysis. **Global Ecology and Biogeography**, [s. l.], v. 22, n. 1, p. 105–117, 2013. Disponível em: <https://onlinelibrary.wiley.com/doi/10.1111/j.1466-8238.2012.00788.x>

MARQUES, T. V; MENDES, K.; MUTTI, P.; MEDEIROS, S.; SILVA, L.; PEREZ-MARIN, A. M.; CAMPOS, S.; LÚCIO, P. S.; LIMA, K.; DOS REIS, J.; RAMOS, T. M.; DA SILVA, D. F.; OLIVEIRA, C. P.; COSTA, G. B.; ANTONINO, A. C. D.; MENEZES, R. S. C.; SANTOS E SILVA, C. M.; BEZERRA, B. Environmental and biophysical controls of evapotranspiration from Seasonally Dry Tropical Forests (Caatinga) in the Brazilian Semiarid. **Agricultural and Forest Meteorology**, [s. l.], v. 287, p. 107957, 2020. Disponível em: <https://www.sciencedirect.com/science/article/pii/S0168192320300599>

MARTINS, A. P.; GALVANI, E. Desempenho do algoritmo SEBAL para estimativa de vazão em bacias hidrográficas do Cerrado Brasileiro. **Sociedade & Natureza**, [s. l.], v. 32, p. 687–698, 2020. Disponível em: <http://www.seer.ufu.br/index.php/sociedadenatureza/article/view/53169>

MARTINS, L. N.; BAPTISTA, G. M. de M. Multitemporal Analysis of Forest Carbon Sink at Carão Settlement Project, Acre. **Revista Brasileira de Geografia Física**, [s. l.], v. 6, n. 6, p. 1648–1657, 2013.

MAYER, S.; KÜHNEL, A.; BURMEISTER, J.; KÖGEL-KNABNER, I.; WIESMEIER, M. Controlling factors of organic carbon stocks in agricultural topsoils and subsoils of Bavaria. **Soil and Tillage Research**, [s. l.], v. 192, p. 22–32, 2019. Disponível em: <https://linkinghub.elsevier.com/retrieve/pii/S0167198719301187>

MCKEE T.B., DOESKEN N.J., KLEIST J., 1993. The relationship of drought frequency and duration to time scales, in: Proc. 8th Conf. on Applied Climatology, Anaheim, California, 179–184. **Eighth Conference on Applied Climatology**, [s. l.], n. January, p. 17–22, 1993. Disponível em:

<https://www.droughtmanagement.info/literature/AMS_Relationship_Drought_Frequency_Duration_Time_Scales_1993.pdf>

MCTI. **Estimativas Anuais de Emissões de Gases de Efeito Estufa no Brasil**, MCTI, Brasília, DF, 2014. Disponível em: <http://www.mct.gov.br/upd_blob/0235/235580.pdf>

MENDES, K. R.; GRANJA, J. A. A.; OMETTO, J. P.; ANTONINO, A. C. D.; MENEZES, R. S. C.; PEREIRA, E. C.; POMPELLI, M. F. Croton blanchetianus modulates its morphophysiological responses to tolerate drought in a tropical dry forest. **Functional Plant Biology**, [s. l.], v. 44, n. 10, p. 1039–1051, 2017.

MERZLYAK, M. N.; GITELSON, A. A.; CHIVKUNOVA, O. B.; RAKITIN, V. Y. Non-destructive optical detection of pigment changes during leaf senescence and fruit ripening. **Physiologia Plantarum**, [s. l.], v. 106, n. 1, p. 135–141, 1999. Disponível em: <http://doi.wiley.com/10.1034/j.1399-3054.1999.106119.x>

MIKHAYLOV, A.; MOISEEV, N.; ALESHIN, K.; BURKHARDT, T. Global climate change and greenhouse effect. **Entrepreneurship and Sustainability Issues**, [s. l.], v. 7, n. 4, p. 2897–2913, 2020. Disponível em: <https://jssidoi.org/jesi/article/560>

MO, J.; ZHANG, W.; ZHU, W.; GUNDERSEN, P.; FANG, Y.; LI, D.; WANG, H. Nitrogen addition reduces soil respiration in a mature tropical forest in southern China. **Global Change Biology**, [s. l.], v. 14, n. 2, p. 403–412, 2008. Disponível em: <https://onlinelibrary.wiley.com/doi/10.1111/j.1365-2486.2007.01503.x>

MOITINHO, M. R.; FERRAUDO, A. S.; PANOSSO, A. R.; DA SILVA BICALHO, E.; TEIXEIRA, D. D. B.; DE ANDRADE BARBOSA, M.; TSAI, S. M.; BORGES, B. M. F.; DE SOUZA CANNAVAN, F.; DE SOUZA, J. A. M.; LA SCALA, N. Effects of burned and unburned sugarcane harvesting systems on soil $CO_2$ emission and soil physical, chemical, and microbiological attributes. **CATENA**, [s. l.], v. 196, p. 104903, 2021. Disponível em: <https://www.sciencedirect.com/science/article/pii/S0341816220304537>

MOITINHO, M. R.; PADOVAN, M. P.; PANOSSO, A. R.; TEIXEIRA, D. D. B.; FERRAUDO, A. S.; LA SCALA, N. On the spatial and temporal dependence of $CO_2$ emission on soil properties in sugarcane (Saccharum spp.) production. **Soil and Tillage Research**, [s. l.], v. 148, p. 127–132, 2015. Disponível em: <https://www.sciencedirect.com/science/article/pii/S0167198714002906>

MORAIS FILHO, L. F. F.; MENESES, K. C. De; SANTOS, G. A. de A.; BICALHO, E. da S.; ROLIM, G. de S.; LA SCALA, N. $xCO_2$ temporal variability above Brazilian agroecosystems: A remote sensing approach. **Journal of Environmental Management**, England, v. 288, p. 112433, 2021.

MURAOKA, H.; SAIGUSA, N.; NASAHARA, K. N.; NODA, H.; YOSHINO, J.; SAITOH, T. M.; NAGAI, S.; MURAYAMA, S.; KOIZUMI, H. Effects of seasonal and interannual variations in leaf photosynthesis and canopy leaf area index on gross primary production of a cool-temperate deciduous broadleaf forest in Takayama, Japan. **Journal of Plant Research**, [s. l.], v. 123, n. 4, p. 563–576, 2010. Disponível em: <http://link.springer.com/10.1007/s10265-009-0270-4>

MÜTZENBERG, D. M. **CARACTERIZAÇÃO DA VEGETAÇÃO, DA COMPOSIÇÃO FÍSICA E QUÍMICA DO SOLO E DA SERAPILHEIRA EM ÁREA DE TRANSIÇÃO AMAZÔNIA-CERRADO**. 2020. Tese (doutorado) - Universidade Federal de Mato Grosso, Instituto de Física, Programa de Pós-Graduação em Física Ambiental, Cuiabá, [s. l.], 2020.

NASROLLAHI, Z.; HASHEMI, M.; BAMERI, S.; MOHAMAD TAGHVAEE, V. Environmental pollution, economic growth, population, industrialization, and technology in weak and strong sustainability: using STIRPAT model. **Environment, Development and Sustainability**, [s. l.], v. 22, n. 2, p. 1105–1122, 2020. Disponível em: <https://doi.org/10.1007/s10668-018-0237-5>

NAYLOR, R.; STEINFELD, H.; FALCON, W.; GALLOWAY, J.; SMIL, V.; BRADFORD, E.; ALDER, J.; MOONEY, H. Losing the links between livestock and land. **Science**, United States, v. 310, n. 5754, p. 1621–1622, 2005.

NEILL, C.; MELILLO, J. M.; STEUDLER, P. A.; CERRI, C. C.; DE MORAES, J. F. L.; PICCOLO, M. C.; BRITO, M. Soil carbon and nitrogen stocks following forest clearing for pasture in the southwestern Brazilian Amazon. **Ecological Applications**, [s. l.], v. 7, n. 4, p. 1216–1225, 1997.

NEPSTAD, D. C.; STICKLER, C. M.; ALMEIDA, O. T. Globalization of the Amazon soy and beef industries: Opportunities for conservation. **Conservation Biology**, United States, v. 20, n. 6, p. 1595–1603, 2006.

NICHOLS, V.; MIGUEZ, F.; SAUER, T.; DIETZEL, R. Maize and prairie root contributions to soil CO2 emissions in the field. **Crop Science**, [s. l.], v. 56, n. 5, p. 2791–2801, 2016.

NOGUEIRA, E. M.; YANAI, A. M.; FONSECA, F. O. R.; FEARNSIDE, P. M. Carbon stock loss from deforestation through 2013 in Brazilian Amazonia. **Global Change Biology**, [s. l.], v. 21, n. 3, p. 1271–1292, 2015.

OERTEL, C.; MATSCHULLAT, J.; ZURBA, K.; ZIMMERMANN, F.; ERASMI, S. Greenhouse gas emissions from soils—A review. **Geochemistry**, [s. l.], v. 76, n. 3, p. 327–352, 2016. Disponível em: <https://www.sciencedirect.com/science/article/pii/S0009281916300551>

OLIVEIRA, I. N. **Qualidade do solo utilizando diferentes coberturas e preparos do solo em área de cana-de-açúcar**. 2018. Universidade Estadual de Campinas, Faculdade de Engenharia Agrícola, [s. l.], 2018.

PAN, Y.; BIRDSEY, R. A.; FANG, J.; HOUGHTON, R.; KAUPPI, P. E.; KURZ, W. A.; PHILLIPS, O. L.; SHVIDENKO, A.; LEWIS, S. L.; CANADELL, J. G.; CIAIS, P.; JACKSON, R. B.; PACALA, S. W.; MCGUIRE, A. D.; PIAO, S.; RAUTIAINEN, A.;

SITCH, S.; HAYES, D. A large and persistent carbon sink in the world’s forests. **Science**, United States, v. 333, n. 6045, p. 988–993, 2011.

PANOSSO, A. R.; SCALA JÚNIOR, N. L.; PEREIRA, G. T.; ZANINI, J. R. Uso de krigagem ordinária e co-krigagem pra estimar a emissão de CO2 do solo após molhamento. In: XXXI CONGRESSO BRASILEIRO DE CIÊNCIA DO SOLO 2007, Gramado - RS. **Anais**... Gramado - RS

PARAZOO, N. C.; BOWMAN, K.; FRANKENBERG, C.; LEE, J. E.; FISHER, J. B.; WORDEN, J.; JONES, D. B. A.; BERRY, J.; COLLATZ, G. J.; BAKER, I. T.; JUNG, M.; LIU, J.; OSTERMAN, G.; O’DELL, C.; SPARKS, A.; BUTZ, A.; GUERLET, S.; YOSHIDA, Y.; CHEN, H.; GERBIG, C. Interpreting seasonal changes in the carbon balance of southern Amazonia using measurements of XCO2 and chlorophyll fluorescence from GOSAT. **Geophysical Research Letters**, [s. l.], v. 40, n. 11, p. 2829–2833, 2013. Disponível em: <https://agupubs.onlinelibrary.wiley.com/doi/abs/10.1002/grl.50452>

PAREDES-TREJO, F. J.; BARBOSA, H. A.; LAKSHMI KUMAR, T. V. Validating CHIRPS-based satellite precipitation estimates in Northeast Brazil. **Journal of Arid Environments**, [s. l.], v. 139, p. 26–40, 2017.

PENG, Y.; LI, F.; ZHOU, G.; FANG, K.; ZHANG, D.; LI, C.; YANG, G.; WANG, G.; WANG, J.; MOHAMMAT, A.; YANG, Y. Nonlinear response of soil respiration to increasing nitrogen additions in a Tibetan alpine steppe. **Environmental Research Letters**, [s. l.], v. 12, n. 2, p. 024018, 2017. Disponível em: <https://iopscience.iop.org/article/10.1088/1748-9326/aa5ba6>

PEÑUELAS, J.; POULTER, B.; SARDANS, J.; CIAIS, P.; VAN DER VELDE, M.; BOPP, L.; BOUCHER, O.; GODDERIS, Y.; HINSINGER, P.; LLUSIA, J.; NARDIN, E.; VICCA, S.; OBERSTEINER, M.; JANSSENS, I. A. Human-induced nitrogen–phosphorus imbalances alter natural and managed ecosystems across the globe. **Nature Communications**, [s. l.], v. 4, n. 1, p. 2934, 2013. Disponível em: <http://www.nature.com/articles/ncomms3934>

PICOLI, M. C. A.; CAMARA, G.; SANCHES, I.; SIMÕES, R.; CARVALHO, A.; MACIEL, A.; COUTINHO, A.; ESQUERDO, J.; ANTUNES, J.; BEGOTTI, R. A.; ARVOR, D.; ALMEIDA, C. Big earth observation time series analysis for monitoring Brazilian agriculture. **ISPRS Journal of Photogrammetry and Remote Sensing**, [s. l.], v. 145, p. 328–339, 2018.

PILI, U. B.; VIOLANDA, R. R. Extracting Earth’s orbital period from atmospheric CO2concentrations using the Fourier transform based on Matlab. **Physics Education**, [s. l.], v. 55, n. 5, p. 1V, 2020.

PINHO-PESSOA, A. C. B.; MENDES, K. R.; JARMA-OROZCO, A.; PEREIRA, M. P. S.; SANTOS, M. A.; MENEZES, R. S. C.; OMETTO, J. P.; PEREIRA, E. C.; POMPELLI, M. F. Interannual variation in temperature and rainfall can modulate the physiological and photoprotective mechanisms of a native semiarid plant species. **Indian J. Sci. Technol**, [s. l.], v. 11, n. 41, p. 1–17, 2018.

PIRES, L. F.; BORGES, J. A. R.; ROSA, J. A.; COOPER, M.; HECK, R. J.; PASSONI, S.; ROQUE, W. L. Soil structure changes induced by tillage systems. **Soil and Tillage Research**, [s. l.], v. 165, p. 66–79, 2017. Disponível em: <https://www.sciencedirect.com/science/article/pii/S0167198716301313>

PIRES, R. L. de O. **Potencial de remoção de gases de efeito estufa do sistema de integração pecuária-floresta em áreas de cerrado**. 2019. [s. l.], 2019.

PONZONI, F. J.; DISPERATI, A. A. Comportamento espectral da vegetação. **Sensoriamento remoto: reflectância de alvos naturais**, [s. l.], v. 1, p. 157–199, 2001.

PRIES, C. E. H.; CASTANHA, C.; PORRAS, R. C.; TORN, M. S. The whole-soil carbon flux in response to warming. **Science**, [s. l.], v. 355, n. 6332, p. 1420–1423, 2017. Disponível em: <https://www.science.org/doi/abs/10.1126/science.aal1319>

QUESADA, B.; ARNETH, A.; ROBERTSON, E.; DE NOBLET-DUCOUDRÉ, N. Potential strong contribution of future anthropogenic land-use and land-cover change to the terrestrial carbon cycle. **Environmental Research Letters**, [s. l.], v. 13, n. 6, p. 64023, 2018.

R CORE TEAM. **R: A Language and Environment for Statistical Computing**, 2022. Disponível em: <https://www.r-project.org/>

RAHMAN, A. F.; GAMON, J. A.; FUENTES, D. A.; ROBERTS, D. A.; PRENTISS, D. Modeling spatially distributed ecosystem flux of boreal forest using hyperspectral indices from AVIRIS imagery. **Journal of Geophysical Research Atmospheres**, [s. l.], v. 106, n. D24, p. 33579–33591, 2001.

REGO, L. F.; VALLADARES, G. S.; AQUINO, R. P.; COELHO, R. M.; CUNHA, C. M. F. Da; CABRAL, L. J. R. S. Teor de Carbono Orgânico nos Horizontes Superficiais de Solos do Sertão Central do Ceará. In: XXXIV CONGRESSO BRASILEIRO DE CIÊNCIA DO SOLO 2013, Florianópolis, SC. **Anais**... Florianópolis, SC: Ciência do Solo: Para que e para quem? Programa Resumos, 2013. Disponível em: <https://eventosolos.org.br/cbcs2013/anais/arquivos/1641.pdf>

REHMAN, A.; MA, H.; AHMAD, M.; IRFAN, M.; TRAORE, O.; CHANDIO, A. A. Towards environmental Sustainability: Devolving the influence of carbon dioxide emission to population growth, climate change, Forestry, livestock and crops production in Pakistan. **Ecological Indicators**, [s. l.], v. 125, p. 107460, 2021. a. Disponível em: <https://www.sciencedirect.com/science/article/pii/S1470160X21001254>

REHMAN, A.; MA, H.; AHMAD, M.; OZTURK, I.; CHISHTI, M. Z. How do climatic change, cereal crops and livestock production interact with carbon emissions? Updated evidence from China. **Environmental Science and Pollution Research**, [s. l.], v. 28, n. 24, p. 30702–30713, 2021. b. Disponível em:

<https://doi.org/10.1007/s11356-021-12948-0>

REHMAN, A.; MA, H.; OZTURK, I.; ULUCAK, R. Sustainable development and pollution: the effects of CO2 emission on population growth, food production, economic development, and energy consumption in Pakistan. **Environmental Science and Pollution Research**, [s. l.], v. 29, n. 12, p. 17319–17330, 2022. Disponível em: <https://doi.org/10.1007/s11356-021-16998-2>

REN, F.; YANG, X.; ZHOU, H.; ZHU, W.; ZHANG, Z.; CHEN, L.; CAO, G.; HE, J.-S. Contrasting effects of nitrogen and phosphorus addition on soil respiration in an alpine grassland on the Qinghai-Tibetan Plateau. **Scientific Reports**, [s. l.], v. 6, n. 1, p. 34786, 2016. Disponível em: <http://www.nature.com/articles/srep34786>

RIBEIRO, H. V; RYBSKI, D.; KROPP, J. P. Effects of changing population or density on urban carbon dioxide emissions. **Nature Communications**, [s. l.], v. 10, n. 1, p. 3204, 2019. Disponível em: <https://doi.org/10.1038/s41467-019-11184-y>

RICHTER, I.; XIE, S. P. Muted precipitation increase in global warming simulations: A surface evaporation perspective. **Journal of Geophysical Research Atmospheres**, [s. l.], v. 113, n. 24, 2008.

RODRIGUES, R. P. Qualidade física de solos sob pastagens submetidas a reflorestamentos em épocas distintas: Pinheiral-RJ. [s. l.], 2021.

ROSSI, F. S.; DE ARAÚJO SANTOS, G. A.; DE SOUZA MARIA, L.; LOURENÇONI, T.; PELISSARI, T. D.; DELLA-SILVA, J. L.; OLIVEIRA JÚNIOR, J. W.; SILVA, A. de A. e; LIMA, M.; TEODORO, P. E.; TEODORO, L. P. R.; DE OLIVEIRA-JÚNIOR, J. F.; LA SCALA JR, N.; SILVA JUNIOR, C. A. Da. Carbon dioxide spatial variability and dynamics for contrasting land uses in central Brazil agricultural frontier from remote sensing data. **Journal of South American Earth Sciences**, [s. l.], v. 116, p. 103809, 2022. Disponível em: <https://www.sciencedirect.com/science/article/pii/S0895981122001006>

ROSSI, F. S.; SANTOS, G. A. de A. Fire dynamics in Mato Grosso State, Brazil: the relative roles of gross primary productivity. **Big Earth Data**, [s. l.], v. 4, n. 1, p. 23–44, 2020.

ROY, P. S.; RAVAN, S. A. Biomass estimation using satellite remote sensing data—An investigation on possible approaches for natural forest. **Journal of Biosciences**, [s. l.], v. 21, n. 4, p. 535–561, 1996. Disponível em: <http://link.springer.com/10.1007/BF02703218>

RUFINO, D. C.; DINIZ NETO, M. A.; MELO, T. de S.; BANDEIRA, L. B.; SILVA, M. D. P. Da; BULHÕES, L. A. De; DINIZ, B. L. M. T.; MESQUITA, E. F. De. Estoque de carbono do solo em agroecossistemas e vegetação secundária. **Research, Society and Development**, [s. l.], v. 11, n. 11, p. e545111133840, 2022. Disponível em: <https://rsdjournal.org/index.php/rsd/article/view/33840>

RUNNING, S. W.; NEMANI, R.; GLASSY, J. M.; THORNTON, P. E. **MODIS daily photosynthesis (PSN) and annual net primary production (NPP) product (MOD17) Algorithm Theoretical Basis Document**, 1999.

RUNNING, S. W.; ZHAO, M. User's Guide Daily GPP and Annual NPP (MOD17A2H/A3H) and Year-end Gap-Filled (MOD17A2HGF/A3HGF) Products NASA Earth Observing System MODIS Land Algorithm (For Collection 6). **University of Montana, Missoula, MT**, [s. l.], 2019.

SÁ, M. M. F.; SCHAEFER, C. E. G. R.; LOUREIRO, D. C.; SIMAS, F. N. B.; ALVES, B. J. R.; DE SÁ MENDONÇA, E.; DE FIGUEIREDO, E. B.; LA SCALA, N.; PANOSSO, A. R. Fluxes of CO2, CH4, and N2O in tundra-covered and Nothofagus forest soils in the Argentinian Patagonia. **Science of The Total Environment**, [s. l.], v. 659, p. 401–409, 2019. Disponível em: <https://www.sciencedirect.com/science/article/pii/S0048969718352136>

SANQUETTA, C. R.; DALLA CORTE, A. P.; SANQUETTA, M. N. I.; MAAS, G. C. B.; TOMÉ, M. Methane emissions and carbon storage from household paper disposal in Brazil during 1901-2016. **Desenvolvimento e Meio Ambiente**, [s. l.], v. 60, 2022. Disponível em: <https://revistas.ufpr.br/made/article/view/71476>

SANTANA, D. C.; DOS SANTOS, R. G.; TEODORO, L. P. R.; DA SILVA JUNIOR, C. A.; BAIO, F. H. R.; CORADI, P. C.; TEODORO, P. E. Structural equation modelling and factor analysis of the relationship between agronomic traits and vegetation indices in corn. **Euphytica**, [s. l.], v. 218, n. 4, p. 44, 2022. Disponível em: <https://link.springer.com/10.1007/s10681-022-02997-y>

SANTILLI, M.; MOUTINHO, P.; SCHWARTZMAN, S.; NEPSTAD, D.; CURRAN, L.; NOBRE, C. Tropical Deforestation and the Kyoto Protocol. **Climatic Change**, [s. l.], v. 71, n. 3, p. 267–276, 2005. Disponível em: <http://link.springer.com/10.1007/s10584-005-8074-6>

SANTOS, C. da C. Sojicultura no Amapá: desafios e oportunidades. [s. l.], 2019.

SANTOS, C. V. B. DOS. **Modelagem Espectral Para Determinação De Fluxo De Co2 Em Áreas De Caatinga Preservada E Em Regeneração Cloves**. 2017. Universidade Estadual de Feira de Santana., [s. l.], 2017.

SANTOS, H. G.; CARVALHO JUNIOR, W. De; DART, R. de O.; ÁGLIO, M. L. D.; DE SOUSA, J. S.; PARES, J. G.; FONTANA, A.; MARTINS, A. L. da S.; DE OLIVEIRA, A. P. O novo mapa de solos do Brasil: legenda atualizada. [s. l.], 2011.

SCHLOERKE, B.; COOK, D.; LARMARANGE, J.; BRIATTE, F.; MARBACH, M.; THOEN, E.; ELBERG, A.; CROWLEY, J. **GGally: Extension to "ggplot2"**, 2021. Disponível em: <https://cran.r-project.org/package=GGally>

SCHOLES, R. J.; VAN BREEMEN, N. The effects of global change on tropical ecosystems. **Geoderma**, [s. l.], v. 79, n. 1–4, p. 9–24, 1997. Disponível em: <https://linkinghub.elsevier.com/retrieve/pii/S0016706197000360>

SCHUMAN, G. .; JANZEN, H. .; HERRICK, J. . Soil carbon dynamics and potential carbon sequestration by rangelands. **Environmental Pollution**, [s. l.], v. 116, n. 3, p. 391–396, 2002. Disponível em: <https://linkinghub.elsevier.com/retrieve/pii/S0269749101002159>

SCHWANDNER, F. M.; GUNSON, M. R.; MILLER, C. E.; CARN, S. A.; ELDERING, A.; KRINGS, T.; VERHULST, K. R.; SCHIMEL, D. S.; NGUYEN, H. M.; CRISP, D.; O'DELL, C. W.; OSTERMAN, G. B.; IRACI, L. T.; PODOLSKE, J. R. Spaceborne detection of localized carbon dioxide sources. **Science**, [s. l.], v. 358, n. 6360, 2017. Disponível em: <https://www.science.org/doi/10.1126/science.aam5782>

SCRIPPS OCEANOGRAPHY. **The Keeling Curve is a daily record of global atmospheric carbon dioxide concentration maintained by Scripps Institution of Oceanography at UC San Diego**. 2022. Disponível em: <https://keelingcurve.ucsd.edu/>. Acesso em: 10 abr. 2022.

SHAHBAZ, M.; KUMAR, A.; KUZYAKOV, Y.; BÖRJESSON, G.; BLAGODATSKAYA, E. Interactive priming effect of labile carbon and crop residues on SOM depends on residue decomposition stage: Three-source partitioning to evaluate mechanisms. **Soil Biology and Biochemistry**, [s. l.], v. 126, p. 179–190, 2018.

SHI, Q.; HUA, J.; CREECH, D.; YIN, Y. Biomass Estimation and Carbon Storage of Taxodium Hybrid Zhongshanshan Plantations in the Yangtze River Basin. **Forests**, [s. l.], v. 13, n. 10, p. 1725, 2022. Disponível em: <https://www.mdpi.com/1999-4907/13/10/1725>

SHIA, R. L.; LIANG, M. C.; MILLER, C. E.; YUNG, Y. L. CO2 in the upper troposphere: Influence of stratosphere- troposphere exchange. **Geophysical Research Letters**, [s. l.], v. 33, n. 14, 2006.

SHIMABUKURO, Y. E.; SMITH, J. A. The Least-Squares Mixing Models to Generate Fraction Images Derived From Remote Sensing Multispectral Data. **IEEE Transactions on Geoscience and Remote Sensing**, [s. l.], v. 29, n. 1, p. 16–20, 1991.

SHUKLA, P. R.; SKEG, J.; BUENDIA, E. C.; MASSON-DELMOTTE, V.; PÖRTNER, H.-O.; ROBERTS, D. C.; ZHAI, P.; SLADE, R.; CONNORS, S.; VAN DIEMEN, S.; FERRAT, M.; HAUGHEY, E.; LUZ, S.; PATHAK, M.; PETZOLD, J.; PEREIRA, J. P.; VYAS, P.; HUNTLEY, E.; KISSICK, K.; BELKACEMI, M.; MALLEY, J. **Climate Change and Land: An Ipcc Special Report on Climate Change, Desertification, Land Degradation, Sustainable Land Management, Food Security, and Greenhouse Gas Fluxes in Terrestrial Ecosystems**. [s.l: s.n.].

SIABI, Z.; FALAHATKAR, S.; ALAVI, S. J. Spatial distribution of XCO2 using OCO-2 data in growing seasons. **Journal of Environmental Management**, [s. l.], v. 244, p. 110–118, 2019.

SILVA-OLAYA, A. M.; CERRI, C. E. P.; LA SCALA JR, N.; DIAS, C. T. S.; CERRI, C. C. Carbon dioxide emissions under different soil tillage systems in mechanically harvested sugarcane. **Environmental Research Letters**, [s. l.], v. 8, n. 1, p. 15014, 2013. a.

SILVA-OLAYA, A. M.; CERRI, C. E. P.; LA SCALA JR, N.; DIAS, C. T. S.; CERRI, C. C. Carbon dioxide emissions under different soil tillage systems in mechanically harvested sugarcane. **Environmental Research Letters**, [s. l.], v. 8, n. 1, p. 015014, 2013. b. Disponível em: <https://iopscience.iop.org/article/10.1088/1748-9326/8/1/015014>

SILVA, B. de O.; MOITINHO, M. R.; SANTOS, G. A. de A.; TEIXEIRA, D. D. B.; FERNANDES, C.; LA SCALA, N. Soil CO2 emission and short-term soil pore class distribution after tillage operations. **Soil and Tillage Research**, [s. l.], v. 186, p. 224–232, 2019. Disponível em: <https://www.sciencedirect.com/science/article/pii/S0167198718304513>

SILVA, C. A.; LIMA, M. Soy Moratorium in Mato Grosso: Deforestation undermines the agreement. **Land Use Policy**, [s. l.], v. 71, p. 540–542, 2018. a.

SILVA, C. A.; LIMA, M. Soy Moratorium in Mato Grosso: Deforestation undermines the agreement. **Land Use Policy**, [s. l.], v. 71, p. 540–542, 2018. b. Disponível em: <https://linkinghub.elsevier.com/retrieve/pii/S0264837717312413>

SILVA, P. A. Da; DE LIMA, B. H.; LA SCALA, N.; PERUZZI, N. J.; CHAVARETTE, F. R.; PANOSSO, A. R. Spatial variation of soil carbon stability in sugarcane crops, central-south of Brazil. **Soil and Tillage Research**, [s. l.], v. 202, p. 104667, 2020. Disponível em: <https://www.sciencedirect.com/science/article/pii/S0167198720304499>

SILVA JUNIOR, C. A. Da; COSTA, G. de M.; ROSSI, F. S.; VALE, J. C. E. Do; LIMA, R. B. De; LIMA, M.; OLIVEIRA-JUNIOR, J. F. De; TEODORO, P. E.; SANTOS, R. C. Remote sensing for updating the boundaries between the brazilian Cerrado-Amazonia biomes. **Environmental Science and Policy**, [s. l.], v. 101, p. 383–392, 2019.

SILVA JUNIOR, C. A. Da; LEONEL-JUNIOR, A. H. S.; ROSSI, F. S.; CORREIA FILHO, W. L. F.; SANTIAGO, D. de B.; DE OLIVEIRA-JÚNIOR, J. F.; TEODORO, P. E.; LIMA, M.; CAPRISTO-SILVA, G. F. Mapping soybean planting area in midwest Brazil with remotely sensed images and phenology-based algorithm using the Google Earth Engine platform. **Computers and Electronics in Agriculture**, [s. l.], v. 169, p. 105194, 2020.

SILVA JUNIOR, C. A. Da; TEODORO, P. E.; TEODORO, L. P. R.; DELLA-SILVA, J. L.; SHIRATSUCHI, L. S.; BAIO, F. H. R.; BOECHAT, C. L.; CAPRISTO-SILVA, G. F. Is it possible to detect boron deficiency in eucalyptus using hyper and multispectral sensors? **Infrared Physics & Technology**, [s. l.], v. 116, p. 103810, 2021. Disponível em: <https://linkinghub.elsevier.com/retrieve/pii/S1350449521001821>

SILVA, M. A.; LIMA, M.; SILVA JUNIOR, C. A.; COSTA, G. M.; PERES, C. A. Achieving low-carbon cattle ranching in the Amazon: ‘Pasture sudden death’ as a window of opportunity. **Land Degradation and Development**, [s. l.], v. 29, n. 10, p. 3535–3543, 2018.

SILVA, M. de A.; SANTOS, C. M. Dos; VITORINO, H. dos S.; RHEIN, L.; OTHERS. Pigmentos fotossintéticos e {\'\i}ndice SPAD como descritores de intensidade do estresse por deficiência h{\'\i}drica em cana-de-açúcar. **Bioscience Journal**, [s. l.], p. 173–181, 2014.

SIQUEIRA, M. G. De; FIORELLI, E. C.; SANTOS, W. P.; MACHADO, C. B.; SANTOS, W. P.; VIEIRA, A. S.; SOUZA, S. P. De; SCHLINDWEIN, J. A. BIOMASSA MICROBIANA E CARBONO ORGÂNICO DO SOLO SOB DIFERENTES MANEJOS E SUCESSÃO DE CULTURAS. In: **Extensão Rural: práticas e pesquisas para o fortalecimento da agricultura familiar - Volume 2**. [s.l.] : Editora Científica Digital, 2021. p. 126–138.

SOARES, P.; SPOLADOR, H. F. S.; OTHERS. Determinantes da eficiência técnica na agricultura: um estudo para as culturas de milho e soja do estado de São Paulo. **ENCONTRO NACIONAL DE ECONOMIA (ANPEC)**, [s. l.], v. 44, p. 1–20, 2016.

SOJAMAPS. **Monitoramento de áreas de soja por meio de imagens de satélite.** 2021.

SOLANO, R.; DIDAN, K.; JACOBSON, A.; HUETE, A. MODIS Vegetation Index User ’ s Guide ( MOD13 Series ). **The University of Arizona**, [s. l.], v. 2010, n. May, p. 38, 2010.

SOMANATHAN, H. et al. **R: A Language and Environment for Statistical Computing. R Foundation for Statistical Computing.**, 2004. Disponível em: <http://tropicalconservationscience.mongabay.com/public/old/tropicalconservationscience/_/ojs/index.php/tcs/article/view/58%5Cnhttp://doi.wiley.com/10.1111/j.1744-7429.2003.tb00280.x%5Cn%3CGo to ISI%3E://A1997XW01300010%5Cn%3CGo to ISI%3E://000253477500007>

SOUZA, A. P.; MOTA, L. L.; ZAMADEI, T.; MARTIN, C. C.; ALMEIDA, F. T.; PAULINO, J. Classificação Climática e Balanço Hídrico Climatológico no Estado de Mato Grosso. **Nativa**, [s. l.], v. 1, n. 1, p. 34–43, 2013. a.

SOUZA, C. M.; ROBERTS, D. A.; COCHRANE, M. A. Combining spectral and spatial information to map canopy damage from selective logging and forest fires. **Remote Sensing of Environment**, [s. l.], v. 98, n. 2–3, p. 329–343, 2005.

SOUZA, C. M.; ROBERTS, D. A.; MONTEIRO, A. Multitemporal Analysis of Degraded Forests in the Southern Brazilian Amazon. **Earth Interactions**, [s. l.], v. 9, n. 19, p. 1–25, 2005. Disponível em: <https://journals.ametsoc.org/doi/10.1175/EI132.1>

SOUZA, C. M.; SIQUEIRA, J. V.; SALES, M. H.; FONSECA, A. V.; RIBEIRO, J. G.; NUMATA, I.; COCHRANE, M. A.; BARBER, C. P.; ROBERTS, D. A.; BARLOW, J. Ten-year landsat classification of deforestation and forest degradation in the brazilian amazon. **Remote Sensing**, [s. l.], v. 5, n. 11, p. 5493–5513, 2013. b.

STRUECKER, J.; DYCKMANS, J.; JOERGENSEN, R. G. Plant residue and native organic matter decomposition under subsoil-specific gas conditions--Comparing topsoils with C-poor and C-rich subsoils. **Geoderma**, [s. l.], v. 292, p. 1–8, 2017.

SUN, Z.; LIU, L.; MA, Y.; YIN, G.; ZHAO, C.; ZHANG, Y.; PIAO, S. The effect of nitrogen addition on soil respiration from a nitrogen-limited forest soil. **Agricultural and Forest Meteorology**, [s. l.], v. 197, p. 103–110, 2014. Disponível em: <https://linkinghub.elsevier.com/retrieve/pii/S0168192314001634>

TCHOBSALA; HAMADOU, A. Z.; HYACENTE, A.; PAUL, K.; DANRA, D. D.; CLAUTILDE, M. Influence of anthropization on flora and the carbon stock of the corridor’s vegetation at the Benoue National Park of Cameroon. **Environmental Challenges**, [s. l.], v. 5, p. 100345, 2021. Disponível em: <https://www.sciencedirect.com/science/article/pii/S2667010021003176>

TEOBALDO, D.; BAPTISTA, G. M. de M. Quantificação da Severidade das Queimadas e da Perda de Sequestro Florestal de Carbono em Unidades de Conservação do Distrito Federal (Measurement of Severity of Fires and Loss of Carbon Forest sink in the Conservation Units at Distrito Federal). **Revista Brasileira de Geografia Física**, [s. l.], v. 9, n. 1, p. 250, 2016. Disponível em: <https://periodicos.ufpe.br/revistas/rbgfe/article/view/233450>

TEODORO, P. E.; CORRÊA, C. C. G.; TORRES, F. E.; DE OLIVEIRA-JÚNIOR, J. F.; DA SILVA JUNIOR, C. A.; GOIS, G.; DELGADO, R. C. Analysis of the occurrence of wet and drought periods using standardized precipitation index in mato grosso do sul state, brazil. **Journal of Agronomy**, [s. l.], v. 14, n. 2, p. 80–86, 2015.

THE WORLD BANK. **<https://data.worldbank.org/>...Accessed March 2021**. [s.d.].

TIWARI, S.; SINGH, C.; SINGH, J. S. Wetlands: A Major Natural Source Responsible for Methane Emission. In: **Restoration of Wetland Ecosystem: A Trajectory Towards a Sustainable Environment**. Singapore: Springer Singapore, 2020. p. 59–74.

TIWARI, Y. K.; REVADEKAR, J. V.; RAVI KUMAR, K. Variations in atmospheric Carbon Dioxide and its association with rainfall and vegetation over India. **Atmospheric Environment**, [s. l.], v. 68, p. 45–51, 2013.

TONELLO, L. L.; AZEREDO, N. S. **Carbono no solo: vantagens para a agricultura e meio ambiente**. 2021. Disponível em: <https://maissoja.com.br/carbono-no-solo-vantagens-para-a-agricultura-e-meio-

ambiente/>. Acesso em: 4 jan. 2023.

TSAI, Y. H.; STOW, D.; AN, L.; CHEN, H. L.; LEWISON, R.; SHI, L. Monitoring land-cover and land-use dynamics in Fanjingshan National Nature Reserve. **Applied Geography**, [s. l.], v. 111, p. 102077, 2019. Disponível em: <https://linkinghub.elsevier.com/retrieve/pii/S0143622818309093>

VALE, N. K. A. Do; CARVALHO, M. T. de M.; ABDALA, K. de O. Caracterização de estudos de impacto ambiental relacionados ao cultivo e expansão da cultura da soja no mundo. **Revista em Agronegócio e Meio Ambiente**, [s. l.], v. 14, n. Supl. 2, p. 1–13, 2021. Disponível em: <https://periodicos.unicesumar.edu.br/index.php/rama/article/view/8954>

VERSINI, A.; NOUVELLON, Y.; LACLAU, J.-P.; KINANA, A.; MARESCHAL, L.; ZELLER, B.; RANGER, J.; EPRON, D. The manipulation of organic residues affects tree growth and heterotrophic CO2 efflux in a tropical Eucalyptus plantation. **Forest Ecology and Management**, [s. l.], v. 301, p. 79–88, 2013. Disponível em: <https://linkinghub.elsevier.com/retrieve/pii/S0378112712004586>

VIERA, M.; RODRÍGUEZ-SOALLEIRO, R. A Complete Assessment of Carbon Stocks in Above and Belowground Biomass Components of a Hybrid Eucalyptus Plantation in Southern Brazil. **Forests**, [s. l.], v. 10, n. 7, p. 536, 2019. Disponível em: <https://www.mdpi.com/1999-4907/10/7/536>

VILLACRÉS, J.; FUENTES, A.; RESZKA, P.; CHEEIN, F. A. Retrieval of Vegetation Indices Related to Leaf Water Content from a Single Index: A Case Study of Eucalyptus globulus (Labill.) and Pinus radiata (D. Don.). **Plants**, [s. l.], v. 10, n. 4, p. 697, 2021. Disponível em: <https://www.mdpi.com/2223-7747/10/4/697>

WAHEED, R.; CHANG, D.; SARWAR, S.; CHEN, W. Forest, agriculture, renewable energy, and CO2 emission. **Journal of Cleaner Production**, [s. l.], v. 172, p. 4231–4238, 2018.

WANG, J.; LIU, Q.-Q.; CHEN, R.-R.; LIU, W.-Z.; SAINJU, U. M. Soil carbon dioxide emissions in response to precipitation frequency in the Loess Plateau, China. **Applied Soil Ecology**, [s. l.], v. 96, p. 288–295, 2015. Disponível em: <https://www.sciencedirect.com/science/article/pii/S0929139315300792>

WANG, J.; ZENG, N.; WANG, M. Interannual variability of the atmospheric CO2 growth rate: Roles of precipitation and temperature. **Biogeosciences**, [s. l.], v. 13, n. 8, p. 2339–2352, 2016.

WANG, X.; LIU, L.; PIAO, S.; JANSSENS, I. A.; TANG, J.; LIU, W.; CHI, Y.; WANG, J.; XU, S. Soil respiration under climate warming: differential response of heterotrophic and autotrophic respiration. **Global Change Biology**, [s. l.], v. 20, n. 10, p. 3229–3237, 2014. Disponível em: <https://onlinelibrary.wiley.com/doi/10.1111/gcb.12620>

WASTI, S. K. A.; ZAIDI, S. W. An empirical investigation between $CO_2$ emission, energy consumption, trade liberalization and economic growth: A case of Kuwait. **Journal of Building Engineering**, [s. l.], v. 28, p. 101104, 2020.

WENCHEN, S.; XIAOJUAN, T.; JINSONG, Z.; PING, M.; JUN, L. Autotrophic and heterotrophic components of soil respiration caused by rhizosphere priming effects in a plantation. **Plant, Soil and Environment**, [s. l.], v. 63, n. 7, p. 295–299, 2017.

WEST, H.; QUINN, N.; HORSWELL, M. Remote sensing for drought monitoring & impact assessment: Progress, past challenges and future opportunities. **Remote Sensing of Environment**, [s. l.], v. 232, p. 111291, 2019. Disponível em: <https://www.sciencedirect.com/science/article/pii/S0034425719303104>

WUNCH, D.; WENNBERG, P. O.; OSTERMAN, G.; FISHER, B.; NAYLOR, B.; ROEHL, C. M.; O'DELL, C.; MANDRAKE, L.; VIATTE, C.; KIEL, M.; OTHERS. Comparisons of the orbiting carbon observatory-2 (OCO-2) X CO 2 measurements with TCCON. **Atmospheric Measurement Techniques**, [s. l.], v. 10, n. 6, p. 2209–2238, 2017.

XAVIER, C. V.; MOITINHO, M. R.; TEIXEIRA, D. D. B.; DE ARAÚJO SANTOS, G. A.; CORÁ, J. E.; LA SCALA JR., N. Crop rotation and sequence effects on temporal variation of $CO_2$ emissions after long-term no-till application. **Science of The Total Environment**, [s. l.], v. 709, p. 136107, 2020. Disponível em: <https://www.sciencedirect.com/science/article/pii/S0048969719361030>

XU, C.; DU, X.; YAN, Z.; FAN, X. ScienceEarth: A Big Data Platform for Remote Sensing Data Processing. **Remote Sensing**, [s. l.], v. 12, n. 4, p. 607, 2020. Disponível em: <https://www.mdpi.com/2072-4292/12/4/607>

XUE, J.; SU, B. Significant Remote Sensing Vegetation Indices: A Review of Developments and Applications. **Journal of Sensors**, [s. l.], v. 2017, p. 1–17, 2017. Disponível em: <https://www.hindawi.com/journals/js/2017/1353691/>

YAO, Q.; LI, Z.; SONG, Y.; WRIGHT, S. J.; GUO, X.; TRINGE, S. G.; TFAILY, M. M.; PAŠA-TOLIĆ, L.; HAZEN, T. C.; TURNER, B. L.; MAYES, M. A.; PAN, C. Community proteogenomics reveals the systemic impact of phosphorus availability on microbial functions in tropical soil. **Nature Ecology & Evolution**, [s. l.], v. 2, n. 3, p. 499–509, 2018. Disponível em: <https://www.nature.com/articles/s41559-017-0463-5>

ZANCHI, F. B.; ROCHA, H. R.; KRUIJT, B.; CARDOSO, F. L.; DEUS, J. A.; AGUIAR, L. J. G. Medição do efluxo de $CO_2$ do solo: monitoramento com câmaras automáticas sobre floresta e pastagem em Rondônia. In: ANAIS VI CONGRESSO DE ECOLOGIA DO BRASIL, FORTALEZA 2003, **Anais**... [s.l: s.n.]

ZÁS, L. R. T.; OTHERS. Relação entre variáveis dendrométricas de eucaliptus e índices de vegetação obtidos com VANT. [s. l.], 2017.

ZENG, X.; SONG, Y.; ZENG, C.; ZHANG, W.; HE, S. Partitioning soil respiration in two typical forests in semi-arid regions, North China. **CATENA**, [s. l.], v. 147, p. 536–544, 2016. Disponível em: <https://linkinghub.elsevier.com/retrieve/pii/S0341816216303204>

ZHANG, Q.; MANZONI, S.; KATUL, G.; PORPORATO, A.; YANG, D. The hysteretic evapotranspiration—Vapor pressure deficit relation. **Journal of Geophysical Research: Biogeosciences**, [s. l.], v. 119, n. 2, p. 125–140, 2014.

ZHANG, X.-Q.; XU, D. Potential carbon sequestration in China's forests. **Environmental Science & Policy**, [s. l.], v. 6, n. 5, p. 421–432, 2003. Disponível em: <https://linkinghub.elsevier.com/retrieve/pii/S1462901103000728>

ZHANG, Y.; WANG, X. Geographical spatial distribution and productivity dynamic change of eucalyptus plantations in China. **Scientific Reports**, [s. l.], v. 11, n. 1, p. 19764, 2021. Disponível em: <https://www.nature.com/articles/s41598-021-97089-7>

ZHENG, X.; STREIMIKIENE, D.; BALEZENTIS, T.; MARDANI, A.; CAVALLARO, F.; LIAO, H. A review of greenhouse gas emission profiles, dynamics, and climate change mitigation efforts across the key climate change players. **Journal of Cleaner Production**, [s. l.], v. 234, p. 1113–1133, 2019. Disponível em: <https://linkinghub.elsevier.com/retrieve/pii/S0959652619320943>